Appl. Comput. Harmon. Anal. ••• (••••) •••–•••

Contents lists available at ScienceDirect

Applied and Computational Harmonic Analysis

journal homepage: www.elsevier.com/locate/acha

Analytic and directional wavelet packets in the space of periodic signals

Amir Averbuch [a], Pekka Neittaanmäki [b], Valery Zheludev [a]

[a] School of Computer Science, Tel Aviv University, Tel Aviv 69978, Israel
[b] Department of Mathematical Information Technology, University of Jyväskylä, Finland

ARTICLE INFO

Article history:
Received 2 July 2019
Received in revised form 7 June 2023
Accepted 16 June 2023
Available online xxxx
Communicated by Erwan Erwan Le Pennec

Keywords:
Directional wavelet packet
Discrete periodic splines
Analytic wavelet packet
Image denoising and impainting

ABSTRACT

The paper presents a versatile library of analytic and quasi-analytic complex-valued wavelet packets (WPs) which originate from discrete splines of arbitrary orders. The real parts of the quasi-analytic WPs are the regular spline-based orthonormal WPs designed in [4]. The imaginary parts are the so-called complementary orthonormal WPs, which, unlike the symmetric regular WPs, they are antisymmetric. Tensor products of 1D quasi-analytic WPs provide a diversity of 2D WPs oriented in multiple directions. The designed computational scheme in the paper enables us to get fast and easy implementation of the WP transforms. The presented WPs proved to be efficient in signal/image processing applications such as restoration of images degraded by either additive noise or missing of up to 90% of their pixels.

1. Introduction

The sparse representation of data is of crucial importance in various applications such as compression, restoration of images degraded by noise and/or missing some portion of pixels (inpainting), deblurring, superresolution, classification, to name a few. Sparse representation of an object means its approximation by a linear combination of a relatively small number of elements from a proper dictionary. To succeed in image processing applications, the dictionary has to adapt to such typical structures of images that comprise smooth regions, oriented edges oriented in various directions and texture that can have an oscillating structure.

For example, dictionaries that have directionality in them are brushlets [33], contourlets, curvelets, bandelets, ridgelets [17,9,8,10,39,31,35], pseudo-polar Fourier transforms [1,2] and related to them shearlets [30,18]. These dictionaries are used in various image processing applications such as Radon transform in tomography, and Affine Shear transforms (DAS-1) [41]. However, while these transforms successfully capture

E-mail address: amir1@tauex.tau.ac.il (A. Averbuch).

https://doi.org/10.1016/j.acha.2023.06.006
1063-5203/

edges in images, the dictionaries did not demonstrate a satisfactory texture restoration due to the lack of oscillating waveforms in their dictionaries.

Since the introduction by Kingsbury ([28,29]) of complex wavelet transforms implemented by the dual-tree scheme, the complex wavelets (DT_CW), M-band wavelets, wavelet frames and wavelet packets (WPs) have become a field of active research that appears in multiple applications ([24,26,25,12,11,40,38,7,21,22], to name a few). The advantages of the DT_CWs over the standard real wavelet transforms stem from their approximate shift invariance and some directionality inherent to tensor-products of the DT_CWs.

However, the directionality of the DT_CWs as well as the M-band wavelets ([11]) is very limited and this is a drawback for image processing applications. The tight tensor-product complex wavelet frames TP_CTF$_n$ with different number of directions, are designed in [21,22] and some of them, in particular TP_CTF$_6$ and TP_CTF$_n^{\downarrow}$, demonstrate excellent performance (in terms of PSNR) for image denoising and inpainting. The number of directions in both 2D TP_CTF$_6$ and TP_CTF$_n^{\downarrow}$ frames is 14 and remains the same for all decomposition levels.

Some of disadvantages of the above 2D TP_CTF$_6$ and TP_CTF$_n^{\downarrow}$ frames are mentioned in [13]. For example, "limited and fixed number of directions is undesirable in practice especially when the resolution of an image is very high that requires large number of directional filters in order to capture as many features with different orientations as possible" ([13]). In addition, "due to the fixed number of 1D filters, the number of free parameters is limited which prevents the search of optimal filter bank systems for image processing" ([13]).

According to [13], the remedy for the above shortcomings is in the incorporation of the two-layer structure that is inherent in the TP_CTF$_6$ and TP_CTF$_n^{\downarrow}$ frames into directional filter banks introduced in [23,41].

The complex wavelet packets (Co_WPs) are an alternative way to overcome the above disadvantages. The first version of complex WPs appears in [24] after the introduction of the complex wavelets by Kingsbury. The complex wavelet transforms in [24,26,25] are extended to the Co_WP transforms by the application of the same filters as used in the DT_CW transforms to the high-frequency bands. Although the low- and high-frequency bands in DT_CW are approximately analytic, this is not the case for the Co_WPs designed in [24,26,25]. In addition, as shown in [7] (Fig. 1), much energy passes into the negative half-bands of the spectra. Another approach to the design of Co_WPs is described in [7]. It is suggested in [7] that in order to retain an approximate analyticity of the dual-tree WP transforms, the filter banks for the second decomposition of the transforms should be the same for both stems of the tree.

The potential advantages of the Co_WP transforms are apparent. In this paper, we design a family of Co_WP transforms which possess properties such as perfect frequency separation, Hilbert transform relation between real and imaginary parts of the Co_WPs, orthonormality of shifts of real and imaginary parts of the Co_WPs, unlimited number of directions in the multidimensional case, a variety of free parameters, and fast and easy implementation. As a base for the design, we use the family of discrete-time WPs originated from periodic discrete splines of different orders that are described in [4] (Chapter 4). The wavelet packets $\psi^{2r}_{[m],l}$, where m is the decomposition level, $l = 0, ..., 2^m - 1$ is the index of the related frequency band and $2r$ is the order of the generating discrete spline, are symmetric, well localized in time domain (although are not compactly supported), their DFTs spectra are flat, and provide a refined split of the frequency domain. The WP transforms are executed in the frequency domain using the Fast Fourier transform (FFT). By varying the order $2r$, we can supply the WPs $\psi^{2r}_{[m],l}$ with any number of local vanishing moments without increase of the computational cost. Different combinations of the shifts in these WPs provide a variety of orthonormal bases of the space of N-periodic signals.

To derive the Co_WPs, we expand the WPs $\psi^{2r}_{[m],l}$ to periodic analytic discrete-time signals $\bar{\psi}^{2r}_{\pm[m],l} = \psi^{2r}_{[m],l} \pm i\,\theta^{2r}_{[m],l}$, where $\theta^{2r}_{[m],l}$ is the discrete periodic Hilbert transform (HT) of the WP $\psi^{2r}_{[m],l}$. The waveforms $\theta^{2r}_{[m],l}$ are antisymmetric, and for all $l \neq 0,\ 2^m-1$, orthonormal properties similar to the properties of the WPs $\psi^{2r}_{[m],l}$ take place. To achieve orthonormality, the waveforms $\theta^{2r}_{[m],l},\ l = 0,\ 2^m - 1$ are slightly corrected at the expense of minor deviation from antisymmetry and we get a new orthonormal complimentary WP (cWP)

Please cite this article in press as: A. Averbuch et al., Analytic and directional wavelet packets in the space of periodic signals, Appl. Comput. Harmon. Anal. (2023), https://doi.org/10.1016/j.acha.2023.06.006

system $\left\{\varphi^{2r}_{[m],l}\right\}$, $m = 1, ..., M,\ l = 0, ..., 2^m - 1$, where for $l \neq 0,\ 2^m - 1$, the WPs satisfy $\varphi^{2r}_{[m],l} = \theta^{2r}_{[m],l}$. The magnitude spectra of the cWPs $\varphi^{2r}_{[m],l}$ coincide with the spectra of the respective WPs $\psi^{2r}_{[m],l}$ and, similarly to the WPs $\psi^{2r}_{[m],l}$, the cWPs $\varphi^{2r}_{[m],l}$ provide a variety of orthonormal bases for the space of N-periodic signals.

Correspondingly, we define the quasi-analytic WP systems (qWP) as

$$\Psi^{2r}_{\pm[m],l} = \psi^{2r}_{[m],l} \pm i\varphi^{2r}_{[m],l}, \quad m = 1, ..., M,\ l = 0, ..., 2^m - 1,$$

where all the WPs with indices other than $l = 0, 2^m - 1$ are analytic. For the implementation of the transforms with the complex qWPs we do not use the dual-tree scheme with different filter banks for real and imaginary wavelets but use the scheme with a single complex filter bank in the first step of the transform, and a real filter bank in the additional steps.

A dual-tree structure type appears in the 2D case when two sets of qWPs are defined as the tensor products of 1D qWPs

$$\Psi^{2r}_{++[m],j,l}[k,n] \stackrel{\text{def}}{=} \Psi^{2r}_{+[m],\kappa}[k]\,\Psi^{2r}_{+[m],l}[n], \quad \Psi^{2r}_{+-[m],j,l}[k,n] \stackrel{\text{def}}{=} \Psi^{2r}_{+[m],\kappa}[k]\,\Psi^{2r}_{-[m],l}[n] \tag{1.1}$$

and processing with the qWPs $\Psi^{2r}_{+\pm[m],j,l}$ is executed separately.

The real and imaginary parts of the qWPs $\Psi^{2r}_{+\pm[m],j,l}$ are the 2D waveforms oriented in multiple directions, specifically the $2(2^{m+1} - 1)$ directions at the m-th decomposition level. Such an abundant directionality proved to be efficient in the examples on image denoising and inpainting. It is worth mentioning that the WPs of one- and two-dimensions have a localized oscillating structure, which is useful for detection of transient oscillating events in 1D signals and oscillating patterns in the images (for example, "Barbara" in Fig. 7.3).

Both one- and two-dimensional transforms are implemented in a fast way by using the Fast Fourier transform (FFT).

The paper is organized as follows: Section 2 outlines briefly periodic discrete-time WPs originated from discrete splines and corresponding transforms that form a basis for the design of Co_WPs. The analysis $\tilde{\mathbf{F}}$ and synthesis $\mathbf{F}$ filter banks for the WP transforms are described. Section 3 outlines the construction of discrete-time periodic analytic signals. This section also introduces complimentary sets of WPs (cWPs), analytic and quasi-analytic WPs (qWPs). Section 4 describes the implementation of the cWP and qWP transforms. The filter banks for one step of analysis and synthesis transforms are introduced. It is interesting to note that subsequent application of the direct and inverse qWP filter banks to a signal $\mathbf{x}$ produces the analytic signal $\bar{\mathbf{x}} = \mathbf{x} + i\,H(\mathbf{x})$. All the subsequent steps of cWP and qWP transforms are implemented with the same filter banks $\tilde{\mathbf{F}}$ and $\mathbf{F}$ as used in the above WP transforms (section 2). Section 5 extends the design of 1D qWPs to the 2D case. The 2D qWPs are defined via tensor products as shown in Eq. (1.1). Directionality of the 2D qWPs is discussed. Section 6 describes the implementation of the 2D qWP transforms by a dual-tree. Section 7 presents a few experimental results for the restoration of images that are degraded by either strong additive noise or by missing many of the pixels. In one example, both the degradation sources are present. Section 8 discusses the results. The Appendix contains the proof of a proposition and the outline of a denoising scheme.

Notations and abbreviations $N = 2^j$, $M = 2^m$, $m < j$, $N_m = 2^{j-m}$ and $\Pi[N]$ is a space of real-valued N-periodic signals. $\Pi[N, N]$ is the space of two-dimensional N-periodic arrays in both vertical and horizontal directions. $\omega \stackrel{\text{def}}{=} e^{2\pi\, i/N}$.

The expression $\bigoplus_{k=P}^{R} f_k$ means the union of elements f_k which are orthogonal to each other. $A \bigoplus B$ means the union of the sets A and B, which are orthogonal to each other that is each element of A is orthogonal to all elements of B and vice versa.

Please cite this article in press as: A. Averbuch et al., Analytic and directional wavelet packets in the space of periodic signals, Appl. Comput. Harmon. Anal. (2023), https://doi.org/10.1016/j.acha.2023.06.006

A signal $\mathbf{x} = \{x[k]\} \in \Pi[N]$ is represented by its inverse discrete Fourier transform (DFT)

$$\begin{array}{l} x[k] \;=\; \frac{1}{N}\sum_{n=0}^{N-1} \hat{x}[n]\,\omega^{kn} = \frac{1}{N}\sum_{n=-N/2}^{N/2-1} \hat{x}[n]\,\omega^{kn}, \\ \hat{x}[n] \;=\; \sum_{k=0}^{N-1} x[k]\,\omega^{-kn}, \quad \hat{x}[-n] = \hat{x}[N-n] = \hat{x}[n]^*, \end{array} \tag{1.2}$$

where $\cdot^*$ means complex conjugate. In particular, $\hat{x}[0] = \sum_{k=0}^{N-1} x[k]$ and $\hat{x}[N/2] = \sum_{k=0}^{N-1}(-1)^k\, x[k]$ are real numbers.

The DFT of an N_m-periodic signal is $\hat{x}[n]_m = \sum_{k=0}^{N_m-1} x[k]\,\omega^{-kn2^m}$. The abbreviation PR means perfect reconstruction. The abbreviations 1D and 2D mean one-dimensional and two-dimensional, respectively. FFT is the fast Fourier transform, HT is the Hilbert transform, $H(\mathbf{x})$ is the discrete periodic HT of a signal $\mathbf{x}$.

The abbreviations WP, cWP and qWP mean wavelet packets (typically spline-based wavelet packets $\psi^{2r}_{[m],l}$), complementary wavelet packets $\varphi^{2r}_{[m],l}$ and quasi-analytic wavelet packets $\Psi^{2r}_{\pm[m],l}$, respectively, in 1D case, and wavelet packets $\psi^{2r}_{[m],j,l}$, complimentary wavelet packets $\varphi^{2r}_{[m],j,l}$ and quasi-analytic wavelet packets $\Psi^{2r}_{+\pm[m],l,j}$, respectively, in 2D case.

$$U^{4r}[n] \stackrel{\text{def}}{=} \frac{1}{2}\left(\cos^{4r}\frac{\pi\, n}{N} + \sin^{4r}\frac{\pi\, n}{N}\right). \tag{1.3}$$

Peak Signal-to-Noise ratio (PSNR) in decibels (dB) is

$$PSNR \stackrel{\text{def}}{=} 10\log_{10}\left(\frac{N\,255^2}{\sum_{k=1}^{N}(x_k - \tilde{x}_k)^2}\right)\; dB.$$

SBI stands for split Bregman iterations and p-filter means periodic filter.

Throughout the paper σ denotes the standard deviation of a signal $\mathbf{x}$ and $\delta[k] = \begin{cases} 1, & \text{if } k = lN,\ l \in \mathbb{Z}; \\ 0, & \text{otherwise} \end{cases}$ denotes the delta sequence in the space $\Pi[N]$.

2. Outline of orthonormal WPs originated from discrete splines: preliminaries

This section provides a brief outline of periodic discrete-time wavelet packets originated from discrete splines and corresponding transforms. For details see Chapter 4 in [4].

2.1. Periodic discrete splines

The centered span-two N-periodic discrete B-spline of order $2r$ is defined as the IDFT of the sequence

$$\hat{b}^{2r}[n] = \cos^{2r}\frac{\pi\, n}{N}, \quad b^{2r}[k] = \frac{1}{N}\sum_{n=-N/2}^{N/2-1} \omega^{kn}\,\cos^{2r}\frac{\pi\, n}{N}.$$

The B-splines are non-negative symmetric finite-length signals (up to periodization). Only the samples $b^{2r}[k],\ k = -r, ...r$, are non-zero.

The signals $s^{2r}[k] \stackrel{\text{def}}{=} \sum_{l=0}^{N/2-1} q[l]\, b^{2r}[k-2l]$, which are referred to as discrete splines, form an $N/2$-dimensional subspace ${}^{2r}\mathcal{S}^0_{[1]}$ of the space $\Pi[N]$ whose basis consists of two-sample shifts of the B-spline $\mathbf{b}^{2r}$. Here $\mathbf{q} = \{q[l]\},\ l = 0, ..., N/2-1$, is a real-valued sequence. The DFT of the discrete spline $\mathbf{s}^{2r}$ is

$$\hat{s}^{2r}[n] = \hat{q}[n]_1\,\hat{b}^{2r}[n] = \hat{q}[n]_1\,\cos^{2r}\frac{\pi\, n}{N}.$$

Please cite this article in press as: A. Averbuch et al., Analytic and directional wavelet packets in the space of periodic signals, Appl. Comput. Harmon. Anal. (2023), https://doi.org/10.1016/j.acha.2023.06.006

A discrete spline $\psi^{2r}_{[1],0} \in {}^{2r}\mathcal{S}^0_{[1]}$ is defined through its inverse DFT (iDFT):

$$\psi^{2r}_{[1],0}[k] \stackrel{\text{def}}{=} \frac{1}{N} \sum_{n=-N/2}^{N/2-1} \omega^{kn} \frac{\cos^{2r} \frac{\pi n}{N}}{\sqrt{U^{4r}[n]}},$$

where $U^{4r}[n]$ is defined in Eq. (1.3).

Proposition 2.1 *([4], Proposition 3.6). Two-sample shifts* $\left\{\psi^{2r}_{[1],0}[\cdot - 2l]\right\}$, $l = 0, ..., N/2-1$, *of the discrete splines* $\psi^{2r}_{[1],0}$ *form an orthonormal basis of the subspace* ${}^{2r}\mathcal{S}^0_{[1]} \subset \Pi[N]$.

The orthogonal projection of a signal $\mathbf{x} \in \Pi[N]$ *onto the space* ${}^{2r}\mathcal{S}^0_{[1]}$ *is the signal* $\mathbf{x}^0_{[1]} \in \Pi[N]$ *such that*

$$x^0_{[1]}[k] = \sum_{l=0}^{N/2-1} y^0_{[1]}[l]\, \psi^{2r}_{[1],0}[k-2l], \quad y^0_{[1]}[l] = \left\langle \mathbf{x},\, \psi^{2r}_{[1],0}[\cdot - 2l] \right\rangle = \sum_{k=0}^{N-1} h^0_{[1]}[k-2l]\, x[k],$$

$$h^0_{[1]}[k] = \psi^{2r}_{[1],0}[k], \quad \hat{h}^0_{[1]}[n] = \hat{\psi}^{2r}_{[1],0}[n] = \frac{\cos^{2r} \frac{\pi n}{N}}{\sqrt{U^{4r}[n]}}. \tag{2.1}$$

2.2. Orthogonal complement for subspace ${}^{2r}\mathcal{S}^0_{[1]}$

The orthogonal complement for ${}^{2r}\mathcal{S}^0_{[1]}$ in the signal space $\Pi[N]$ is denoted by ${}^{2r}\mathcal{S}^1_{[1]}$. Thus, $\Pi[N] = \mathcal{S}_{[0]} = {}^{2r}\mathcal{S}^0_{[1]} \bigoplus {}^{2r}\mathcal{S}^1_{[1]}$. The orthonormal basis in the subspace is formed by the two-sample shifts $\left\{\psi^{2r}_{[1],1}[\cdot - 2l]\right\}$, $l = 0, ..., N/2-1$, of the signal $\psi^{2r}_{[1],1}$, which is defined through its inverse DFT (iDFT):

$$\psi^{2r}_{[1],1}[k] \stackrel{\text{def}}{=} \frac{1}{N} \sum_{n=-N/2}^{N/2-1} \omega^{kn} \frac{\omega^n \sin^{2r} \frac{\pi n}{N}}{\sqrt{U^{4r}[n]}}.$$

Proposition 2.2 *([4], Proposition 4.1). The orthogonal projection of a signal* $\mathbf{x} \in \Pi[N]$ *onto the space* ${}^{2r}\mathcal{S}^1_{[1]}$ *is the signal* $\mathbf{x}^1_{[1]} \in \Pi[N]$ *such that*

$$x^1_{[1]}[k] = \sum_{l=0}^{N/2-1} y^1_{[1]}[l]\, \psi^{2r}_{[1],1}[k-2l], \quad y^1_{[1]}[l] = \left\langle \mathbf{x},\, \psi^{2r}_{[1],1}[\cdot - 2l] \right\rangle = \sum_{k=0}^{N-1} h^1_{[1]}[k-2l]\, x[k],$$

$$h^1_{[1]}[k] = \psi^{2r}_{[1],1}[k], \quad \hat{h}^1_{[1]}[n] = \hat{\psi}^{2r}_{[1],1}[n] = \frac{\omega^n \sin^{2r} \frac{\pi n}{N}}{\sqrt{U^{4r}[n]}}. \tag{2.2}$$

The signals $\psi^{2r}_{[1],0}$ and $\psi^{2r}_{[1],1}$ are referred to as the discrete-spline wavelet packets of order $2r$ from the first decomposition level. They are the impulse responses of the low- and high-pass periodic filters (p-filters) $\mathbf{h}^0_{[1]}$ and $\mathbf{h}^1_{[1]}$, respectively.

Remark 2.1. We emphasise that the DFTs $\hat{\psi}^{2r}_{[1],0}[n] = \begin{cases} \sqrt{2}, & \text{if } n = 0; \\ 0, & \text{if } n = N/2, \end{cases}$

and $\hat{\psi}^{2r}_{[1],1}[n] = \begin{cases} -\sqrt{2}, & \text{if } n = N/2; \\ 0, & \text{if } n = 0. \end{cases}$ It is seen from Eqs. (2.1) and (2.2).

Fig. 2.1 displays the discrete-spline wavelet packets $\psi^{2r}_{[1],0}$ and $\psi^{2r}_{[1],1}$ of different orders and magnitudes of their DFT spectra (which are the p-filters $\mathbf{h}^0_{[1]}$ and $\mathbf{h}^1_{[1]}$ magnitude responses). It is seen that the wavelets

Please cite this article in press as: A. Averbuch et al., Analytic and directional wavelet packets in the space of periodic signals, Appl. Comput. Harmon. Anal. (2023), https://doi.org/10.1016/j.acha.2023.06.006

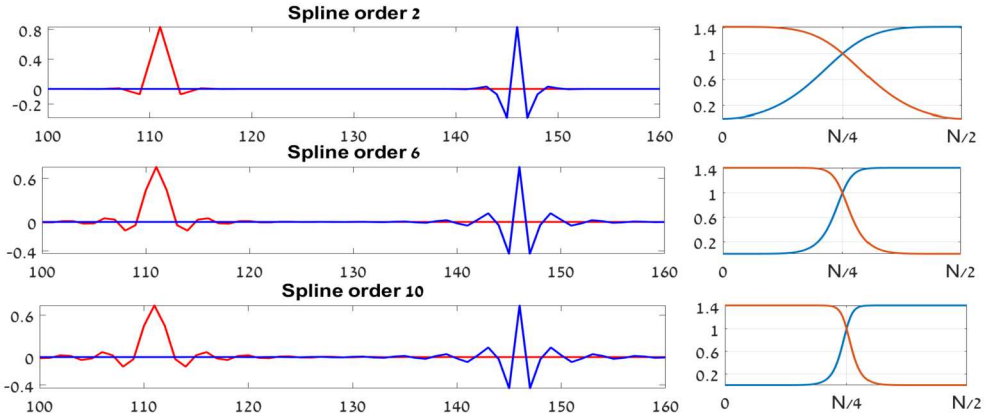

Fig. 2.1. Left: wavelet packets $\psi^{2r}_{[1],0}$ (red lines) and $\psi^{2r}_{[1],1}$ (blue lines), $r = 1, 3, 5$. Right: magnitude spectra of $\psi^{2r}_{[1],0}$ (red lines) and $\psi^{2r}_{[1],1}$ (blue lines). (For interpretation of the colors in the figure(s), the reader is referred to the web version of this article.)

are well localized in time domain. The spectra are flat and their shapes tend to rectangular as their orders increase.

2.3. One-level wavelet packet transform of a signal

The transform of a signal $\mathbf{x} \in \Pi[N]$ into the pair $\left\{\mathbf{y}^0_{[1]}, \mathbf{y}^1_{[1]}\right\}$ of signals from $\Pi[N/2]$ is referred to as the one-level wavelet packet transform (WPT) of the signal $\mathbf{x}$. According to Propositions 2.1 and 2.2, the transform is implemented by filtering $\mathbf{x}$ with time-reversed half-band low- and high-pass p-filters $\mathbf{h}^0_{[1]}$ and $\mathbf{h}^1_{[1]}$, respectively, which is followed by downsampling. Thus the p-filters $\mathbf{h}^0_{[1]}$ and $\mathbf{h}^1_{[1]}$ form a critically sampled analysis p-filter bank $\tilde{\mathbf{H}}^1_{[1]}$. Eqs. (2.1) and (2.2) imply that its modulation matrix is

$$\begin{aligned} \tilde{\mathbf{M}}[n] &= \begin{pmatrix} \hat{h}^0_{[1]}[n] & \hat{h}^0_{[1]}\left[n+\frac{N}{2}\right] \\ \hat{h}^1_{[1]}[n] & \hat{h}^1_{[1]}\left[n+\frac{N}{2}\right] \end{pmatrix} = \begin{pmatrix} \beta[n] & \beta\left[n+\frac{N}{2}\right] \\ \alpha[n] & \alpha\left[n+\frac{N}{2}\right] \end{pmatrix} = \begin{pmatrix} \beta[n] & \omega^{-n}\alpha[n] \\ \alpha[n] & -\omega^n\beta[n] \end{pmatrix}, \\ \beta[n] &= \frac{\cos^{2r}\frac{\pi n}{N}}{\sqrt{U^{4r}[n]}}, \quad \alpha[n] = \omega^n\,\beta\left[n+\tfrac{N}{2}\right] = \omega^n\,\frac{\sin^{2r}\frac{\pi n}{N}}{\sqrt{U^{4r}[n]}}. \end{aligned} \tag{2.3}$$

The analysis modulation matrix $\tilde{\mathbf{M}}[n]/\sqrt{2}$, as well as the matrix $\tilde{\mathbf{M}}[-n]/\sqrt{2}$ are unitary matrices. Therefore, the synthesis modulation matrix is

$$\mathbf{M}[n] = \begin{pmatrix} \beta[n] & \alpha[n] \\ \omega^{-n}\alpha[n] & -\omega^n\beta[n] \end{pmatrix} = \tilde{\mathbf{M}}[n]^T. \tag{2.4}$$

Consequently, the synthesis p-filter bank coincides with the analysis p-filter bank and, together, they form a perfect reconstruction (PR) p-filter bank.

The one-level WP transform of a signal $\mathbf{x}$ and its inverse are represented in a matrix form:

$$\begin{pmatrix} \hat{y}^0_{[1]}[n]_1 \\ \hat{y}^1_{[1]}[n]_1 \end{pmatrix} = \frac{1}{2}\tilde{\mathbf{M}}[-n] \cdot \begin{pmatrix} \hat{x}[n] \\ \hat{x}[\vec{n}] \end{pmatrix}, \quad \begin{pmatrix} \hat{x}[n] \\ \hat{x}[\vec{n}] \end{pmatrix} = \mathbf{M}[n] \cdot \begin{pmatrix} \hat{y}^0_{[1]}[n]_1 \\ \hat{y}^1_{[1]}[n]_1 \end{pmatrix} \tag{2.5}$$

where $\vec{n} = n + N/2$.

Please cite this article in press as: A. Averbuch et al., Analytic and directional wavelet packets in the space of periodic signals, Appl. Comput. Harmon. Anal. (2023), https://doi.org/10.1016/j.acha.2023.06.006

2.4. Extension of transforms to deeper decomposition levels

2.4.1. Second-level p-filter banks

The signals $\mathbf{y}^{\lambda}_{[1]},\ \lambda = 0, 1$, belong to the space $\Pi[N/2] \subset \Pi[N]$. The space $\Pi[N/2]$ can be split into mutually orthogonal subspaces, which we denote by $\Pi^0[N/2]$ and $\Pi^1[N/2]$, in a way that is similar to the split of the space $\Pi[N]$. Projection of a signal $\mathbf{Y} \in \Pi[N/2]$ onto these subspaces and the inverse operation are done using the analysis and synthesis p-filter banks $\tilde{\mathbf{H}}_{[2]} = \left\{\mathbf{h}^0_{[2]}, \mathbf{h}^1_{[2]}\right\} = \mathbf{H}_{[2]}$ (Eq. (2.6)), which operate in the space $\Pi[N/2]$. The frequency responses of the p-filters are

$$\hat{h}^0_{[2]}[n]_1 = \beta[2n] \quad \hat{h}^1_{[2]}[n]_1 = \alpha[2n], \tag{2.6}$$

where $\beta[n]$ and $\alpha[n]$ are defined in Eq. (2.3). The impulse responses of the p-filters $\mathbf{h}^0_{[2]}$ and $\mathbf{h}^1_{[2]}$ are orthogonal to each other in the space $\Pi[N/2]$ and their 2-sample shifts are mutually orthogonal

$$\sum_{k=0}^{N/2-1} h^{\lambda}_{[2]}[k-2l]\, h^{\mu}_{[2]}[k-2p] = \delta[\lambda-\mu]\,\delta[l-p], \quad \lambda, \mu = 0, 1.$$

The orthogonal projections of a signal $\mathbf{Y} \in \Pi[N/2]$ onto the subspaces $\Pi^0[N/2]$ and $\Pi^1[N/2]$ are

$$Y^{\mu}[k] = \sum_{l=0}^{N/4-1} y^{\mu}_{[2]}[l]\, h^{\mu}_{[2]}[k-2l], \quad y^{\mu}_{[2]}[l] = \sum_{k=0}^{N/2-1} h^{\mu}_{[2]}[k-2l] Y[k],$$

where $\mu = 0, 1$. The modulation matrices of the p-filter bank $\mathbf{H}_{[2]}$ are

$$\tilde{\mathbf{M}}_{[2]}[n] = \tilde{\mathbf{M}}[2n], \quad \mathbf{M}_{[2]}[n] = \mathbf{M}[2n], \tag{2.7}$$

where the modulation matrices $\tilde{\mathbf{M}}[n]$ and $\mathbf{M}[n]$ are defined in Eqs. (2.3) and (2.4), respectively.

2.4.2. Second-level WPTs

By the application of the analysis p-filter bank $\tilde{\mathbf{H}}_{[2]}$ (Section 2.4.1 and Eq. (2.6)) to the signals $y^{\lambda}_{[1]}[k] = \sum_{n=0}^{N-1} h^{\lambda}_{[1]}[n-2k]x[n],\ \mu,\ \lambda = 0, 1$, that belong to $\Pi[N/2]$, we get their orthogonal projections $\mathbf{y}^{\lambda,0}_{[1]}$ and $\mathbf{y}^{\lambda,1}_{[1]} \in \Pi[N/2]$ onto the subspaces $\Pi^0[N/2]$ and $\Pi^1[N/2]$:

$$\begin{aligned} y^{\lambda,\mu}_{[1]}[k] &= \sum_{l=0}^{N/4-1} y^{\rho}_{[2]}[l]\, h^{\mu}_{[2]}[k-2l], \quad y^{\rho}_{[2]}[l] = \sum_{k=0}^{N/2-1} h^{\mu}_{[2]}[k-2l]\, y^{\lambda}_{[1]}[k] \\ &= \sum_{k=0}^{N/2-1} h^{\mu}_{[2]}[k-2l] \sum_{n=0}^{N-1} h^{\lambda}_{[1]}[n-2k]x[n] = \sum_{n=0}^{N-1} x[n]\, \psi^{2r}_{[2],\rho}[n-4l], \\ \psi^{2r}_{[2],\rho}[n] &\stackrel{\text{def}}{=} \sum_{k=0}^{N/2-1} h^{\mu}_{[2]}[k]\, h^{\lambda}_{[1]}[n-2k] = \sum_{k=0}^{N/2-1} h^{\mu}_{[2]}[k]\, \psi^{2r}_{[1],\lambda}[n-2k]. \end{aligned}$$

where $\rho = \begin{cases} \mu, & \text{if } \lambda = 0; \\ 3-\mu, & \text{if } \lambda = 1. \end{cases}$

The signal $\psi^{2r}_{[2],\rho}$ is a linear combination of 2-sample shifts of the discrete-spline WP $\psi^{2r}_{[1],\lambda}$, therefore $\psi^{2r}_{[2],\rho} \in {}^{2r}\mathcal{S}^{\lambda}_{[1]} \subset \Pi[N]$. Its DFT is

Please cite this article in press as: A. Averbuch et al., Analytic and directional wavelet packets in the space of periodic signals, Appl. Comput. Harmon. Anal. (2023), https://doi.org/10.1016/j.acha.2023.06.006

$$\hat{\psi}^{2r}_{[2],\rho}[n] = \hat{\psi}^{2r}_{[1],\lambda}[n]\,\hat{h}^{\mu}_{[2]}[n]_1,$$
$$\hat{\psi}^{2r}_{[2],0}[n] = \frac{\cos^{2r}\frac{\pi n}{N}}{\sqrt{U^{4r}[n]}}\,\frac{\cos^{2r}\frac{2\pi n}{N}}{\sqrt{U^{4r}[2n]}}, \quad \hat{\psi}^{2r}_{[2],1}[n] = \frac{\cos^{2r}\frac{\pi n}{N}}{\sqrt{U^{4r}[n]}}\,\omega^{2n}\,\frac{\sin^{2r}\frac{2\pi n}{N}}{\sqrt{U^{4r}[2n]}}, \tag{2.8}$$
$$\hat{\psi}^{2r}_{[2],2}[n] = \omega^{n}\,\frac{\sin^{2r}\frac{\pi n}{N}}{\sqrt{U^{4r}[n]}}\,\omega^{2n}\,\frac{\sin^{2r}\frac{2\pi n}{N}}{\sqrt{U^{4r}[2n]}}, \quad \hat{\psi}^{2r}_{[2],3}[n] = w^{n}\,\frac{\sin^{2r}\frac{\pi n}{N}}{\sqrt{U^{4r}[n]}}\,\frac{\cos^{2r}\frac{2\pi n}{N}}{\sqrt{U^{4r}[2n]}}.$$

Remark 2.2. It is seen from Eq. (2.8) that the magnitude DFT spectra $\left|\hat{\psi}^{2r}_{[2],0}[n]\right| = \begin{cases} 2, & \text{if } n = 0; \\ 0, & \text{if } n = N/2, \end{cases}$ and $\left|\hat{\psi}^{2r}_{[2],3}[n]\right| = \begin{cases} 2, & \text{if } n = N/2; \\ 0, & \text{if } n = 0. \end{cases}$ The DFTs $\hat{\psi}^{2r}_{[2],1}[n]$ and $\hat{\psi}^{2r}_{[2],2}[n]$ are zeros as $n = 0$ and $n = N/2$.

Proposition 2.3 *([4]). The norms of the signals $\psi^{2r}_{[2],\rho} \in \Pi[N]$ are equal to one. The 4-sample shifts $\left\{\psi^{2r}_{[2],\rho}[\cdot - 4l]\right\}$, $l = 0, ..., N/4 - 1$, of this signal are mutually orthogonal and signals with different indices ρ are orthogonal to each other.*

Thus, the signal space $\Pi[N]$ splits into four mutually orthogonal subspaces $\Pi[N] = \bigoplus_{\rho=0}^{3} {}^{2r}\mathcal{S}^{\rho}_{[2]}$ whose orthonormal bases are formed by 4-sample shifts $\left\{\psi^{2r}_{[2],\rho}[\cdot - 4l]\right\}$, $l = 0, ..., N/4 - 1$, of the signals $\psi^{2r}_{[2],\rho}$, which are referred to as the second-level discrete-spline wavelet packets of order $2r$.

The orthogonal projection of a signal $\mathbf{x} \in \Pi[N]$ onto the subspace ${}^{2r}\mathcal{S}^{\rho}_{[2]}$ is the signal

$$x^{\rho}_{[2]}[k] = \sum_{l=0}^{N/4-1} \left\langle \mathbf{x},\, \psi^{2r}_{[2],\rho}[\cdot - 4l] \right\rangle \psi^{2r}_{[2],\rho}[k - 4l] = \sum_{l=0}^{N/4-1} y^{\rho}_{[2]}[l]\,\psi^{2r}_{[2],\rho}[k - 4l], \quad k = 0, \ldots, N-1.$$

Practically, derivation of the wavelet packet transform coefficients $\mathbf{y}^{\lambda}_{[1]}$, $\lambda = 0, 1$, from $\mathbf{x}$ and the inverse operation are implemented using Eq. (2.5), while the transform $\mathbf{y}^{\lambda}_{[1]} \longleftrightarrow \mathbf{y}^{\rho}_{[2]}$ are implemented similarly using the modulation matrices of the p-filter bank $\mathbf{H}_{[2]}$ defined in Eq. (2.7). The second-level wavelet packets $\psi^{2r}_{[2],\rho}$ are derived from the first-level wavelet packets $\psi^{2r}_{[1],\lambda}$ by filtering the latter with the p-filters $\mathbf{h}^{\mu}_{[2]}$, $\lambda, \mu = 0, 1$, $\rho = \begin{cases} \mu, & \text{if } \lambda = 0; \\ 3 - \mu, & \text{if } \lambda = 1. \end{cases}$.

Fig. 2.2 displays the second-level wavelet packets originating from discrete splines of orders 2, 6 and 10 and their DFTs. One can observe that the wavelet packets are symmetric and well localized in time domain. Their spectra are flat and their shapes tend to rectangular as their orders increase. They split the frequency domain into four quarter-bands.

2.4.3. Transforms to deeper levels

The WPTs to deeper decomposition levels are implemented iteratively, while the transform coefficients $\left\{\mathbf{y}^{\rho}_{[m+1]}\right\}$ are derived by filtering the coefficients $\left\{\mathbf{y}^{\lambda}_{[m]}\right\}$ with the p-filters $\mathbf{h}^{\mu}_{[m+1]}$, where $\lambda = 0, ..., 2^m - 1$, $\mu = 0, 1$ and $\rho = \begin{cases} 2\lambda + \mu, & \text{if } \lambda \text{ is even}; \\ 2\lambda + (1 - \mu), & \text{if } \lambda \text{ is odd}. \end{cases}$ The transform coefficients are $y^{\lambda}_{[m]}[l] = \left\langle \mathbf{x}, \psi^{2r}_{[m],\lambda}[\cdot, -2^m l] \right\rangle$, where the signals $\psi^{2r}_{[m],\lambda}$ are normalized, orthogonal to each other in the space $\Pi[N]$, and their $2^m l$-sample shifts are mutually orthogonal. They are referred to as level-m discrete-spline wavelet packets of order $2r$. The set $\left\{\psi^{2r}_{[m],\lambda}[\cdot, -2^m l]\right\}$, $\lambda = 0, ..., 2^m - 1$, $l = 0, ...N/2^m - 1$, constitutes an orthonormal basis of the space $\Pi[N]$ and generates its split into 2^m orthogonal subspaces. The next-level wavelet packets $\psi^{2r}_{[m+1],\rho}$ are derived by filtering the wavelet packets $\psi^{2r}_{[m],\lambda}$ with the p-filters $\mathbf{h}^{\mu}_{[m+1]}$ such that

Please cite this article in press as: A. Averbuch et al., Analytic and directional wavelet packets in the space of periodic signals, Appl. Comput. Harmon. Anal. (2023), https://doi.org/10.1016/j.acha.2023.06.006

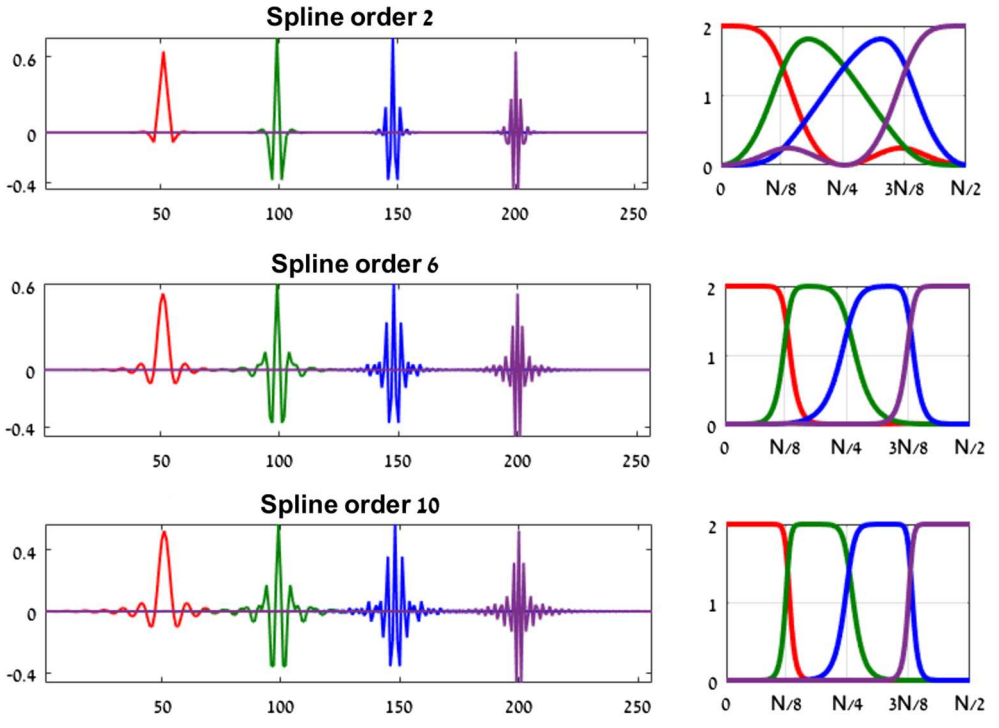

Fig. 2.2. Left: second-level discrete-spline wavelet packets of different orders; left to right: $\psi^{2r}_{[2],0} \to \psi^{2r}_{[2],1} \to \psi^{2r}_{[2],2} \to \psi^{2r}_{[2],3}$. Right: magnitude DFT spectra of these wavelet packets.

$$\psi^{2r}_{[m+1],\rho}[n] = \sum_{k=0}^{N/2^m-1} h^{\mu}_{[m+1]}[k]\, \psi^{2r}_{[m],\lambda}[n-2^m k], \quad \hat{\psi}^{2r}_{[m+1],\rho}[n] = \hat{\psi}^{2r}_{[m],\lambda}[n]\, \hat{h}^{\mu}_{[m+1]}[n]_m. \tag{2.9}$$

Proposition 2.4. *For any* $M \in \mathbb{N}$

1. *the DFTs* $\hat{\psi}^{2r}_{[M],0}[0] \neq 0$ *and* $\hat{\psi}^{2r}_{[M],2^M-1}[N/2] \neq 0$*;*
2. *The DFTs of the wavelet packets* $\left\{\hat{\psi}^{2r}_{[M],l}[n]\right\}$, $l = 1, ..., 2^m - 1$ *are zero when* $n = 0$*. The DFTs of the wavelet packets* $\left\{\hat{\psi}^{2r}_{[M],l}[n]\right\}$, $l = 0, ..., 2^m - 2$*, are zero when* $n = N/2$*.*

Proof. Note that the frequency response of an m-level p-filter is $\hat{h}^{\mu}_{[m]}[n] = \hat{h}^{\mu}_{[1]}[2^{m-1}n]$, $\mu = 0, 1$. The claims are true for $M = 1$, 2. Assume that it holds for $M = m$.

1. Then, due to Eq. (2.9),

$$\hat{\psi}^{2r}_{[m+1],0}[0] = \hat{\psi}^{2r}_{[m],0}[0]\, \hat{h}^{0}_{[m+1]}[n]_m = \hat{\psi}^{2r}_{[m],0}[0]\, \frac{\cos^{2r}\frac{2^m \pi\, n}{N}}{\sqrt{U^{4r}[2^m n]}} \neq 0 \quad \text{as } n = 0.$$

   If $\lambda = 2^m - 1$ and $\rho = 2^{m+1} - 1$ then $\mu = 0$ and we apply the filter $h^{0}_{[m+1]}[k]$. Hence, we have

$$\hat{\psi}^{2r}_{[m+1],2^{m+1}-1}[N/2] = \hat{\psi}^{2r}_{[m],2^m-1}[N/2]\, \frac{\cos^{2r}(2^{m-1}\pi)}{\sqrt{U^{4r}[2^m n]}} \neq 0.$$

2. Equation (2.9) implies that if $\hat{\psi}^{2r}_{[m],\lambda}[n] = 0$ with either $n = 0$ or $n = N/2$ then both $\hat{\psi}^{2r}_{[m+1],\rho}[n]$, $\rho = 2\lambda$, $2\lambda + 1$, has the same property. If $\lambda = 0$ then

Please cite this article in press as: A. Averbuch et al., Analytic and directional wavelet packets in the space of periodic signals, Appl. Comput. Harmon. Anal. (2023), https://doi.org/10.1016/j.acha.2023.06.006

$$\hat{\psi}^{2r}_{[m+1],1}[0] = \hat{\psi}^{2r}_{[m],0}[0]\,\hat{h}^{1}_{[m+1]}[n]_m = \hat{\psi}^{2r}_{[m],0}[0]\,\frac{\sin^{2r}\frac{2^m\pi\,n}{N}}{\sqrt{U^{4r}[2^m n]}} = 0 \quad \text{as } n = 0.$$

Similarly we can establish that $\hat{\psi}^{2r}_{[m+1],2^{m+1}-2}[N/2] = 0$. □

A scheme of fast implementation of the discrete-spline-based WPT is described in [4]. The transforms are executed in the spectral domain using the Fast Fourier transform (FFT) by the application of critically sampled two-channel filter banks to the half-band spectral components of a signal. For example, the Matlab execution of the 8-level 12-th-order WPT of a signal comprising 245760 samples, takes 0.2324 seconds.

2.5. 2D WPTs

A standard way to extend the one-dimensional (1D) WPTs to multiple dimensions is the tensor-product extension. The 2D one-level WPT of a signal $\mathbf{x} = \{x[k,n]\}\,,\ k,n = 0,...,N-1$, which belongs to $\Pi[N,N]$, consists of the application of 1D WPT to columns of $\mathbf{x}$, which is followed by the application of the transform to rows of the coefficients array. As a result of the 2D WPT of signals from $\Pi[N,N]$, the space becomes split into four mutually orthogonal subspaces $\Pi[N,N] = \bigoplus_{j,l=0}^{1} {}^{2r}\mathcal{S}^{j,l}_{[1]}$.

The subspace ${}^{2r}\mathcal{S}^{j,l}_{[1]}$ is a linear hull of two-sample shifts of the 2D wavelet packets $\left\{\psi^{2r}_{[1],j,l}[k-2p,n-2t]\right\},\ p,t,= 0,...,N/2-1$, that form an orthonormal basis of ${}^{2r}\mathcal{S}^{j,l}_{[1]}$. The orthogonal projection of the signal $\mathbf{x} \in \Pi[N,N]$ onto the subspace ${}^{2r}\mathcal{S}^{j,l}_{[1]}$ is the signal $\mathbf{x}^{j,l}_{[1]} \in \Pi[N,N]$ such that

$$x^{j,l}_{[1]}[k,n] = \sum_{p,t=0}^{N/2-1} y^{j,l}_{[1]}[p,t]\,\psi^{2r}_{[1],j,l}[k-2p,n-2t], \quad j,l = 0,1,$$

The 2D wavelet packets are $\psi^{2r}_{[1],j,l}[n,m] \stackrel{\text{def}}{=} \psi^{2r}_{[1],j}[n]\,\psi^{2r}_{[1],l}[m], \quad j,l = 0,1$. They are normalized and orthogonal to each other in the space $\Pi[N,N]$. It means that $\sum_{n,m=0}^{N-1}\psi^{2r}_{[1],j1,l1}[n,m]\,\psi^{2r}_{[1],j2,l2}[n,m] = \delta[j1-j2]\,\delta[l1-l2]$. Their two-sample shifts in either direction are mutually orthogonal. The transform coefficients are

$$y^{j,l}_{[1]}[p,t] = \left\langle \mathbf{x}, \psi^{2r}_{[1],j,l}[\cdot-2p,\cdot-2t]\right\rangle = \sum_{n,m=0}^{N-1}\psi^{2r}_{[1],j,l}[n-2p,m-2t]\,x[n,m].$$

By the application of the above transforms iteratively to blocks of the transform coefficients down to m-th level, we get that the space $\Pi[N,N]$ is decomposed into 4^m mutually orthogonal subspaces $\Pi[N,N] = \bigoplus_{j,l=0}^{2^m-1} {}^{2r}\mathcal{S}^{j,l}_{[m]}$. The orthogonal projection of the signal $\mathbf{x} \in \Pi[N,N]$ onto the subspace ${}^{2r}\mathcal{S}^{j,l}_{[m]}$ is the signal $\mathbf{x}^{j,l}_{[m]} \in \Pi[N,N]$ such that

$$x^{j,l}_{[m]}[k,l] = \sum_{p,t=0}^{N/2^m-1} y^{j,l}_{[m]}[p,t]\,\psi^{2r}_{[m],j,l}[k-2^m p,l-2^m t], \quad j,l = 0,...,2^m-1,$$

$$\psi^{2r}_{[m],j,l}[k,n] = \psi^{2r}_{[m],j}[k]\,\psi^{2r}_{[m],l}[n], \quad y^{j,l}_{[m]}[p,t] = \left\langle \mathbf{x}, \psi^{2r}_{[m],j,l}[\cdot-2^m p,\cdot-2^m t]\right\rangle.$$

The 2D tensor-product wavelet packets $\psi^{2r}_{[m],j,l}$ are well localized in the spatial domain, their 2D DFT spectra are flat and provide a refined split of the frequency domain of signals from $\Pi[N,N]$.[1] The drawback is that the wavelet packets are oriented in either horizontal or vertical directions or are not oriented at all.

[1] Especially it is true for WPs derived from higher-order discrete splines.

Please cite this article in press as: A. Averbuch et al., Analytic and directional wavelet packets in the space of periodic signals, Appl. Comput. Harmon. Anal. (2023), https://doi.org/10.1016/j.acha.2023.06.006

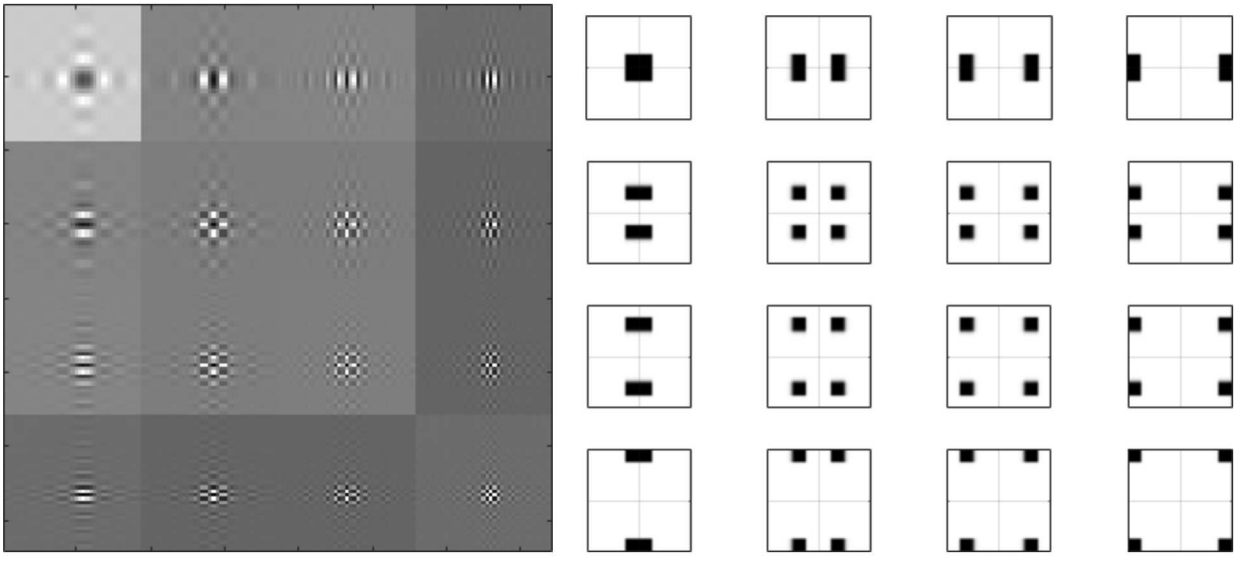

Fig. 2.3. WPs from the second decomposition level (left) and their magnitude spectra (right).

Fig. 2.3 displays the tenth-order 2D wavelet packets from the second decomposition level and their magnitude spectra.

3. (Quasi-)analytic and complementary WPs

In this section we define analytic and the so-called quasi-analytic WPs related to the discrete-spline-based WPs discussed in Section 2 and introduce an orthonormal set of waveforms which are complementary to the above WPs.

3.1. Analytic periodic signals

A real-valued N-periodic signal $\mathbf{x} \in \Pi[N]$ is represented by its inverse DFT. Then, Eq. (1.2) can be written as follows:

$$x[k] = \frac{\hat{x}[0] + (-1)^k \hat{x}[N/2]}{N} + \frac{2}{N} \sum_{n=1}^{N/2-1} \frac{\hat{x}[n]\,\omega^{kn} + (\hat{x}[n]\,\omega^{kn})^*}{2}.$$

Define the real-valued signal $\mathbf{h} \in \Pi[N]$ and two complex-valued signals $\bar{\mathbf{x}}_+$ and $\bar{\mathbf{x}}_-$ such that

$$\begin{aligned} h[k] &\stackrel{\text{def}}{=} \tfrac{2}{N} \textstyle\sum_{n=1}^{N/2-1} \frac{\hat{x}[n]\,\omega^{kn} - \hat{x}[n]^*\,\omega^{-kn}}{2i}, \\ \bar{x}_\pm[k] &\stackrel{\text{def}}{=} x[k] \pm i h[k] = \tfrac{\hat{x}[0] + (-1)^k \hat{x}[N/2]}{N} \\ &\quad + \tfrac{2}{N} \textstyle\sum_{n=1}^{N/2-1} \begin{cases} \hat{x}[n]\,\omega^{kn}, & \text{for } \bar{x}_+; \\ \hat{x}[n]^*\,\omega^{-kn} = \hat{x}[N-n]\,\omega^{-k(N-n)}, & \text{for } \bar{x}_-. \end{cases} \end{aligned} \tag{3.1}$$

Please cite this article in press as: A. Averbuch et al., Analytic and directional wavelet packets in the space of periodic signals, Appl. Comput. Harmon. Anal. (2023), https://doi.org/10.1016/j.acha.2023.06.006

The signals' $\bar{\mathbf{x}}_{\pm}$ DFT spectra are

$$\hat{\bar{x}}_{+}[n] = \begin{cases} \hat{x}[n], & \text{if } n = 0, \text{ or } n = N/2\ ; \\ 2\hat{x}[n], & \text{if } 0 < n < N/2; \\ 0, & \text{if } -N/2 < n < 0 \Longleftrightarrow N/2 < n < N, \end{cases}$$
$$\hat{\bar{x}}_{-}[n] = \begin{cases} \hat{x}[n], & \text{if } n = 0, \text{ or } n = N/2\ ; \\ 2\hat{x}[n], & \text{if } -N/2 < n < 0 \Longleftrightarrow N/2 < n < N; \\ 0, & \text{if } n = 0, \text{ or } n = N/2. \end{cases} \tag{3.2}$$

The spectrum of $\bar{\mathbf{x}}_{+}$ comprises only non-negative frequencies and vice versa for $\bar{\mathbf{x}}_{-}$. $\mathbf{x} = \mathfrak{Re}(\bar{\mathbf{x}}_{\pm})$ and $\mathfrak{Im}(\bar{\mathbf{x}}_{\pm}) = \pm\mathbf{h}$. The signals $\bar{\mathbf{x}}_{\pm}$ are referred to as periodic analytic signals.

The signal's $\mathbf{h}$ DFT spectrum is

$$\hat{h}[n] = \begin{cases} -i\,\hat{x}[n], & \text{if } 0 < n < N/2; \\ i\,\hat{x}[n], & \text{if } -N/2 < n < 0 \Longleftrightarrow N/2 < n < N; \\ 0, & \text{if } n = 0, \text{ or } n = N/2. \end{cases}$$

Thus, the signal $\mathbf{h}$ where $\mathbf{h} = H(\mathbf{x})$ can be regarded as the Hilbert transform (HT) of a discrete-time periodic signal $\mathbf{x}$, (see [34], for example).

Proposition 3.1.

1. *The operator $H(\cdot)$ of the HT $\mathbf{h} = H(\mathbf{x})$ is cyclic-invariant in the space $\Pi[N]$. That means that for a circular m-sample shift $\tilde{\mathbf{h}} = \mathbf{h}[\cdot + m]$ is the HT of $\tilde{\mathbf{x}} = \mathbf{x}[\cdot + m]$.*
2. *If the signal $\mathbf{x} \in \Pi[N]$ is symmetric about a grid point $k = K$ then $\mathbf{h} = H(\mathbf{x})$ is antisymmetric about* K *and $h[K] = 0$.*
3. *Assume that a signal $\mathbf{x} \in \Pi[N]$ and $\hat{x}[0] = \hat{x}[N/2] = 0$. Then,*
   (a) *The norm of its HT is $\|H(\mathbf{x})\| = \|\mathbf{x}\|$.*
   (b) *Magnitude spectra of the signals $\mathbf{x}$ and $\mathbf{h} = H(\mathbf{x})$ coincide.*

Proof. 1. The DFT of the signal $\tilde{\mathbf{x}}$ is $\hat{\tilde{x}}[n] = \omega^{mn}\,\hat{x}[n]$. Denote by $\bar{\tilde{\mathbf{x}}}_{+}$ the analytic signal related to $\tilde{\mathbf{x}}$. Equation (3.2) implies that $\hat{\bar{\tilde{x}}}_{+}[n] = \omega^{mn}\,\hat{\bar{x}}[n]$. Consequently, $\bar{\tilde{x}}_{+}[k] = \bar{x}_{+}[k + m]$. The same relation holds for $\tilde{\mathbf{h}} = \mathfrak{Im}(\bar{\tilde{\mathbf{x}}})$.

2. Assume that $\mathbf{x} \in \Pi[N]$ is symmetric about $K = 0$. Then, its DFT obeys

$$\hat{x}[n] = x[0] + (-1)^n x[N/2] + 2\sum_{k=1}^{N/2-1} x[k]\,\cos(2\pi kn/N) = \hat{x}[-n].$$

   Then, due to Eq. (3.1), $h[k] = 2/N\sum_{n=1}^{N/2-1} x[n]\sin(2\pi kn/N) = h[-k]$ and $h[0] = 0$. Extension of the proof to $K \neq 0$ is straightforward.

3. If $\hat{x}[0] = \hat{x}[N/2] = 0$ then $x[k] = \frac{1}{N}\sum_{n=1}^{N/2-1}\left(\hat{x}[n]\,\omega^{kn} + (\hat{x}[n]\,\omega^{kn})^*\right)$. In that case we have
   (a) The squared norm is $\|\mathbf{h}\|^2 = \frac{1}{N}\sum_{n=-N/2}^{N/2-1}|\hat{h}[n]|^2 = \frac{1}{N}\sum_{n=-N/2}^{N/2-1}|\hat{x}[n]|^2$.
   (b) The coincidence of the magnitude spectra is straightforward. □

Please cite this article in press as: A. Averbuch et al., Analytic and directional wavelet packets in the space of periodic signals, Appl. Comput. Harmon. Anal. (2023), https://doi.org/10.1016/j.acha.2023.06.006

3.2. Analytic WPs

The analytic spline-based WPs and their DFT spectra are derived from the corresponding WPs $\left\{\psi^{2r}_{[m],l}\right\}$, $m = 1, ..., M$, $l = 0, ..., 2^m - 1$, in line with the scheme in Section 3.1. Recall that for all $l \neq 0$, the DFT $\hat{\psi}^{2r}_{[m],l}[0] = 0$ and for all $l \neq 2^m - 1$, the DFT $\hat{\psi}^{2r}_{[m],l}[N/2] = 0$.

Denote by $\theta^{2r}_{[m],l} = H(\psi^{2r}_{[m],l})$ the discrete periodic HT of the wavelet packet $\psi^{2r}_{[m],l}$, such that the DFT is

$$\hat{\theta}^{2r}_{[m],l}[n] = \begin{cases} -i\,\hat{\psi}^{2r}_{[m],l}[n], & \text{if } 0 < n < N/2; \\ i\,\hat{\psi}^{2r}_{[m],l}, & \text{if } -N/2 < n < 0; \\ 0, & \text{if } n = 0, \text{ or } n = N/2\ . \end{cases}$$

Then, the corresponding analytic WPs are

$$\bar{\psi}^{2r}_{\pm[m],l} = \psi^{2r}_{[m],l} \pm i\theta^{2r}_{[m],l}.$$

Properties of the analytic WPs

1. The DFT spectra of the analytic WPs $\bar{\psi}^{2r}_{+[m],l}$ and $\bar{\psi}^{2r}_{-[m],l}$ are located within the bands $[0, N/2]$ and $[N/2, N] \Longleftrightarrow [-N/2, 0]$, respectively.
2. The real component $\psi^{2r}_{[m],l}$ is the same for both WPs $\bar{\psi}^{2r}_{\pm[m],l}$. It is a symmetric oscillating waveform.
3. The HT WPs $\theta^{2r}_{[m],l} = H(\psi^{2r}_{[m],l})$ are antisymmetric oscillating waveforms.
4. For all $l \neq 0$, $2^m - 1$, the norms $\left\|\theta^{2r}_{[m],l}\right\| = 1$. Their magnitude spectra $\left|\hat{\theta}^{2r}_{[m],l}[n]\right|$ coincide with the magnitude spectra of the respective WPs $\psi^{2r}_{[m],l}$.
5. When $l = 0$ or $l = 2^m - 1$, the magnitude spectra of $\theta^{2r}_{[m],l}$ coincide with that of $\psi^{2r}_{[m],l}$ everywhere except for the points $n = 0$ or $N/2$, respectively, and the waveforms' norms are no longer equal to 1.

Properties in items 3–5 follow directly from Proposition 3.1.

Remark 3.1. Comment on Property 5: The DFT of the HT signal $\hat{\theta}^{2r}_{[m],0}[0] = 0$ while Proposition 2.4 implies that $\hat{\psi}^{2r}_{[m],0}[0] \neq 0$. Therefore, as in the proof of Proposition 3.1, we have

$$\|\theta^{2r}_{[m],0}\|^2 = \frac{1}{N}\sum_{n=-N/2}^{N/2-1} |\hat{\theta^{2r}_{[m],0}}[n]|^2 = \frac{1}{N}\left(\sum_{n=-N/2}^{N/2-1} |\hat{\psi}^{2r}_{[m],0}[n]|^2 - |\hat{\psi}^{2r}_{[m],0}[0]|^2\right) = 1 - \frac{1}{N}|\hat{\psi}^{2r}_{[m],0}[0]|^2.$$

Similarly we have $\|\theta^{2r}_{[m],2^m-1}\|^2 \neq 1$.

Proposition 3.2. *For all $l \neq 0$, $2^m - 1$, the shifts of the HT WPs $\left\{\theta^{2r}_{[m],l}[\cdot - 2^m k]\right\}$ are orthogonal to each other in the space $\Pi[N]$. The orthogonality does not take place for $\theta^{2r}_{[m],0}$ and $\theta^{2r}_{[m],2^m-1}$.*

Proof. For all $l \neq 0$, $2^m - 1$, the inner product is

$$\left\langle \theta^{2r}_{[m],l}, \theta^{2r}_{[m],l}[\cdot - 2^m k]\right\rangle = \frac{1}{N}\sum_{n=-N/2}^{N/2-1} \omega^{2^m kn}\left|\hat{\theta}^{2r}_{[m],l}[n]\right|^2$$

$$= \frac{1}{N}\sum_{n=-N/2}^{N/2-1} \omega^{2^m kn}\left|\hat{\psi}^{2r}_{[m],l}[n]\right|^2 = \left\langle \psi^{2r}_{[m],l}, \psi^{2r}_{[m],l}[\cdot - 2^m l]\right\rangle = 0.$$

Please cite this article in press as: A. Averbuch et al., Analytic and directional wavelet packets in the space of periodic signals, Appl. Comput. Harmon. Anal. (2023), https://doi.org/10.1016/j.acha.2023.06.006

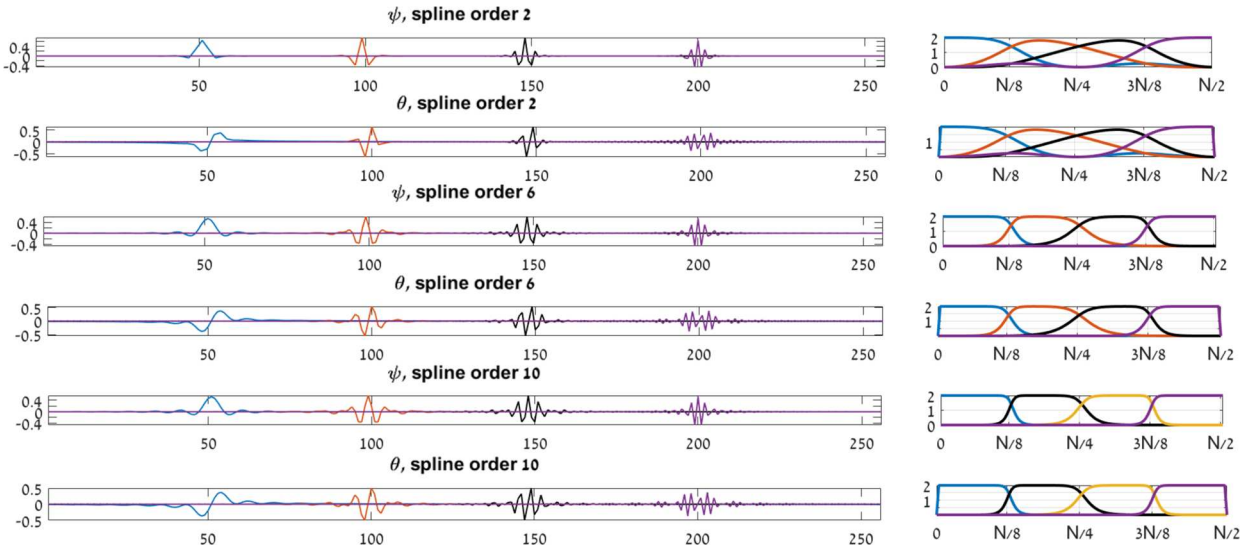

Fig. 3.1. WPs $\psi^{2r}_{[2],l}$ (first, third and fifth from the top left frames) and $\theta^{2r}_{[2],l}$ (second, fourth and sixth from the top left frames) from the second decomposition level and their magnitude spectra, respectively (right frames).

If $l = 0$, we have

$$\left\langle \theta^{2r}_{[m],0}, \theta^{2r}_{[m],0}[\cdot - 2^m k] \right\rangle = \frac{1}{N} \sum_{n=-N/2}^{N/2-1} \omega^{2^m kn} \left| \hat{\psi}^{2r}_{[m],0}[n] \right|^2 - \frac{1}{N} |\hat{\psi}^{2r}_{[m],0}[0]|^2 = -\frac{1}{N} |\hat{\psi}^{2r}_{[m],0}[0]|^2 \neq 0.$$

Similarly we have $\left\langle \theta^{2r}_{[m],2^m-1}, \theta^{2r}_{[m],2^m-1}[\cdot - 2^m k] \right\rangle \neq 0$. □

Fig. 3.1 displays the wavelet packets $\psi^{2r}_{[2],l}$ and $\theta^{2r}_{[2],l}$, $r = 1, 3, 5$, $l = 0, 1, 2, 3$, and their magnitude spectra.

3.3. Complementary set of wavelet packets and quasi-analytic WPs

3.3.1. Complementary orthonormal WPs

The discrete-spline-based WPs $\left\{\psi^{2r}_{[m],l}\right\}$ are normalized and their 2^m-sample shifts are mutually orthogonal. Combinations of shifts of several wavelet packets can form orthonormal bases for the signal space $\Pi[N]$. On the other hand, it is not true for the set $\left\{\theta^{2r}_{[m],l}\right\}$, $l = 0, ...2^m - 1$, of the antisymmetric waveforms, which are the HTs of the WPs $\left\{\psi^{2r}_{[m],l}\right\}$. At the decomposition level m, the waveforms $\left\{\theta^{2r}_{[m],l}\right\}$, $l = 1, ...2^m - 2$, are normalized and their 2^m-sample shifts are mutually orthogonal, but the norms of the waveforms $\theta^{2r}_{[m],0}$ and $\theta^{2r}_{[m],2^m-1}$ are close but not equal to 1 and their shifts are not mutually orthogonal. It happens because the values $\hat{\theta}^{2r}_{[m],j}[0]$ and $\hat{\theta}^{2r}_{[m],j}[N/2]$ are missing in their DFT spectra.[2] Keeping this in mind, we upgrade the set $\left\{\theta^{2r}_{[m],l}\right\}$, $l = 0, ...2^m - 1$ in the following way.

Define a set $\left\{\varphi^{2r}_{[m],l}\right\}$, $m = 1, ..., M$, $l = 0, ..., 2^m - 1$, of signals from the space $\Pi[N]$ via their DFTs:

$$\hat{\varphi}^{2r}_{[m],l}[n] = \begin{cases} -i\,\hat{\psi}^{2r}_{[m],l}[n], & \text{if } 0 < n < N/2; \\ i\,\hat{\psi}^{2r}_{[m],l}[n], & \text{if } -N/2 < n < 0\ ; \\ \hat{\psi}^{2r}_{[m],l}[n], & \text{if } n = 0, \text{ or } n = N/2. \end{cases} \tag{3.3}$$

[2] Recall that these values are real.

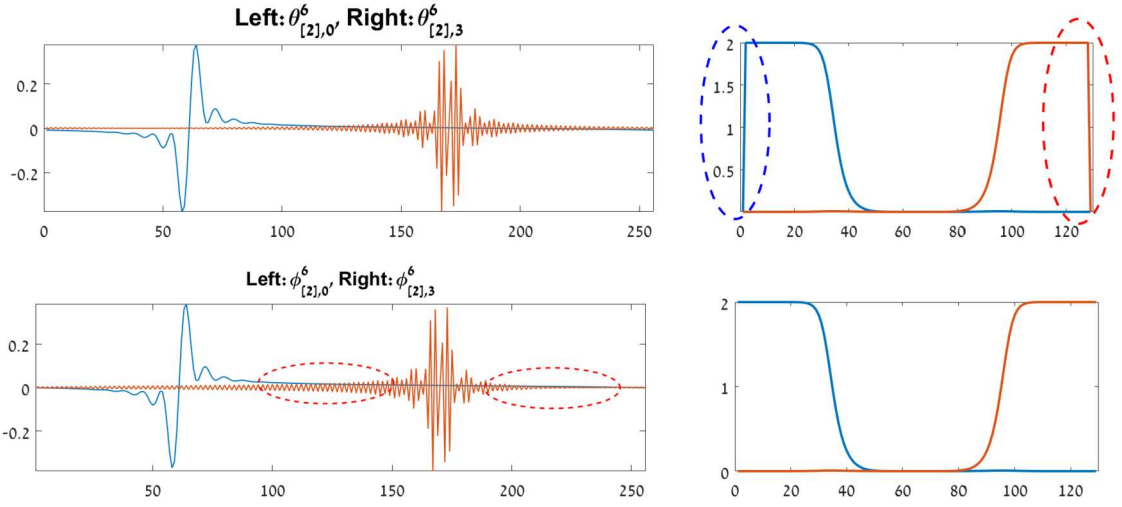

Fig. 3.2. Left: signals $\theta^6_{[2],l},\ l=0,3$ (top), and $\varphi^6_{[2],l},\ l=0,3$ (bottom). Right: their magnitude DFT spectra, respectively.

For all $l \neq 0, 2^m-1$, the signals $\varphi^{2r}_{[m],l}$ coincide with $\theta^{2r}_{[m],l} = H(\psi^{2r}_{[m],l})$.

Proposition 3.3.

- *The magnitude spectra* $\left|\hat{\varphi}^{2r}_{[m],l}[n]\right|$ *coincide with the magnitude spectra of the respective WPs* $\psi^{2r}_{[m],l}$.
- *For any* $m=1,...,M$, *and* $l=1,...,2^m-2$, *the signals* $\varphi^{2r}_{[m],l}$ *are antisymmetric oscillating waveforms. For* $l=0$ *and* $l=2^m-1$, *the shapes of the signals slightly deviate from the antisymmetry.*
- *The orthonormality properties that are similar to the properties of WPs* $\psi^{2r}_{[m],l}$ *hold for the signals* $\varphi^{2r}_{[m],l}$ *such that*

$$\left\langle \varphi^{2r}_{[m],l}[\cdot - p\,2^m], \varphi^{2r}_{[m],\lambda}[\cdot - s\,2^m] \right\rangle = \delta[\lambda,l]\,\delta[p,s].$$

The proof of Proposition 3.3 is similar to the proof of Proposition 3.2.

Fig. 3.2 displays the signals $\theta^6_{[2],l},\ l=0,3$ and $\varphi^6_{[2],l},\ l=0,3$, from the second decomposition level and their magnitude spectra. Lack of the values $\hat{\theta}^{2r}_{[m],j}[0]$ and $\hat{\theta}^{2r}_{[m],j}[N/2]$ in the DFTs of $\theta^6_{[2],l},\ l=0,3$, are seen. Addition of $\hat{\psi}^{2r}_{[m],j}[0]$ and $\hat{\psi}^{2r}_{[m],j}[N/2]$ to the above spectra results in the antisymmetry distortion.

We call the signals $\left\{\varphi^{2r}_{[m],l}\right\},\ m=1,...,M,\ l=0,...,2^m-1$, the *complementary wavelet packets* (cWPs). Similarly to the WPs $\left\{\psi^{2r}_{[m],l}\right\}$, different combinations of the cWPs can provide different orthonormal bases for the space $\Pi[N]$. These can be, for example, the wavelet bases

$$\left\{\bigoplus_{r=0}^{N/2^M} \varphi^{2r}_{[M],0}[\cdot - r\,2^M]\right\} \bigoplus_{m=1}^{M} \left\{\bigoplus_{r=0}^{N/2^m} \varphi^{2r}_{[m],1}[\cdot - r\,2^m]\right\}.$$

or a Best Basis [14] type.

3.3.2. Quasi-analytic WPs

The sets of complex-valued WPs, which we refer to as the quasi-analytic wavelet packets (qWP), are defined as

$$\Psi^{2r}_{\pm[m],l} = \psi^{2r}_{[m],l} \pm i\varphi^{2r}_{[m],l}, \quad m=1,...,M,\ l=0,...,2^m-1,$$

where $\varphi^{2r}_{[m],l}$ are the cWPs defined in Eq. (3.3). The qWPs $\Psi^{2r}_{\pm[m],l}$ differ from the analytic WPs $\bar{\psi}^{2r}_{\pm[m],l}$ by the addition of the two values $\pm i\,\hat{\psi}^{2r}_{[m],l}[0]$ and $\pm i\,\hat{\psi}^{2r}_{[m],l}[N/2]$ into their DFT spectra, respectively. For a given decomposition level m, these values are zero for all l except for $l_0 = 0$ and $l_m = 2^m - 1$ (see Proposition 2.4). It means that for all l except for l_0 and l_m, the qWPs $\Psi^{2r}_{\pm[m],l}$ are analytic. The DFTs of qWPs are

$$\hat{\Psi}^{2r}_{+[m],l}[n] = \begin{cases} (1+i)\hat{\psi}^{2r}_{[m],l}[n], & \text{if } n = 0 \text{ or } n = N/2; \\ 2\hat{\psi}^{2r}_{[m],l}[n], & \text{if } 0 < n < N/2; \\ 0 & \text{if } N/2 < n < N, \end{cases} \tag{3.4}$$

$$\hat{\Psi}^{2r}_{-[m],l}[n] = \begin{cases} (1-i)\hat{\psi}^{2r}_{[m],l}[n], & \text{if } n = 0 \text{ or } n = N/2; \\ 0 & \text{if } 0 < n < N/2; \\ 2\hat{\psi}^{2r}_{[m],l}[n], & \text{if } N/2 < n < N. \end{cases}$$

3.3.3. Design of cWPs and qWPs

The DFTs of the first-level WPs are

$$\hat{\psi}^{2r}_{[1],0}[n] = \frac{\cos^{2r}\frac{\pi n}{N}}{\sqrt{U^{4r}[n]}} = \beta[n], \quad \hat{\psi}^{2r}_{[1],1}[n] = \frac{\omega^n \sin^{2r}\frac{\pi n}{N}}{\sqrt{U^{4r}[n]}} = \alpha[n],$$

where the sequence $U^{4r}[n]$ is defined in Eq. (1.3). Consequently, the DFTs of the first-level cWPs are

$$\hat{\varphi}^{2r}_{[1],0}[n] = \begin{cases} -i\,\beta[n], & \text{if } 0 < n < N/2; \\ i\,\beta[n], & \text{if } N/2 < n < N; \\ \sqrt{2}, & \text{if } n = 0; \\ 0, & \text{if } n = N/2, \end{cases} \quad \hat{\varphi}^{2r}_{[1],1}[n] = \begin{cases} -i\,\alpha[n], & \text{if } 0 < n < N/2; \\ i\,\alpha[n], & \text{if } N/2 < n < N; \\ 0, & \text{if } n = 0; \\ -\sqrt{2}, & \text{if } n = N/2. \end{cases} \tag{3.5}$$

Due to Eq. (2.8), the DFT of the second-level WPs are

$$\hat{\psi}^{2r}_{[2],\rho}[n] = \hat{\psi}^{2r}_{[1],\lambda}[n]\,\hat{h}^{\mu}_{[2]}[n]_1, \quad \lambda,\mu = 0,1,\ \rho = 2\lambda + \begin{cases} \mu, & \text{if } \lambda = 0; \\ 1-\mu, & \text{if } \lambda = 1. \end{cases},$$

$$\hat{h}^0_{[2]}[n]_1 = \beta[2n], \quad \hat{h}^1_{[2]}[n]_1 = \alpha[2n]. \tag{3.6}$$

For example, assume $\lambda = \mu = 0$ then we have

$$\hat{\psi}^{2r}_{[2],0}[n] = \hat{\psi}^{2r}_{[1],0}[n]\,\hat{h}^0_{[2]}[n]_1 = \frac{\cos^{2r}\frac{\pi n}{N}}{\sqrt{U^{4r}[n]}}\,\frac{\cos^{2r}\frac{2\pi n}{N}}{\sqrt{U^{4r}[2n]}}.$$

Keeping in mind that the sequence $\beta[2n] = \cos^{2r}(2\pi n/N)/\sqrt{U^{4r}[2n]}$ is $N/2$-periodic, we have that the DFT of the corresponding cWP is

$$\hat{\varphi}^{2r}_{[2],0}[n] = \widehat{H(\psi^{2r}_{[2],0})}[n] = \beta[2n] \begin{cases} -i\,\beta[n], & \text{if } 0 < n < N/2; \\ i\,\beta[n], & \text{if } N/2 < n < N; \\ 2, & \text{if } n = 0; \\ 0, & \text{if } n = N/2, \end{cases} = \hat{\varphi}^{2r}_{[1],0}[n]\,\hat{h}^0_{[2]}[n]_1 = \hat{\varphi}^{2r}_{[1],0}[n]\,\hat{h}^0_{[1]}[2n]_1.$$

Similar relations hold for all the second-level cWPs and a general statement is true.

Please cite this article in press as: A. Averbuch et al., Analytic and directional wavelet packets in the space of periodic signals, Appl. Comput. Harmon. Anal. (2023), https://doi.org/10.1016/j.acha.2023.06.006

Proposition 3.4. *Assume that for a WP $\psi^{2r}_{[m+1],\rho}$ the relation in Eq. (2.9) holds. Then, for the cWP $\varphi^{2r}_{[m+1],\rho}$ we have*

$$\varphi^{2r}_{[m+1],\rho}[n] = \sum_{k=0}^{N/2^m-1} h^{\mu}_{[m+1]}[k]\, \varphi^{2r}_{[m],\lambda}[n-2^m k] \Longleftrightarrow \hat{\varphi}^{2r}_{[m+1],\rho}[\nu] = \hat{h}^{\mu}_{[1]}[2^m\nu]_m\, \hat{\varphi}^{2r}_{[m],\lambda}[\nu],$$
$$\hat{h}^0_{[1]}[\nu] = \hat{\psi}^{2r}_{[1],0}[\nu] = \beta[\nu], \quad \hat{h}^1_{[1]}[\nu] = \hat{\psi}^{2r}_{[1],1}[\nu] = \alpha[\nu].$$

Corollary 3.5. *Assume that for a WP $\psi^{2r}_{[m+1],\rho}$, the relation in Eq. (2.9) holds. Then, for the qWP $\Psi^{2r}_{\pm[m+1],\rho}$ we have*

$$\Psi^{2r}_{\pm[m+1],\rho}[n] = \sum_{k=0}^{N/2^m-1} h^{\mu}_{[m+1]}[k]\, \Psi^{2r}_{\pm[m],\lambda}[n-2^m k] \Longleftrightarrow \hat{\Psi}^{2r}_{\pm[m+1],\rho}[\nu] = \hat{h}^{\mu}_{[1]}[2^m\nu]_m\, \hat{\Psi}^{2r}_{\pm[m],\lambda}[\nu]. \tag{3.7}$$

4. Implementation of cWP and qWP transforms

Implementation of transforms with WPs $\psi^{2r}_{[m],\lambda}$ was discussed in Section 2. In this section, we extend the transform scheme to the transforms with cWPs $\varphi^{2r}_{[m],\lambda}$ and qWPs $\Psi^{2r}_{[m],\lambda}$.

4.1. One-level transforms

Denote by ${}^{2r}\mathcal{C}^0_{[1]}$ the subspace of the signal space $\Pi[N]$, which is the linear hull of the set $\mathbf{W}^0_{[1]} = \left\{\varphi^{2r}_{[1],0}[\cdot - 2k]\right\}$, $k = 0, ..., N/2-1$. The signals from the set $\mathbf{W}^0_{[1]}$ form an orthonormal basis of the subspace ${}^{2r}\mathcal{C}^0_{[1]}$. Denote by ${}^{2r}\mathcal{C}^1_{[1]}$ the orthogonal complement of the subspace ${}^{2r}\mathcal{C}^0_{[1]}$ in the space $\Pi[N]$. The signals from the set $\mathbf{W}^1_{[1]} = \left\{\varphi^{2r}_{[1],1}[\cdot - 2k]\right\}$, $k = 0, ..., N/2-1$ form an orthonormal basis of the subspace ${}^{2r}\mathcal{C}^1_{[1]}$.

Proposition 4.1. *The orthogonal projections of a signal $\mathbf{x} \in \Pi[N]$ onto the spaces ${}^{2r}\mathcal{C}^{\mu}_{[1]}$, $\mu = 0, 1$ are the signals $\mathbf{x}^{\mu}_{[1]} \in \Pi[N]$ such that*

$$x^{\mu}_{[1]}[k] = \sum_{l=0}^{N/2-1} c^{\mu}_{[1]}[l]\, \varphi^{2r}_{[1],\mu}[k-2l], \quad c^{\mu}_{[1]}[l] = \left\langle \mathbf{x},\, \varphi^{2r}_{[1],\mu}[\cdot - 2l] \right\rangle = \sum_{k=0}^{N-1} g^{\mu}_{[1]}[k-2l]\, x[k],$$
$$g^{\mu}_{[1]}[k] = \varphi^{2r}_{[1],\mu}[k], \quad \hat{g}^{\mu}_{[1]}[n] = \hat{\varphi}^{2r}_{[1],\mu}[n], \quad \mu = 0, 1.$$

The DFTs $\hat{\varphi}^{2r}_{[1],\mu}[n]$ of the first-level cWPs are given in Eq. (3.5).

The transforms $\mathbf{x} \to \mathbf{c}^0_{[1]} \bigcup \mathbf{c}^1_{[1]}$ and back are implemented using the analysis $\tilde{\mathbf{M}}^c[n]$ and the synthesis $\mathbf{M}^c[n]$ modulation matrices:

$$\tilde{\mathbf{M}}^c[n] \stackrel{\text{def}}{=} \begin{pmatrix} \hat{g}^0_{[1]}[n] & \hat{g}^0_{[1]}\left[n+\frac{N}{2}\right] \\ \hat{g}^1_{[1]}[n] & \hat{g}^1_{[1]}\left[n+\frac{N}{2}\right] \end{pmatrix} = \begin{pmatrix} \check{\beta}[n] & -\check{\beta}\left[n+\frac{N}{2}\right] \\ \check{\alpha}[n] & -\check{\alpha}\left[n+\frac{N}{2}\right] \end{pmatrix},$$
$$\mathbf{M}^c[n] \stackrel{\text{def}}{=} \begin{pmatrix} \check{\beta}[n] & \check{\alpha}[n] \\ -\check{\beta}\left[n+\frac{N}{2}\right] & -\check{\alpha}\left[n+\frac{N}{2}\right] \end{pmatrix}, \tag{4.1}$$
$$\check{\beta}[n] = \begin{cases} \beta[0], & \text{if } n = 0; \\ -i\beta[n], & \text{otherwise,} \end{cases} \quad \check{\alpha}[n] = \begin{cases} \alpha[N/2], & \text{if } n = N/2; \\ -i\alpha[n], & \text{otherwise.} \end{cases}$$

The sequences $\beta[n]$ and $\alpha[n]$ are given in Eq. (2.3).

Please cite this article in press as: A. Averbuch et al., Analytic and directional wavelet packets in the space of periodic signals, Appl. Comput. Harmon. Anal. (2023), https://doi.org/10.1016/j.acha.2023.06.006

Similarly to Eq. (2.5), the one-level cWP transform of a signal $\mathbf{x}$ and its inverse are:

$$\begin{pmatrix} \hat{c}^0_{[1]}[n]_1 \\ \hat{c}^1_{[1]}[n]_1 \end{pmatrix} = \frac{1}{2}\tilde{\mathbf{M}}^c[-n] \cdot \begin{pmatrix} \hat{x}[n] \\ \hat{x}[\vec{n}] \end{pmatrix}, \quad \begin{pmatrix} \hat{x}[n] \\ \hat{x}[\vec{n}] \end{pmatrix} = \mathbf{M}^c[n] \cdot \begin{pmatrix} \hat{c}^0_{[1]}[n]_1 \\ \hat{c}^1_{[1]}[n]_1 \end{pmatrix},$$

where $\vec{n} = n + N/2$.

Define the p-filters

$$\mathbf{q}^l_{\pm[1]} \stackrel{\text{def}}{=} \mathbf{h}^j_{[1]} \pm i\,\mathbf{g}^j_{[1]} = \psi^{2r}_{[1],l} \pm i\,\varphi^{2r}_{[1],l} = \Psi^{2r}_{\pm[1],l}, \quad l = 0, 1.$$

Equation (3.4) implies that their frequency responses are

$$\hat{q}^0_{+[1]}[n] = \begin{cases} (1+i)\sqrt{2}, & \text{if } n = 0; \\ 2\beta[n], & \text{if } 0 < n < N/2; \\ 0 & \text{if } N/2 \le n < N, \end{cases} \quad \hat{q}^1_{+[1]}[n] = \begin{cases} -(1+i)\sqrt{2}, & \text{if } n = N/2; \\ 2\alpha[n], & \text{if } 0 < n < N/2; \\ 0, & \text{if } N/2 < n \le N. \end{cases}$$

$$\hat{q}^0_{-[1]}[n] = \begin{cases} (1-i)\sqrt{2}, & \text{if } n = 0; \\ 2\beta[n], & \text{if } N/2 < n < N, \\ 0 & \text{if } 0 < n \le N/2; \end{cases} \quad \hat{q}^1_{-[1]}[n] = \begin{cases} -(1-i)\sqrt{2}, & \text{if } n = N/2; \\ 2\alpha[n] & \text{if } N/2 < n \le N; \\ 0, & \text{if } 0 \le n < N/2. \end{cases}$$

Thus, the analysis modulation matrices for the p-filters $\mathbf{q}^l_{\pm[1]}$ are

$$\tilde{\mathbf{M}}^q_+[n] = \begin{pmatrix} \hat{q}^0_{+[1]}[n] & 0 \\ \hat{q}^1_{+[1]}[n] & -\sqrt{2}(1+i)\,\delta[n - N/2] \end{pmatrix} = \tilde{\mathbf{M}}[n] + i\,\tilde{\mathbf{M}}^c[n], \tag{4.2}$$

$$\tilde{\mathbf{M}}^q_-[n] = \begin{pmatrix} (1-i)\sqrt{2}\delta[n] & \hat{q}^0_{-[1]}[n] \\ 0 & \hat{q}^1_{-[1]}[n] \end{pmatrix} = \tilde{\mathbf{M}}[n] - i\,\tilde{\mathbf{M}}^c[n], \tag{4.3}$$

where the modulation matrix $\tilde{\mathbf{M}}[n]$ is defined in Eq. (2.3) and $\tilde{\mathbf{M}}^c[n]$ is defined in Eq. (4.1). Application of the matrices $\tilde{\mathbf{M}}^q_\pm[n]$ to the vector $(\hat{x}[n], \hat{x}[\vec{n}])^T$ produces the vectors

$$\begin{pmatrix} \hat{z}^0_{\pm[1]}[n]_1 \\ \hat{z}^1_{\pm[1]}[n]_1 \end{pmatrix} = \frac{1}{2}(\tilde{\mathbf{M}}^q_\pm[n])^* \cdot \begin{pmatrix} \hat{x}[n] \\ \hat{x}[\vec{n}] \end{pmatrix} = \begin{pmatrix} \hat{y}^0_{[1]}[n]_1 \\ \hat{y}^1_{[1]}[n]_1 \end{pmatrix} \mp i \begin{pmatrix} \hat{c}^0_{[1]}[n]_1 \\ \hat{c}^1_{[1]}[n]_1 \end{pmatrix}.$$

Define the matrices $\mathbf{M}^q_\pm[n] \stackrel{\text{def}}{=} \tilde{\mathbf{M}}^q_\pm[n] = \mathbf{M}[n] \pm i\,\mathbf{M}^c[n]$ and apply these matrices to the vectors $(\hat{z}^0_{\pm[1]}[n]_1, \hat{z}^1_{\pm[1]}[n]_1)^T$. Here the modulation matrix $\mathbf{M}[n]$ is defined in Eq. (2.4) and $\mathbf{M}^c[n]$ is defined in Eq. (4.1).

Proposition 4.2. *The following relations hold*

$$\begin{aligned} &\mathbf{M}^q_\pm[n] \cdot \begin{pmatrix} \hat{z}^0_{\pm[1]}[n]_1 \\ \hat{z}^1_{\pm[1]}[n]_1 \end{pmatrix} = \mathbf{M}[n] \cdot \begin{pmatrix} \hat{y}^0_{[1]}[n]_1 \\ \hat{y}^1_{[1]}[n]_1 \end{pmatrix} + \mathbf{M}^c[n] \cdot \begin{pmatrix} \hat{c}^0_{[1]}[n]_1 \\ \hat{c}^1_{[1]}[n]_1 \end{pmatrix} \\ &\pm i \left(\mathbf{M}^c[n] \cdot \begin{pmatrix} \hat{y}^0_{[1]}[n]_1 \\ \hat{y}^1_{[1]}[n]_1 \end{pmatrix} - \mathbf{M}[n] \cdot \begin{pmatrix} \hat{c}^0_{[1]}[n]_1 \\ \hat{c}^1_{[1]}[n]_1 \end{pmatrix} \right) \\ &= 2 \left(\begin{pmatrix} \hat{x}[n] \\ \hat{x}[n + N/2] \end{pmatrix} \pm i \begin{pmatrix} \hat{h}[n] \\ \hat{h}[n + N/2] \end{pmatrix} \right) = 2 \begin{pmatrix} \hat{\bar{x}}_\pm[n] \\ \hat{\bar{x}}_\pm[n + N/2] \end{pmatrix}, \end{aligned}$$

where $\mathbf{h}$ *is the HT of the signal* $\mathbf{x} \in \Pi[N]$ *and* $\bar{\mathbf{x}}_\pm$ *are the analytic signals associated with* $\mathbf{x}$.

Please cite this article in press as: A. Averbuch et al., Analytic and directional wavelet packets in the space of periodic signals, Appl. Comput. Harmon. Anal. (2023), https://doi.org/10.1016/j.acha.2023.06.006

Proof. In Appendix section A. □

Definition 4.3. The matrices $\tilde{\mathbf{M}}^q_{\pm}[n]$ and $\mathbf{M}^q_{\pm}[n]$ are called the analysis and synthesis modulation matrices for the qWP transform, respectively.

Corollary 4.4. *Successive application of filter banks defined by the analysis and synthesis modulation matrices* $\tilde{\mathbf{M}}^q_{\pm}[n]$ *and* $\mathbf{M}^q_{\pm}[n]$ *to a signal* $\mathbf{x} \in \Pi[N]$ *produces the analytic signals* $\bar{\mathbf{x}}_{\pm}$ *associated with* $\mathbf{x}$.

Corollary 4.5. *A signal* $\mathbf{x} \in \Pi[N]$ *is represented by the redundant orthonormal system*

$$x[k] = \frac{1}{2}\sum_{\mu=0}^{1}\sum_{l=0}^{N/2-1}\left(y^{\mu}_{[1]}[l]\psi^{2r}_{[1],\mu}[k-2l] + c^{\mu}_{[1]}[l]\varphi^{2r}_{[1],\mu}[k-2l]\right),$$
$$y^{\mu}_{[1]}[l] = \left\langle \mathbf{x},\, \psi^{2r}_{[1],\mu}[\cdot-2l]\right\rangle, \quad c^{\mu}_{[1]}[l] = \left\langle \mathbf{x},\, \varphi^{2r}_{[1],\mu}[\cdot-2l]\right\rangle.$$

Thus, the system

$$\mathbf{F} \stackrel{\text{def}}{=} \left\{\psi^{2r}_{[1],0}[\cdot-2l]\right\} \bigoplus \left\{\psi^{2r}_{[1],1}[\cdot-2l]\right\} \bigcup \left\{\varphi^{2r}_{[1],0}[\cdot-2l]\right\} \bigoplus \left\{\varphi^{2r}_{[1],1}[\cdot-2l]\right\}$$

form a tight frame of the space $\Pi[N]$.

4.2. Multi-level transforms

It was explained in Section 2.4.2 that the second-level transform coefficients $\mathbf{y}^{\rho}_{[2]}$ are

$$y^{\rho}_{[2]}[l] = \sum_{n=0}^{N-1} x[n]\,\psi^{2r}_{[2],\rho}[n-4l], \quad \psi^{2r}_{[2],\rho}[n] = \sum_{k=0}^{N/2-1} h^{\mu}_{[2]}[k]\,\psi^{2r}_{[1],\lambda}[n-2k] \Longrightarrow$$
$$y^{\rho}_{[2]}[l] = \sum_{k=0}^{N/2-1} h^{\mu}_{[2]}[k-2l]\,y^{\lambda}_{[1]}[k], \quad \lambda,\mu = 0,1,\ \rho = \begin{cases}\mu, & \text{if } \lambda = 0\ ;\\ 3-\mu, & \text{if } \lambda = 1.\end{cases}$$

The frequency responses of the p-filters $\mathbf{h}^{\mu}_{[2]}$ are given in Eq. (2.6) and Eq. (3.6). Recall that $\hat{h}^{\mu}_{[2]}[n] = \hat{h}^{\mu}_{[1]}[2n]$. The direct and inverse transforms $\mathbf{y}^{\lambda}_{[1]} \longleftrightarrow \mathbf{y}^{2\lambda}_{[2]} \bigcup \mathbf{y}^{2\lambda+1}_{[2]}$ are implemented using the analysis and synthesis modulation matrices $\tilde{\mathbf{M}}[2n]$ and $\mathbf{M}[2n]$, that are defined in Eqs. (2.3) and (2.4) respectively:

$$\begin{pmatrix}\hat{y}^{\rho 0}_{[2]}[n]_2\\ \hat{y}^{\rho 1}_{[2]}[n]_2\end{pmatrix} = \frac{1}{2}\tilde{\mathbf{M}}[-2n]\cdot\begin{pmatrix}\hat{y}^{\lambda}_{[1]}[n]_1\\ \hat{y}^{\lambda}_{[1]}[\vec{n}]_1\end{pmatrix}, \quad \begin{pmatrix}\hat{y}^{\lambda}_{[1]}[n]_1\\ \hat{y}^{\lambda}_{[1]}[\vec{n}]_1\end{pmatrix} = \mathbf{M}[2n]\cdot\begin{pmatrix}\hat{y}^{\rho 0}_{[2]}[n]_2\\ \hat{y}^{\rho 1}_{[2]}[n]_2\end{pmatrix},$$

where

$$\rho 0 = \begin{cases}0, & \text{if } \lambda = 0;\\ 3, & \text{if } \lambda = 1,\end{cases} \quad \rho 1 = \begin{cases}1, & \text{if } \lambda = 0;\\ 2, & \text{if } \lambda = 1,\end{cases} \quad \vec{n} = n + N/4.$$

The second-level transform coefficients $\mathbf{c}^{\rho}_{[2]}$ are

$$c^{\rho}_{[2]}[l] = \sum_{n=0}^{N-1} x[n]\,\varphi^{2r}_{[2],\rho}[n-4l], \quad \varphi^{2r}_{[2],\rho}[n] = \sum_{k=0}^{N/2-1} h^{\mu}_{[2]}[k]\,\varphi^{2r}_{[1],\lambda}[n-2k] \Longrightarrow$$

Please cite this article in press as: A. Averbuch et al., Analytic and directional wavelet packets in the space of periodic signals, Appl. Comput. Harmon. Anal. (2023), https://doi.org/10.1016/j.acha.2023.06.006

$$c^{\rho}_{[2]}[l] = \sum_{k=0}^{N/2-1} h^{\mu}_{[2]}[k-2l]\, c^{\lambda}_{[1]}[k], \quad \lambda,\mu = 0,1,\ \rho = \begin{cases} \mu, & \text{if } \lambda = 0\ ; \\ 3-\mu, & \text{if } \lambda = 1. \end{cases}$$

We emphasise that the p-filters $\mathbf{h}^{\mu}_{[2]}$ for the transform $\mathbf{c}^{\lambda}_{[1]} \longleftrightarrow \mathbf{c}^{2\lambda}_{[2]} \bigcup \mathbf{c}^{2\lambda+1}_{[2]}$ are the same that the p-filters for the transform $\mathbf{y}^{\lambda}_{[1]} \longleftrightarrow \mathbf{y}^{2\lambda}_{[2]} \bigcup \mathbf{y}^{2\lambda+1}_{[2]}$. Therefore, the direct and inverse transforms $\mathbf{c}^{\lambda}_{[1]} \longleftrightarrow \mathbf{c}^{2\lambda}_{[2]} \bigcup \mathbf{c}^{2\lambda+1}_{[2]}$ are implemented using the same analysis and synthesis modulation matrices $\tilde{\mathbf{M}}[2n]$ and $\mathbf{M}[2n]$. Apparently, it is the case also for the transforms $\mathbf{z}^{\lambda}_{\pm[1]} \longleftrightarrow \mathbf{z}^{2\lambda}_{\pm[2]} \bigcup \mathbf{z}^{2\lambda+1}_{\pm[2]}$. The transforms to subsequent decomposition levels are implemented in an iterative way:

$$\begin{pmatrix} \hat{z}^{\rho 0}_{\pm[m+1]}[n]_{m+1} \\ \hat{z}^{\rho 1}_{\pm[m+1]}[n]_{m+1} \end{pmatrix} = \frac{1}{2}\tilde{\mathbf{M}}[-2^m n] \cdot \begin{pmatrix} \hat{z}^{\lambda}_{\pm[m]}[n]_m \\ \hat{z}^{\lambda}_{\pm[m]}[\vec{n}]_m \end{pmatrix},$$

$$\begin{pmatrix} \hat{z}^{\lambda}_{\pm[m]}[n]_m \\ \hat{z}^{\lambda}_{\pm[m]}[\vec{n}]_m \end{pmatrix} = \mathbf{M}[2^m n] \cdot \begin{pmatrix} \hat{z}^{\rho 0}_{\pm[m+1]}[n]_{m+1} \\ \hat{z}^{\rho 1}_{\pm[m+1]}[n]_{m+1} \end{pmatrix},$$

where $\rho 0 = \begin{cases} 2\lambda, & \text{if } \lambda \text{ is even;} \\ 2\lambda+1, & \text{if } \lambda \text{ is odd,} \end{cases}$ and vice versa for $\rho 1$, $\vec{n} = n + N/2^{m+1}$ and $m = 1, ..., M$. By the application of the inverse DFT to the arrays $\left\{\hat{z}^{\rho}_{\pm[m+1]}[n]_{m+1}\right\}$, we get the arrays $\left\{z^{\rho}_{\pm[m+1]}[k] = y^{\rho}_{[m+1]}[k] \pm i\, c^{\rho}_{[m+1]}[k]\right\}$ of the transform coefficients with the qWPs $\Psi^{2r}_{\pm[m+1],\rho}$.

Remark 4.1. We stress that by operating on the transform coefficients $\left\{z^{\rho}_{\pm[m]}[k]\right\}$, we simultaneously operate on the arrays $\left\{y^{\rho}_{[m]}[k]\right\}$ and $\left\{c^{\rho}_{[m]}[k]\right\}$, which are the coefficients for the transforms with the WPs $\psi^{2r}_{[m],\rho}$ and cWPs $\varphi^{2r}_{[m],\rho}$, respectively. The execution speed of the transform with the qWPs $\left\{\Psi^{2r}_{\pm[m]}\right\} = \psi^{2r}_{[m]} \pm i\varphi^{2r}_{[m]}$ is the same as the speed of the transforms with either WPs $\left\{\psi^{2r}_{[m]}\right\}$ or cWPs $\left\{\varphi^{2r}_{[m]}\right\}$.

The transforms are executed in the spectral domain using the FFT by the application of critically sampled two-channel filter banks to the half-band spectral components $(\hat{x}[n], \hat{x}[n+N/2])^T$ of a signal.

The diagrams in Figs. 4.1 and 4.2 illustrate the three-level forward and inverse qWPTs of a signal with quasi-analytic wavelet packets, which use the analysis $\tilde{\mathbf{M}}^q[n]$ and the synthesis $\mathbf{M}^q[n]$ modulation matrices, respectively, for the transforms to and from the first decomposition level, respectively, and the modulation matrices $\tilde{\mathbf{M}}[2^m n]$ and $\mathbf{M}[2^m n]$ for the subsequent levels.

Remark 4.2. The decomposition of a signal $\mathbf{x} \in \Pi[N]$ down to the M-th level produces $2MN$ transform coefficients $\left\{y^{\rho}_{[m]}[k]\right\} \bigcup \left\{c^{\rho}_{[m]}[k]\right\}$. Such a redundancy provides many options for the signal reconstruction. Some of them are listed below.

- A basis compiled from either WPs $\left\{\psi^{2r}_{[m]}\right\}$ or $\left\{\varphi^{2r}_{[m]}\right\}$.
  - Wavelet basis.
  - Best bases [14], Local discriminant bases [36,37].
  - WPs from a single decomposition level.
- Combination of bases compiled from both $\left\{\psi^{2r}_{[m]}\right\}$ and $\left\{\varphi^{2r}_{[m]}\right\}$ WPs generates a tight frame of the space $\Pi[N]$ with redundancy rate 2. The bases for $\left\{\psi^{2r}_{[m]}\right\}$ and $\left\{\varphi^{2r}_{[m]}\right\}$ can have a different structure.
- Frames with increased redundancy rate. For example, a combined reconstruction from several decomposition levels.

Please cite this article in press as: A. Averbuch et al., Analytic and directional wavelet packets in the space of periodic signals, Appl. Comput. Harmon. Anal. (2023), https://doi.org/10.1016/j.acha.2023.06.006

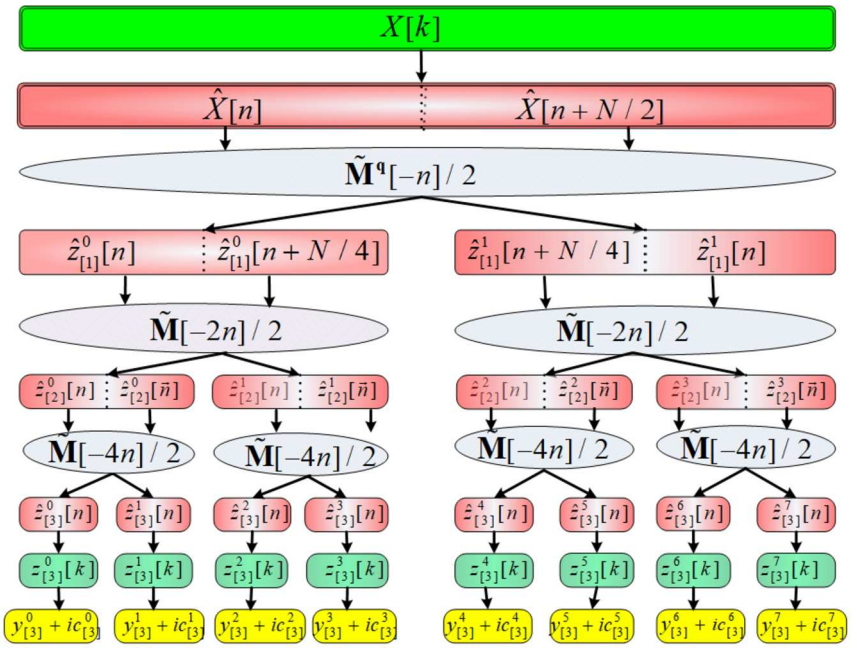

Fig. 4.1. Forward qWTP of a signal $\mathbf{X}$ down to the third decomposition level with quasi-analytic wavelet packets. Here $\vec{n}$ means $n + N/8$.

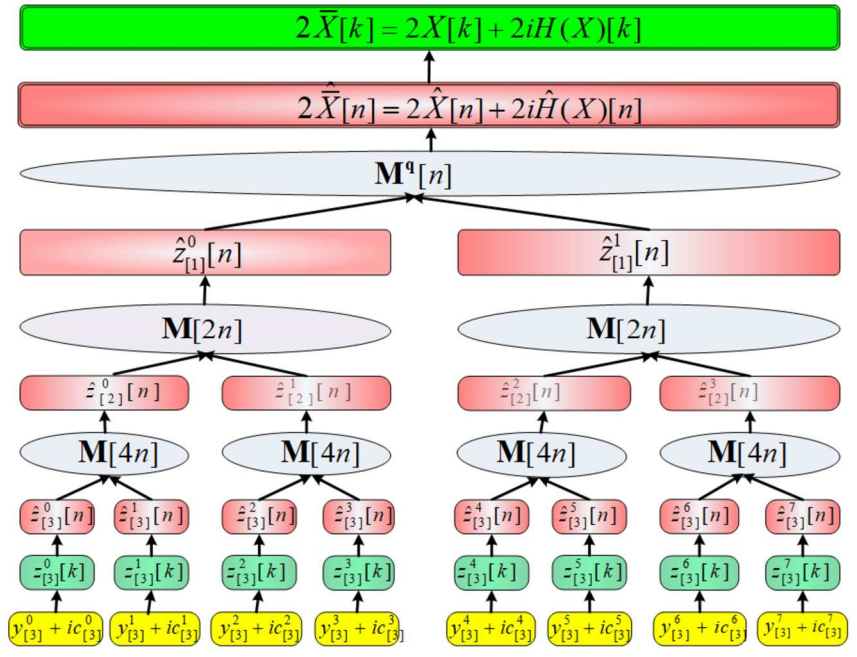

Fig. 4.2. Inverse qWTP from the transform coefficients from the third decomposition level that results in restoration of the signal $\mathbf{X}$ and its HT $H(\mathbf{X})$.

The collection of WPs $\left\{\psi^{2r}_{[m]}\right\}$ and cWPs $\left\{\varphi^{2r}_{[m]}\right\}$, which originate from discrete splines of different orders $2r$, provides a variety of waveforms that are (anti)symmetric, well localized in time domain. Their DFT spectra are flat and the spectra shapes tend to rectangles when the order $2r$ increases. Therefore, they can be utilized as a collection of band-pass filters which produce a refined split of the frequency domain into

Please cite this article in press as: A. Averbuch et al., Analytic and directional wavelet packets in the space of periodic signals, Appl. Comput. Harmon. Anal. (2023), https://doi.org/10.1016/j.acha.2023.06.006

bands of different widths. The (c)WPs can be used as testing waveforms for the signal analysis, such as a dictionary for the Matching Pursuit procedures [32,5].

5. Two-dimensional complex wavelet packets

A standard design scheme for 2D wavelet packets is outlined in Section 2.5. The 2D wavelet packets are defined as the tensor products of 1D WPs such that

$$\psi^{2r}_{[m],j,l}[k,n] = \psi^{2r}_{[m],j}[k]\,\psi^{2r}_{[m],l}[n].$$

The 2^m-sample shifts of the WPs $\left\{\psi^{2r}_{[m],j,l}\right\}$, $j,l = 0,...,2^m-1$, in both directions form an orthonormal basis for the space $\Pi[N,N]$ of arrays that are N-periodic in both directions. The DFT spectrum of such a WP is concentrated in four symmetric spots in the frequency domain as it is seen in Fig. 2.3.

Similar properties are inherent to the 2D cWPs such that

$$\varphi^{2r}_{[m],j,l}[k,n] = \varphi^{2r}_{[m],j}[k]\,\varphi^{2r}_{[m],l}[n].$$

5.1. Design of 2D directional WPs

5.1.1. 2D complex WPs and their spectra

The WPs $\left\{\psi^{2r}_{[m],j,l}\right\}$ as well as the cWPs $\left\{\varphi^{2r}_{[m],j,l}\right\}$ lack the directionality property which is needed in many applications that process 2D data. However, real-valued 2D wavelet packets oriented in multiple directions can be derived from tensor products of complex quasi-analytic qWPs $\Psi^{2r}_{\pm[m],\rho}$.

The complex 2D qWPs are defined as follows:

$$\Psi^{2r}_{++[m],j,l}[k,n] \stackrel{\text{def}}{=} \Psi^{2r}_{+[m],j}[k]\,\Psi^{2r}_{+[m],l}[n],$$
$$\Psi^{2r}_{+-[m],j,l}[k,n] \stackrel{\text{def}}{=} \Psi^{2r}_{+[m],j}[k]\,\Psi^{2r}_{-[m],l}[n],$$

where $m = 1,...,M$, $j,l = 0,...,2^m-1$, and $k,n = -N/2,...,N/2-1$. The real and imaginary parts of these 2D qWPs are

$$\begin{aligned}\vartheta^{2r}_{+[m],j,l}[k,n] &\stackrel{\text{def}}{=} \mathfrak{Re}(\Psi^{2r}_{++[m],j,l}[k,n]) = \psi^{2r}_{[m],j,l}[k,n] - \varphi^{2r}_{[m],j,l}[k,n],\\ \vartheta^{2r}_{-[m],j,l}[k,n] &\stackrel{\text{def}}{=} \mathfrak{Re}(\Psi^{2r}_{+-[m],j,l}[k,n]) = \psi^{2r}_{[m],j,l}[k,n] + \varphi^{2r}_{[m],j,l}[k,n],\end{aligned} \tag{5.1}$$

$$\begin{aligned}\theta^{2r}_{+[m],j,l}[k,n] &\stackrel{\text{def}}{=} \mathfrak{Im}(\Psi^{2r}_{++[m],j,l}[k,n]) = \psi^{2r}_{[m],j}[k]\,\varphi^{2r}_{[m],l}[n] + \varphi^{2r}_{[m],j}[k]\,\psi^{2r}_{[m],l}[n],\\ \theta^{2r}_{-[m],j,l}[k,n] &\stackrel{\text{def}}{=} \mathfrak{Im}(\Psi^{2r}_{+-[m],j,l}[k,n]) = \varphi^{2r}_{[m],j}[k]\,\psi^{2r}_{[m],l}[n] - \psi^{2r}_{[m],j}[k]\,\varphi^{2r}_{[m],l}[n].\end{aligned} \tag{5.2}$$

The DFT spectra of the 2D qWPs $\Psi^{2r}_{++[m],j,l}$, $j,l = 0,...,2^m-1$, are the tensor products of the one-sided spectra of the qWPs:

$$\hat{\Psi}^{2r}_{++[m],j,l}[p,q] = \hat{\Psi}^{2r}_{+[m],j}[p]\,\hat{\Psi}^{2r}_{+[m],l}[q]$$

and, as such, they fill the quadrant $k,n = 0,...,N/2-1$ of the frequency domain, while the spectra of $\Psi^{2r}_{+-[m],j,l}$, $j,l = 0,...,2^m-1$, fill the quadrant $k = 0,...,N/2-1$, $n = -N/2,...,-1$. Fig. 5.1 displays the magnitude spectra of the tenth-order 2D qWPs $\Psi^{10}_{++[2],j,l}$ and $\Psi^{10}_{+-[2],j,l}$ from the second decomposition level.

Please cite this article in press as: A. Averbuch et al., Analytic and directional wavelet packets in the space of periodic signals, Appl. Comput. Harmon. Anal. (2023), https://doi.org/10.1016/j.acha.2023.06.006

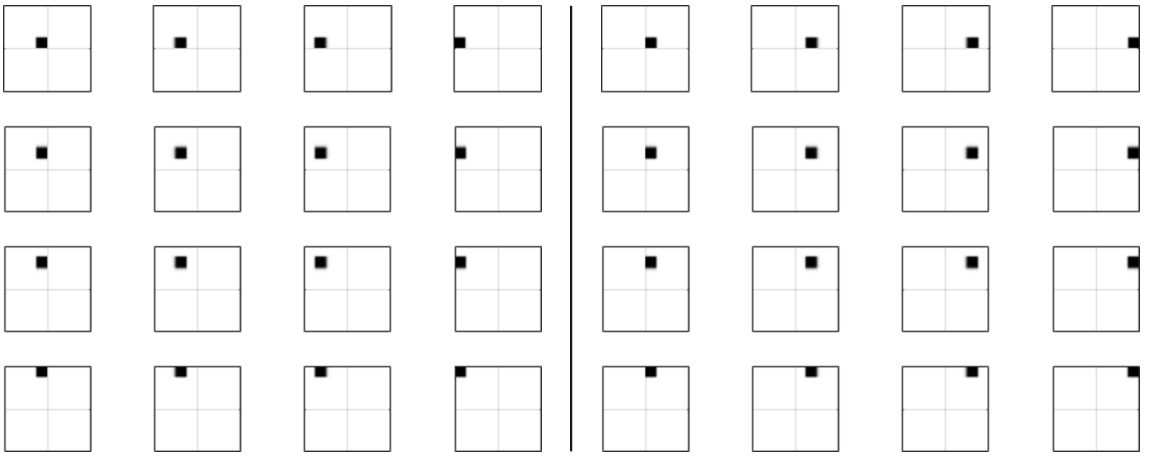

Fig. 5.1. Magnitude spectra of 2D qWPs $\Psi^{10}_{+-[2],j,l}$ (left) and $\Psi^{10}_{++[2],j,l}$ (right) from the second decomposition level.

Remark 5.1. The 2D qWPs $\Psi^{2r}_{+\pm[m],j,l}$ are the tensor products of 1D qWPs from the decomposition level m. However, there are no problems to design the 2D qWPs as tensor products of 1D qWPs from different decomposition levels such as $\Psi^{2r}_{+\pm[m,s],j,l}[k,n] \stackrel{\text{def}}{=} \Psi^{2r}_{+[m],j}[k]\,\Psi^{2r}_{\pm[s],l}[n]$.

5.1.2. Directionality of real-valued 2D WPs

It is seen in Fig. 5.1 that the DFT spectra of the qWPs $\Psi^{10}_{\pm[m],j,l}$ effectively occupy relatively small squares in the frequency domain. For deeper decomposition levels, sizes of the corresponding squares decrease in geometric progression. Such configurations of the spectra lead to the directionality of the real-valued 2D WPs $\vartheta^{2r}_{\pm[m],j,l}$ and $\theta^{2r}_{\pm[m],j,l}$.

Assume, for example, that $N = 512,\ m = 3,\ j = 2,\ l = 5$ and denote $\Psi[k,n] \stackrel{\text{def}}{=} \Psi^{2r}_{++[3],2,5}[k,n]$ and $\vartheta[k,n] \stackrel{\text{def}}{=} \mathfrak{Re}(\Psi[k,n])$. Its magnitude spectrum $\left|\hat{\Psi}[j,l]\right|$, displayed in Fig. 5.2, effectively occupies the square of size 40×40 *pixels* centered around the point $\mathbf{C} = [\kappa_0, \nu_0]$, where $\kappa_0 = 78,\ \nu_0 = 178$. Thus, the WP Ψ is represented by

$$\Psi[k,n] \;=\; \frac{1}{N^2}\sum_{\kappa,\nu=0}^{N/2-1} \omega^{k\kappa+n\nu}\,\hat{\Psi}[\kappa,\nu] \approx \omega^{\kappa_0 k+\nu_0 n}\,\underline{\Psi}[k,n]$$

$$\underline{\Psi}[k,n] \stackrel{\text{def}}{=} \frac{1}{N^2}\sum_{\kappa,\nu=-20}^{19} \omega^{k\kappa+n\nu}\,\hat{\Psi}[\kappa+\kappa_0,\nu+\nu_0].$$

Consequently, the real-valued WP ϑ, whose magnitude spectrum is displayed in Fig, 5.2 (second from left), is represented as follows:

$$\vartheta[k,n] \approx \cos\frac{2\pi(\kappa_0 k+\nu_0 n)}{N}\,\mathfrak{Re}(\underline{\Psi}[k,n]) + \cos\left(\frac{2\pi(\kappa_0 k+\nu_0 n)}{N} - \frac{\pi}{2}\right)\mathfrak{Im}(\underline{\Psi}[k,n]).$$

The spectrum of the 2D signal $\underline{\vartheta}$ comprises only low frequencies in both directions and it does not have a directionality. But the 2D signal $\cos\frac{2\pi(\kappa_0 k+\nu_0 n)}{N}$ is oscillating in the direction of the vector $\vec{D}$, which is orthogonal to the vector $\vec{V}_{++[2],2,5} = 178\vec{\mathbf{i}} + 78\vec{\mathbf{j}}$. The 2D WP $\vartheta[k,n]$ is well localized in the spatial domain as is seen from Eq. (5.1) and the same is true for the low-frequency signal $\underline{\vartheta}$. Therefore, WP $\vartheta[k,n]$ can be regarded as the directional cosine modulated by the localized low-frequency signal $\underline{\vartheta}$.

The same arguments are applicable to the 2D WPs $\vartheta^{p}_{-[m],j,l}[k,n] = \mathfrak{Re}(\Psi^{p}_{+-[m],j,l}[k,n])$. Fig. 5.2 displays the low-frequency signal $\underline{\vartheta}$, its magnitude spectrum and the 2D WP $\vartheta[k,n]$.

Please cite this article in press as: A. Averbuch et al., Analytic and directional wavelet packets in the space of periodic signals, Appl. Comput. Harmon. Anal. (2023), https://doi.org/10.1016/j.acha.2023.06.006

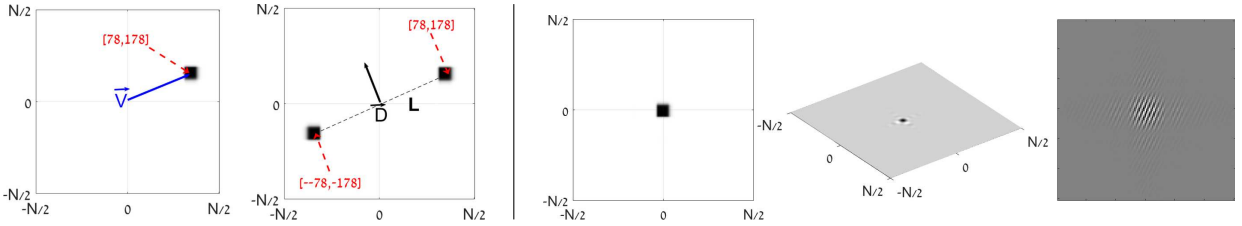

Fig. 5.2. Magnitude spectra of 2D qWP $\Psi[k,n]$ (left) and $\mathfrak{Re}(\Psi) = \vartheta[k,n]$ (second from left). Center: magnitude spectrum of low-frequency signal $\underline{\vartheta}[k,n]$. Second from right: signal $\underline{\vartheta}[k,n]$. Right: 2D WP $\vartheta[k,n]$ (magnified).

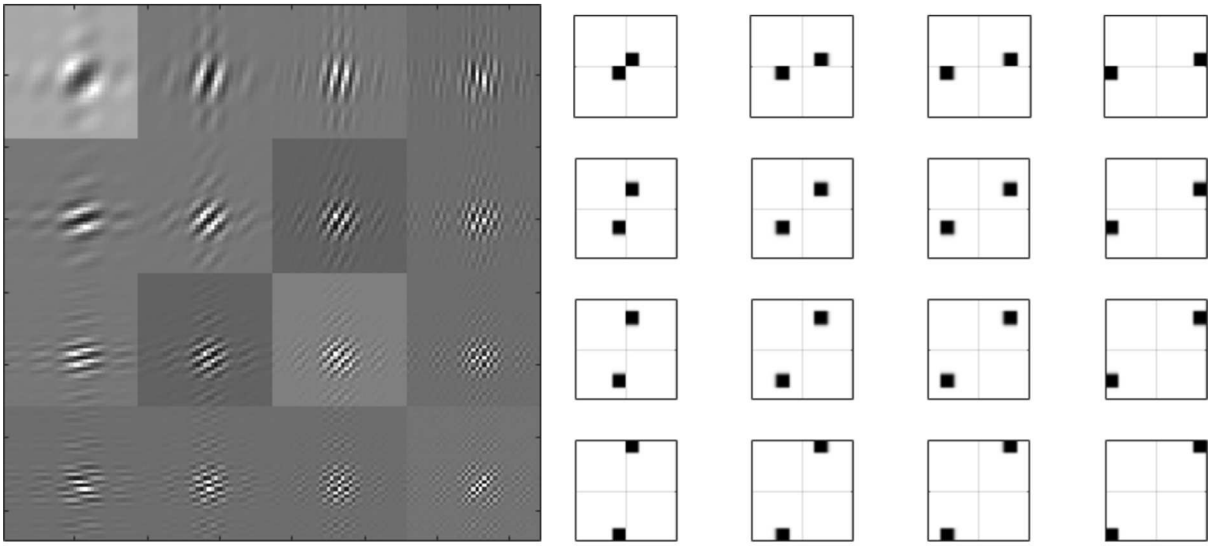

Fig. 5.3. WPs $\vartheta^{10}_{+[2],j,l}$ from the second decomposition level (left) and their magnitude spectra (right).

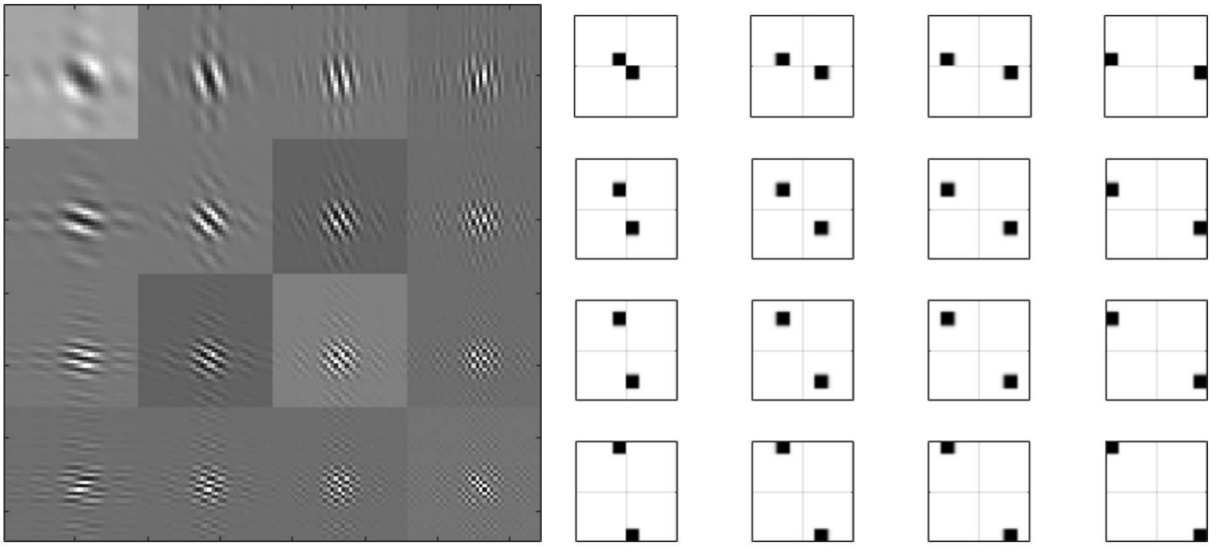

Fig. 5.4. WPs $\vartheta^{10}_{-[2],j,l}$ from the second decomposition level (left) and their magnitude spectra (right).

Fig. 5.3 displays WPs $\vartheta^{10}_{+[2],j,l}$, $j,l = 0,1,2,3$, from the second decomposition level and their magnitude spectra, respectively. Fig. 5.4 displays WPs $\vartheta^{10}_{-[2],j,l}$, $j,l = 0,1,2,3$, from the second decomposition level and their magnitude spectra, respectively.

Please cite this article in press as: A. Averbuch et al., Analytic and directional wavelet packets in the space of periodic signals, Appl. Comput. Harmon. Anal. (2023), https://doi.org/10.1016/j.acha.2023.06.006

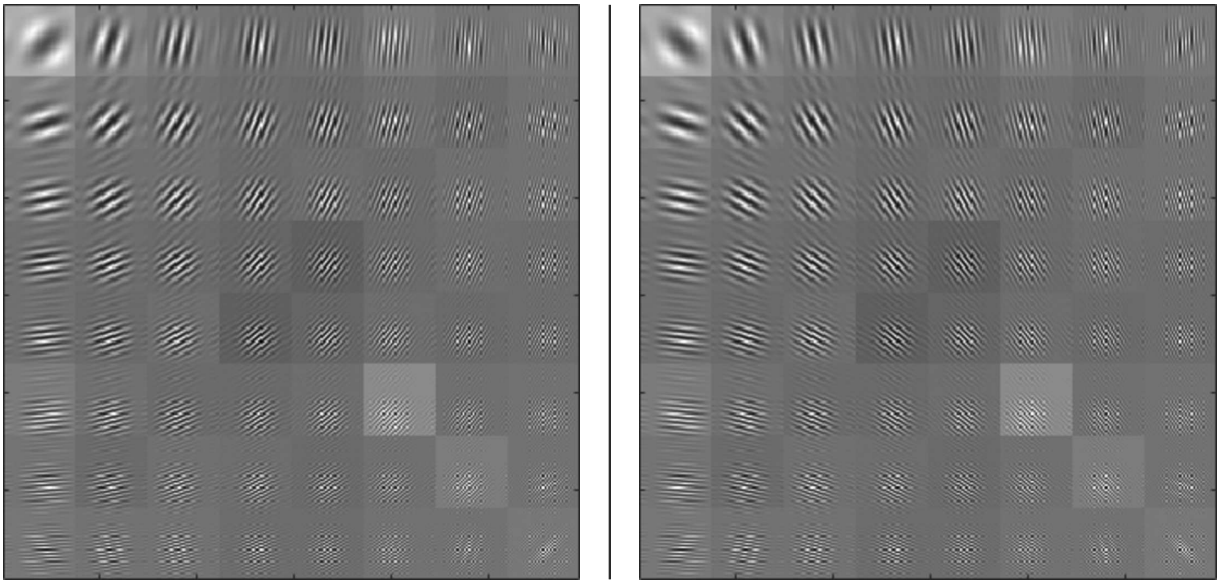

Fig. 5.5. WPs $\vartheta^{10}_{+[3],j,l}$ (left) and $\vartheta^{10}_{-[3],j,l}$ (right) from the third decomposition level.

Fig. 5.5 displays the WPs $\vartheta^{2r}_{\pm[3],j,l}$ from the third decomposition level.

6. Implementation of 2D qWP transforms

The spectra of 1D qWPs $\left\{\Psi^{2r}_{+[m],j}\right\}$, $j = 0, ..., 2^m - 1$, fill the non-negative half-band $[0, N/2]$, and vice versa for the qWPs $\left\{\Psi^{2r}_{-[m],j}\right\}$, $j = 0, ..., 2^m - 1$. Therefore, the spectra of 2D qWPs $\left\{\Psi^{2r}_{++[m],j,l}\right\}$, $j, l = 0, ..., 2^m - 1$ fill the quadrant $[0, N/2 - 1] \times [0, N/2 - 1]$ of the frequency domain, while the spectra of 2D qWPs $\left\{\Psi^{2r}_{+-[m],j,l}\right\}$ fill the quadrant $[0, N/2 - 1] \times [-N/2, -1]$. It is clearly seen in Fig. 6.1.

Consequently, the spectra of the real-valued 2D WPs $\left\{\vartheta^{2r}_{+[m],j,l}\right\}$, $j, l = 0, ..., 2^m - 1$, and $\left\{\vartheta^{2r}_{-[m],j,l}\right\}$ fill the pairs of quadrant $\mathbf{Q}_+ \stackrel{\text{def}}{=} [0, N/2-1] \times [0, N/2-1] \bigcup [-N/2, -1] \times [-N/2, -1]$ and $\mathbf{Q}_- \stackrel{\text{def}}{=} [0, N/2-1] \times [-N/2, -1] \bigcup [-N/2, -1] \times [0, N/2-1]$, respectively (Fig. 6.1).

By this reason, no linear combination of the WPs $\left\{\vartheta^{2r}_{+[m],j,l}\right\}$ and their shifts can serve as a basis in the signal space $\Pi[N, N]$. The same is true for WPs $\left\{\vartheta^{2r}_{-[m],j,l}\right\}$. However, combinations of the WPs $\left\{\vartheta^{2r}_{\pm[m],j,l}\right\}$ provide frames of the space $\Pi[N, N]$.

6.1. One-level 2D transforms

The one-level 2D qWP transforms of a signal $\mathbf{X} = \{X[k, n]\} \in \Pi[N, N]$ are implemented by a tensor-product scheme mentioned in Section 2.5.

6.1.1. Direct transforms with qWPs $\Psi^{2r}_{+\pm[1]}$

Denote by $\tilde{\mathbf{T}}^h_\pm$ the 1D transforms of row signals from $\Pi[N]$ with the analysis modulation matrices $\tilde{\mathbf{M}}^q_\pm$ which are defined in Eq. (4.2). Application of these transforms to rows of a signal $\mathbf{X}$ produces the coefficient arrays

$$\tilde{\mathbf{T}}^h_+ \cdot \mathbf{X} = \left(\zeta^0_+, \zeta^1_+\right), \quad \zeta^j_+[k, n] = \eta^j[k, n] - i\,\xi^j[k, n],$$
$$\tilde{\mathbf{T}}^h_- \cdot \mathbf{X} = \left(\zeta^0_-, \zeta^1_-\right), \quad \zeta^j_-[k, n] = \eta^j[k, n] + i\,\xi^j[k, n] = (\zeta^j_+[k, n])^*,$$

Please cite this article in press as: A. Averbuch et al., Analytic and directional wavelet packets in the space of periodic signals, Appl. Comput. Harmon. Anal. (2023), https://doi.org/10.1016/j.acha.2023.06.006

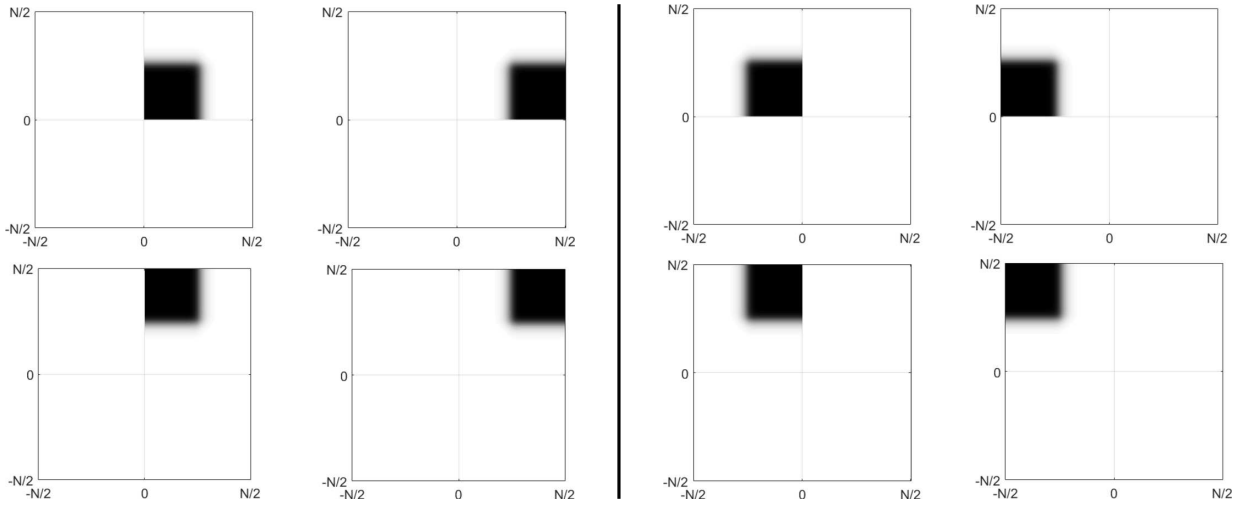

Fig. 6.1. Magnitude spectra of qWPs $\Psi^{10}_{++[1],j,l}$ (left) and $\Psi^{10}_{+-[1],j,l}$ (right) from the first decomposition level.

$$\eta^j[k,n] = \left\langle \mathbf{X}[k,\cdot], \psi^{2r}_{[1],j}[\cdot - 2n] \right\rangle, \quad \xi^j[k,n] = \left\langle \mathbf{X}[k,\cdot], \varphi^{2r}_{[1],j}[\cdot - 2n] \right\rangle, \ j = 0,1.$$

Denote by $\mathbf{T}^h_\pm$ the 1D inverse transforms with the synthesis modulation matrices $\mathbf{M}^q_\pm$. Due to Proposition 4.2, application of these transforms to rows of the coefficient arrays $\zeta_\pm = \left(\zeta^0_\pm, \zeta^1_\pm\right)$, respectively, produces the 2D analytic signals:

$$\mathbf{T}^h_\pm \cdot (\zeta^0_\pm, \zeta^1_\pm) = 2\bar{\mathbf{X}}_\pm = 2(\mathbf{X} \pm i\, H(\mathbf{X})), \tag{6.1}$$

where H($\mathbf{X}$) is the 2D signal consisting of the HTs of rows of the signal $\mathbf{X}$.

Denote by $\tilde{\mathbf{T}}^v_+$ the direct 1D transform determined by the modulation matrix $\tilde{\mathbf{M}}^q_+$ applicable to columns of the corresponding signals. The next step of the tensor product transform consists of the application of the 1D transform $\tilde{\mathbf{T}}^v_+$ to columns of the arrays ζ^j, $j = 0,1$. As a result, we get four transform coefficients arrays:

$$\tilde{\mathbf{T}}^v_+ \cdot \zeta^l_+ = \tilde{\mathbf{T}}^v_+ \cdot \left(\eta^l - i\,\xi^l\right) = \begin{cases} \left(\alpha^{0,l} - i\,\beta^{0,l}\right) - i\left(\gamma^{0,l} - i\,\delta^{0,l}\right) \\ \left(\alpha^{1,l} - i\,\beta^{1,l}\right) - i\left(\gamma^{1,l} - i\,\delta^{1,l}\right) \end{cases}$$

$$= \begin{cases} \mathbf{Z}^{0,l}_{+[1]} = \mathbf{Y}^{0,l}_{+[1]} - i\,\mathbf{C}^{0,l}_{+[1]}, & \mathbf{Y}^{0,l}_{+[1]} = \alpha^{0,l} - \delta^{0,l}, \quad \mathbf{C}^{0,l}_{+[1]} = \beta^{0,l} + \gamma^{0,l} \\ \mathbf{Z}^{1,l}_{+[1]} = \mathbf{Y}^{1,l}_{+[1]} - i\,\mathbf{C}^{1,l}_{+[1]}, & \mathbf{Y}^{1,l}_{+[1]} = \alpha^{1,l} - \delta^{1,l}, \quad \mathbf{C}^{1,l}_{+[1]} = \beta^{1,l} + \gamma^{1,l} \end{cases},$$

$$\alpha^{j,l}[k,n] = \sum_{\lambda,\mu=0}^{N-1} X[\lambda,\mu], \psi^{2r}_{[1],j}[\lambda - 2k]\psi^{2r}_{[1],l}[\mu - 2n],$$

$$\delta^{j,l}[k,n] = \sum_{\lambda,\mu=0}^{N-1} X[\lambda,\mu], \varphi^{2r}_{[1],j}[\lambda - 2k]\varphi^{2r}_{[1],l}[\mu - 2n],$$

$$\beta^{j,l}[k,n] = \sum_{\lambda,\mu=0}^{N-1} X[\lambda,\mu], \psi^{2r}_{[1],j}[\lambda - 2k]\varphi^{2r}_{[1],l}[\mu - 2n],$$

$$\gamma^{j,l}[k,n] = \sum_{\lambda,\mu=0}^{N-1} X[\lambda,\mu], \varphi^{2r}_{[1],j}[\lambda - 2k]\psi^{2r}_{[1],l}[\mu - 2n], \quad j,l = 0,1.$$

Hence, it follows that

Please cite this article in press as: A. Averbuch et al., Analytic and directional wavelet packets in the space of periodic signals, Appl. Comput. Harmon. Anal. (2023), https://doi.org/10.1016/j.acha.2023.06.006

$$\begin{aligned} Y^{j,l}_{+[1]}[k,n] &= \sum_{\lambda,\mu=0}^{N-1} X[\lambda,\mu]\, \vartheta^{2r}_{+[1],j,l}[\lambda-2k,\mu-2n], \\ C^{j,l}_{+[1]}[k,n] &= \sum_{\lambda,\mu=0}^{N-1} X[\lambda,\mu]\, \theta^{2r}_{+[1],j,l}[\lambda-2k,\mu-2n], \\ Z^{j,l}_{+[1]}[k,n] &= \sum_{\lambda,\mu=0}^{N-1} X[\lambda,\mu]\, \Psi^{2r}_{++[1],j,l}[\lambda-2k,\mu-2n], \quad j,l=0,1. \end{aligned} \tag{6.2}$$

Remark 6.1. Recall that the DFT spectra of WPs $\vartheta^{2r}_{+[1],j,l}$ and $\theta^{2r}_{+[1],j,l}$, $j,l=0,1$, which are the real and imaginary parts of the qWP $\Psi^{2r}_{++[1],j,l}$, are confined within the area $\mathbf{Q}_+$ of the frequency domain. It is seen from Eq. (6.2) that if at least a part of the spectrum of a signal $\mathbf{X}\in\Pi[N,N]$ is located in the area $\mathbf{Q}_-$, then the signal $\mathbf{X}\in\Pi[N,N]$ cannot be fully restored from the transform coefficients $Z^{j,l}_{+[1]}[k,n]$, although their number is the same as the number of samples in the signal $\mathbf{X}$. To achieve a perfect reconstruction, the coefficients from the arrays $\mathbf{Z}^{j,l}_{-[1]}$ should be incorporated.

The coefficient arrays $\mathbf{Z}^{j,l}_{-[1]}$ are derived in the same way as the arrays $\mathbf{Z}^{j,l}_{+[1]}$. The only difference is that, for the 1D transform $\tilde{\mathbf{T}}^h_-$ the modulation matrix $\tilde{\mathbf{M}}^q_-$ is used instead of $\tilde{\mathbf{M}}^q_+$. For the transform $\tilde{\mathbf{T}}^v_-$, the modulation matrix $\tilde{\mathbf{M}}^q_+$ is used. Consequently, to derive the coefficient arrays $\mathbf{Z}^{j,l}_{-[1]}$, the transform $\tilde{\mathbf{T}}^v_+$ should be applied to columns of the arrays $\zeta^l_- = (\zeta^l_+)^*$. As a result, we get

$$\mathbf{Z}^{j,l}_{-[1]} = \mathbf{Y}^{j,l}_{-[1]} + i\,\mathbf{C}^{j,l}_{-[1]} = \sum_{\lambda,\mu=0}^{N-1} X[\lambda,\mu], \Psi^{2r}_{+-[1],j,l}[\lambda-2k,\mu-2n],\ j,l=0,1.$$

6.1.2. Inverse transforms with qWPs $\Psi^{2r}_{+\pm[1]}$

Denote by $\mathbf{T}^v_+$ the 1D inverse transform with the synthesis modulation matrix $\mathbf{M}^q_+$ applicable to columns of the coefficient arrays. Denote by $H(\zeta^l_\pm)$, $l=0,1$, the HTs of the arrays consisting of columns of the coefficient arrays $\zeta^j_\pm$. Proposition 4.2 implies that

$$\mathbf{T}^v_+\cdot\begin{pmatrix}\mathbf{Z}^{0,l}_{+[1]}\\ \mathbf{Z}^{1,l}_{+[1]}\end{pmatrix} = 2\bar{\zeta}^l_+, \quad \mathbf{T}^v_+\cdot\begin{pmatrix}\mathbf{Z}^{0,l}_{-[1]}\\ \mathbf{Z}^{1,l}_{-[1]}\end{pmatrix} = 2\bar{\zeta}^l_-,$$

where $l=0,1$ and $\bar{\zeta}^l_\pm = \zeta^l_\pm + i\,H(\zeta^l_\pm)$ are analytic coefficient arrays. Denote by $\mathbf{G}$ a signal from $\Pi[N,N]$ such that

$$\tilde{\mathbf{T}}^h_\pm\cdot\mathbf{G} = \big(H(\zeta^0_\pm), H(\zeta^1_\pm)\big) \Longrightarrow \mathbf{T}^h_\pm\cdot\big(H(\zeta^0_\pm), H(\zeta^1_\pm)\big) = 4(\mathbf{G}\pm i\,H(\mathbf{G})). \tag{6.3}$$

Equations (6.1) and (6.3) imply that the applications of the transforms $\mathbf{T}^h_\pm$ to rows of the respective coefficient arrays results in the following relations:

$$\begin{aligned} \mathbf{X}_+ &\stackrel{\text{def}}{=} \mathbf{T}^h_+\cdot\big(\bar{\zeta}^0_+, \bar{\zeta}^1_+\big) = 4\left(\mathbf{X} + i\,H(\mathbf{X}) + i\mathbf{G} - H(\mathbf{G})\right), \\ \mathbf{X}_- &\stackrel{\text{def}}{=} \mathbf{T}^h_-\cdot\big(\bar{\zeta}^0_-, \bar{\zeta}^1_-\big) = 4\left(\mathbf{X} - i\,H(\mathbf{X}) + i\mathbf{G} + H(\mathbf{G})\right). \end{aligned} \tag{6.4}$$

Finally, we have the signal $\mathbf{X}$ restored by $\mathbf{X} = \mathfrak{Re}(\mathbf{X}_+ + \mathbf{X}_-)/8$.

Figs. 6.2 and 6.3 illustrate the image "Barbara" restoration by the 2D signals $\mathfrak{Re}(\mathbf{X}_\pm)$ and $\mathbf{X} = \mathfrak{Re}(\mathbf{X}_+ + \mathbf{X}_-)/8$. The signal $\mathfrak{Re}(\mathbf{X}_-)$ captures edges oriented to *north-west*, while $\mathfrak{Re}(\mathbf{X}_+)$ captures edges oriented to *north-east*. The signal $\mathbf{X}$ perfectly restores the image achieving PSNR=313.8596 dB.

6.2. Multi-level 2D transforms

It was established in Section 4.2 that the 1D qWP transforms of a signal $\mathbf{x}\in\Pi[N]$ to the second and further decomposition levels are implemented by the iterated application of the filter banks, that are

Please cite this article in press as: A. Averbuch et al., Analytic and directional wavelet packets in the space of periodic signals, Appl. Comput. Harmon. Anal. (2023), https://doi.org/10.1016/j.acha.2023.06.006

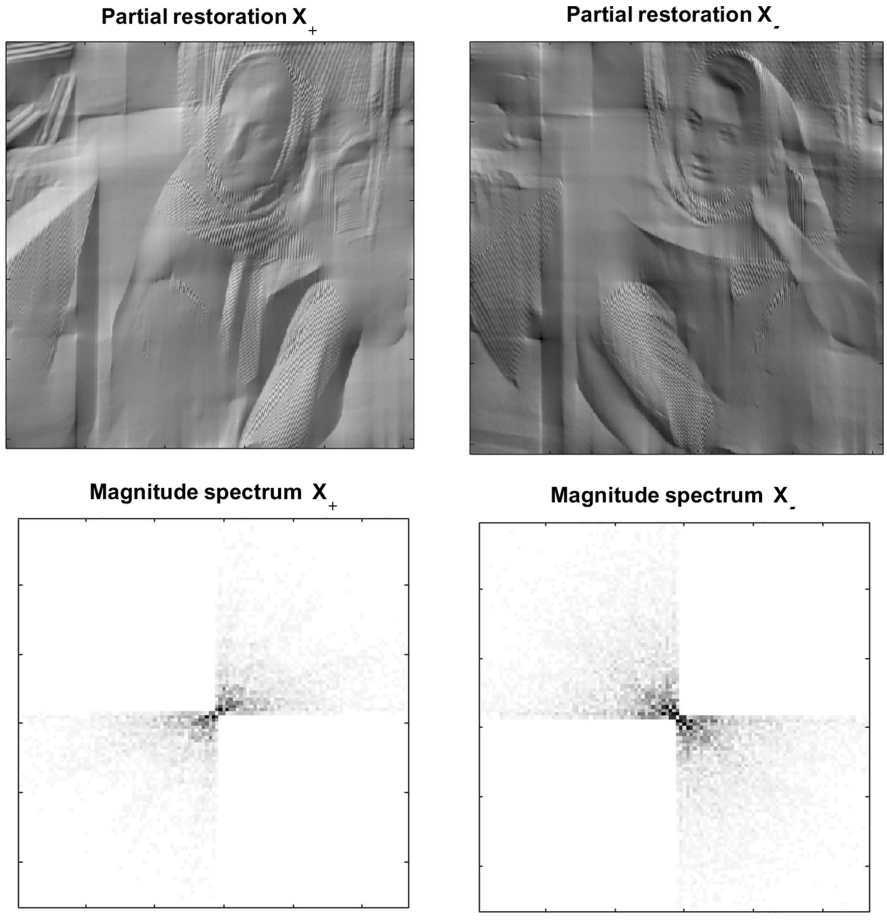

Fig. 6.2. Top: Partially restored "Barbara" image by $\mathfrak{Re}(\mathbf{X}_+)$ (left) and by $\mathfrak{Re}(\mathbf{X}_-)$ (right). Bottom: Magnitude DFT spectrum of $\mathbf{X}_+$ (left) and spectrum of $\mathbf{X}_-$ (right).

Fig. 6.3. Left: Original "Barbara" image. Right: Fully restored image by $\mathfrak{Re}(\mathbf{X}_+ + \mathbf{X}_-)/8$.

determined by their analysis modulation matrices $\tilde{\mathbf{M}}[2^m n],\ m = 1, ..., M-1$, to the coefficients arrays $\mathbf{z}^{\lambda}_{\pm[m]}$. The transforms applied to the arrays $\mathbf{z}^{\lambda}_{\pm[m]}$ produce the arrays $\mathbf{z}^{\rho}_{\pm[m+1]}$, respectively. The inverse transform consists of the iterated application of the filter banks that are determined by their synthesis modulation

Please cite this article in press as: A. Averbuch et al., Analytic and directional wavelet packets in the space of periodic signals, Appl. Comput. Harmon. Anal. (2023), https://doi.org/10.1016/j.acha.2023.06.006

matrices $\mathbf{M}[2^m n],\ m = 1, ..., M-1$, to the coefficients arrays $\mathbf{z}^{\rho}_{\pm[m+1]}$. In that way the first-level coefficient arrays $\mathbf{z}^{\lambda}_{\pm[1]},\ \lambda = 0, 1$ are restored.

The tensor-product of the 2D transforms of a signal $\mathbf{X} \in \Pi[N, N]$ consists of the subsequent application of the 1D transforms to columns and rows of the signal and coefficients arrays. By application of filter banks, which are determined by the analysis modulation matrix $\tilde{\mathbf{M}}[2n]$ to columns and rows of coefficients array $\mathbf{Z}^{j,l}_{\pm[1]}$, we derive four second-level arrays $\mathbf{Z}^{\rho,\tau}_{\pm[2]},\ \rho = 2j, 2j+1;\ \tau = 2l, 2l+1$. The arrays $\mathbf{Z}^{j,l}_{\pm[1]}$ are restored by the application of the filter banks that are determined by their synthesis modulation matrices $\mathbf{M}[2n]$ to rows and columns of the coefficients arrays $\mathbf{Z}^{\rho,\tau}_{\pm[2]},\ \rho = 2j, 2j+1;\ \tau = 2l, 2l+1$. The transition from the second to further levels and back are executed similarly using the modulation matrices $\tilde{\mathbf{M}}[2^m n]$ and $\mathbf{M}[2^m n]$, respectively. The inverse transforms produce the coefficients arrays $\mathbf{Z}^{j,l}_{\pm[1]},\ j, l = 0, 1$, from which the signal $\mathbf{X} \in \Pi[N, N]$ is restored using the synthesis modulation matrices $\mathbf{M}^{q}_{\pm}[n]$ as it is explained in Section 6.1.2.

All the computations are implemented in the frequency domain using the FFT. For example, the Matlab execution of the 2D qWP transform of a 512×512 image down to the sixth decomposition level takes 1.34 seconds. The four-level transform takes 0.28 second.

Summary The 2D qWP processing of a signal $\mathbf{X} \in \Pi[N, N]$ is implemented by a dual-tree scheme. The first step produces two sets of the coefficients arrays: $\mathbf{Z}_{+[1]} = \left\{\mathbf{Z}^{j,l}_{+[1]}\right\},\ j, l, = 0, 1$, which are derived using the analysis modulation matrix $\tilde{\mathbf{M}}^{q}_{+}[n]$, and $\mathbf{Z}_{-[1]} = \left\{\mathbf{Z}^{j,l}_{-[1]}\right\},\ j, l, = 0, 1$, which are derived using the analysis modulation matrix $\tilde{\mathbf{M}}^{q}_{-}[n]$. Further decomposition steps are implemented in parallel on the sets $\mathbf{Z}_{+[1]}$ and $\mathbf{Z}_{-[1]}$ using the same analysis modulation matrix $\tilde{\mathbf{M}}[2^m n]$, thus producing two multi-level sets of the coefficients arrays $\left\{\mathbf{Z}^{j,l}_{+[m]}\right\}$ and $\left\{\mathbf{Z}^{j,l}_{-[m]}\right\},\ m = 2, ..., M,\ j, l = 0, 2^m - 1$.

By parallel implementation of the inverse transforms on the coefficients from the sets $\left\{\mathbf{Z}^{j,l}_{+[m]}\right\}$ and $\left\{\mathbf{Z}^{j,l}_{-[m]}\right\}$ using the same synthesis modulation matrix $\mathbf{M}[2^m n]$, the sets $\mathbf{Z}_{+[1]}$ and $\mathbf{Z}_{-[1]}$ are restored, which, in turn, provide the signals $\mathbf{X}_{+}$ and $\mathbf{X}_{-}$, using the synthesis modulation matrices $\mathbf{M}^{q}_{+}[n]$ and $\mathbf{M}^{q}_{-}[n]$, respectively. Typical signals $\mathbf{X}_{\pm}$ and their DFT spectra are displayed in Fig. 6.2.

Prior to the reconstruction, some structures, possibly different, are defined in the sets $\left\{\mathbf{Z}^{j,l}_{+[m]}\right\}$ and $\left\{\mathbf{Z}^{j,l}_{-[m]}\right\},\ m = 1, ...M$, (2D wavelet or Best Basis structures, for example) and some manipulations on the coefficients, (thresholding, l_1 minimization, for example) are executed.

7. Numerical examples

In this section, we present examples of application of the 2D qWPs to image restoration. The experiments are aimed to confirm the feasibility of the qWPs for such problems rather than to achieve state-of-the-art results. The examples illustrate the ability of the qWPs to restore edges and texture details even from severely damaged images. Certainly, this ability stems from the fact that the designed 2D qWP transforms provide a variety of 2D waveforms oriented in multiple directions, from perfect frequency resolution of these waveforms and, last but not least, from oscillatory structure of many waveforms.

7.1. Denoising examples

One of the best image denoising methods is the BM3D algorithm ([16]), which exploits the non-local self-similarity (NSS) and sparsity of images in a transform domain. This method is especially efficient with restoration of moderately noised images. However, the BM3D tends to over-smooth and smear the image fine structure and edges when noise is strong. Also, the BM3D is not success when the image contains many edges

Please cite this article in press as: A. Averbuch et al., Analytic and directional wavelet packets in the space of periodic signals, Appl. Comput. Harmon. Anal. (2023), https://doi.org/10.1016/j.acha.2023.06.006

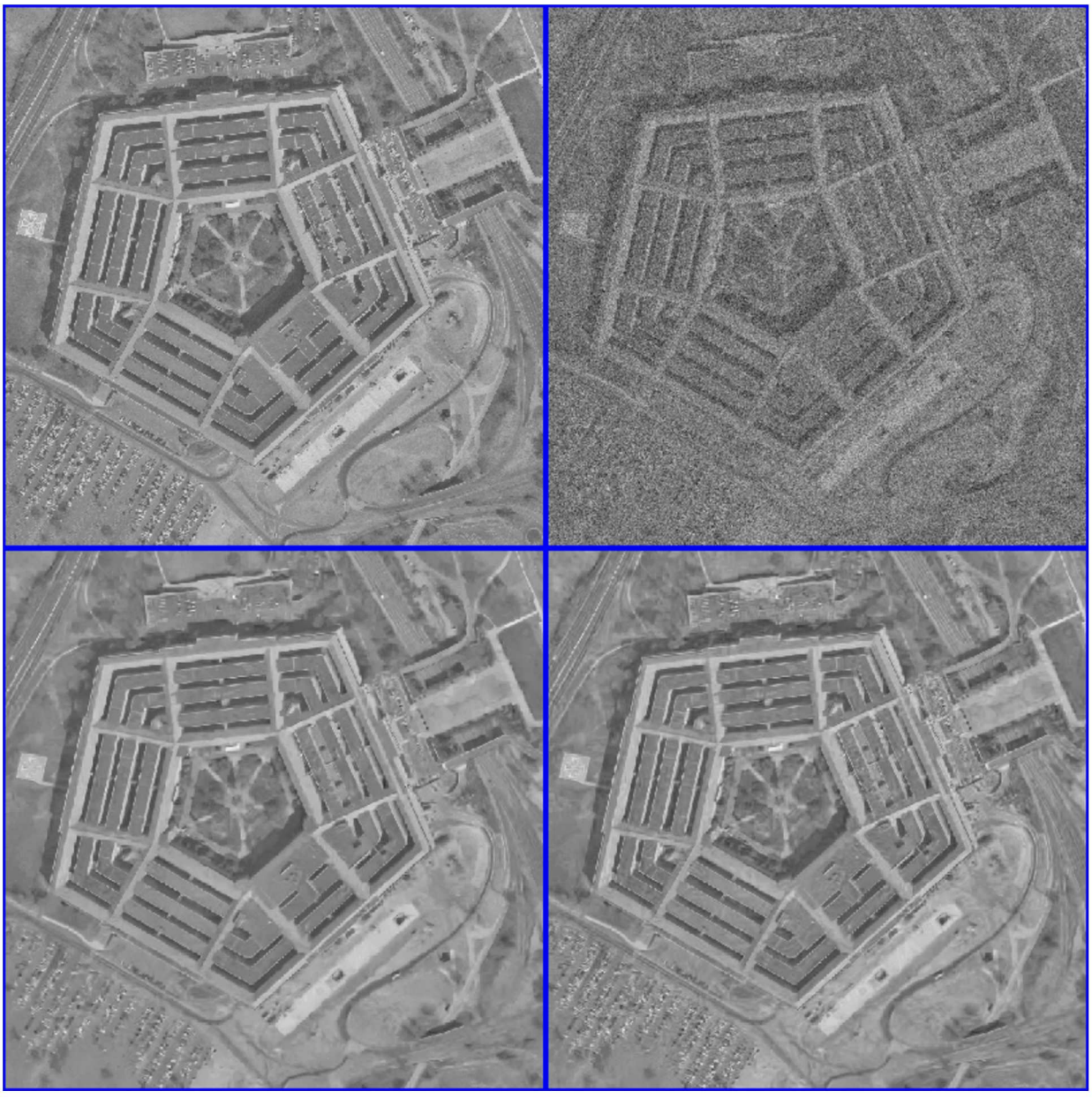

Fig. 7.1. Top left: Original "Pentagon" image. Top right: Image corrupted by noise with $\sigma = 40$ dB, PSNR=16.09 dB. Bottom right: The hybrid-restored image $\mathbf{X}_h$, PSNR=27.29 dB. Bottom left: BM3D-restored image $\mathbf{X}_{bm}$, PSNR=27.09 dB.

oriented in multiple directions. On the other hand, algorithms that use directional oscillating waveforms provide an opportunity to capture lines, edges and texture details. Therefore, it is natural to combine the qWP-based and BM3D algorithms in order to retain strong features of both algorithms and to get rid of their drawbacks. The qWP-based denoising method (qWPdn) consists of multiscale qWP transform of the degraded image, application of adaptive localized soft thresholding to the transform coefficients using the *Bivariate Shrinkage* methodology [15], and restoration of the image from the thresholded coefficients from several decomposition levels. The hybrid qWPdn–BM3D method consists of several iterations of qWPdn and BM3D algorithms in a way that at each iteration, the output from one algorithm boosts the input to the other. The scheme is outlined in Appendix.

Please cite this article in press as: A. Averbuch et al., Analytic and directional wavelet packets in the space of periodic signals, Appl. Comput. Harmon. Anal. (2023), https://doi.org/10.1016/j.acha.2023.06.006

Fig. 7.2. Fragments of the images shown in Fig. 7.1.

A couple of following examples illustrate advantages of such a hybrid method over the original BM3D algorithm.

7.1.1. Example I: "pentagon" image

The "Pentagon" image $\mathbf{X}$ of size 1024×1024 was corrupted by additive Gaussian noise with σ=40 dB. As a result, the PSNR of the corrupted image $\mathbf{X}_\sigma$ was 16.09 dB.

The corrupted image was restored by the BM3D and hybrid algorithms. For the latter algorithm, directional qWPs $\Psi^8_{++[m]}$ and $\Psi^8_{+-[m]}$ originating from the eighth-order discrete splines were used.

Figs. 7.1 and 7.2 display the outputs from the "Pentagon" image reconstruction by the hybrid and the original BM3D algorithms. The hybrid-restored image $\mathbf{X}_h$ has PSNR=27.29 dB versus PSNR=27.09 dB for the BM3D-restored image $\mathbf{X}_{bm}$. Visually, image $\mathbf{X}_h$ is cleaner in comparison to $\mathbf{X}_{bm}$ and more fine details are restored.

7.1.2. Example II: "barbara" image

We present two cases with the "Barbara" image. In one case, the image was corrupted by an additive Gaussian noise with σ=40 dB and in the other, the noise was more intensive with σ=60 dB. In both cases, the "Barbara" image was restored by the same scheme as the "Pentagon" image above.

Noise with σ=40 dB: Figs. 7.3 and 7.4 are the outputs from the image reconstruction by using the hybrid qWPT-BM3D algorithm and the original BM3D algorithm. The qWPT-BM3D-restored image $\mathbf{X}_h$ has

Please cite this article in press as: A. Averbuch et al., Analytic and directional wavelet packets in the space of periodic signals, Appl. Comput. Harmon. Anal. (2023), https://doi.org/10.1016/j.acha.2023.06.006

Fig. 7.3. Top left: Original "Barbara" image. Top right: Image corrupted by noise with σ=40 dB, PSNR=16.09 dB. Bottom right: The hybrid-restored image $\mathbf{X}_h$, PSNR=28.55 dB. Bottom left: BM3D restored image $\mathbf{X}_{bm}$, PSNR=28.19 dB.

PSNR=28.55 dB versus PSNR=28.19 dB for the BM3D-restored image $\mathbf{X}_{bm}$. Visually, the image $\mathbf{X}_h$ is cleaner in comparison to $\mathbf{X}_{bm}$ and almost all edges and the texture structure are restored.

Noise with σ=60 dB: In this case, the PSNR of the corrupted image was 12.57 dB. The same operations as in the previous case were applied to the corrupted image. Figs. 7.5 and 7.6 display results of the image reconstruction by using the hybrid qWPT-BM3D algorithm and the original BM3D algorithm. The hybrid-restored image $\mathbf{X}_h$ has PSNR=26.51 dB versus PSNR=26.34 dB for the BM3D-restored image $\mathbf{X}_{bm}$. Visually, the image $\mathbf{X}_h$ is much cleaner in comparison to $\mathbf{X}_{bm}$ and many edges and the texture structure are restored.

7.2. Image restoration examples

In this section we present a few cases of image restoration using directional qWPs. Images to be restored were degraded by blurring, aggravated by random noise and random loss of significant number of pixels. In our previous work ([3] and Chapter 18 in [6]) we developed the image restoration scheme utilizing 2D wavelet frames designed in Chapter 18 of [6]. In the examples presented below we use, generally, the same

Please cite this article in press as: A. Averbuch et al., Analytic and directional wavelet packets in the space of periodic signals, Appl. Comput. Harmon. Anal. (2023), https://doi.org/10.1016/j.acha.2023.06.006

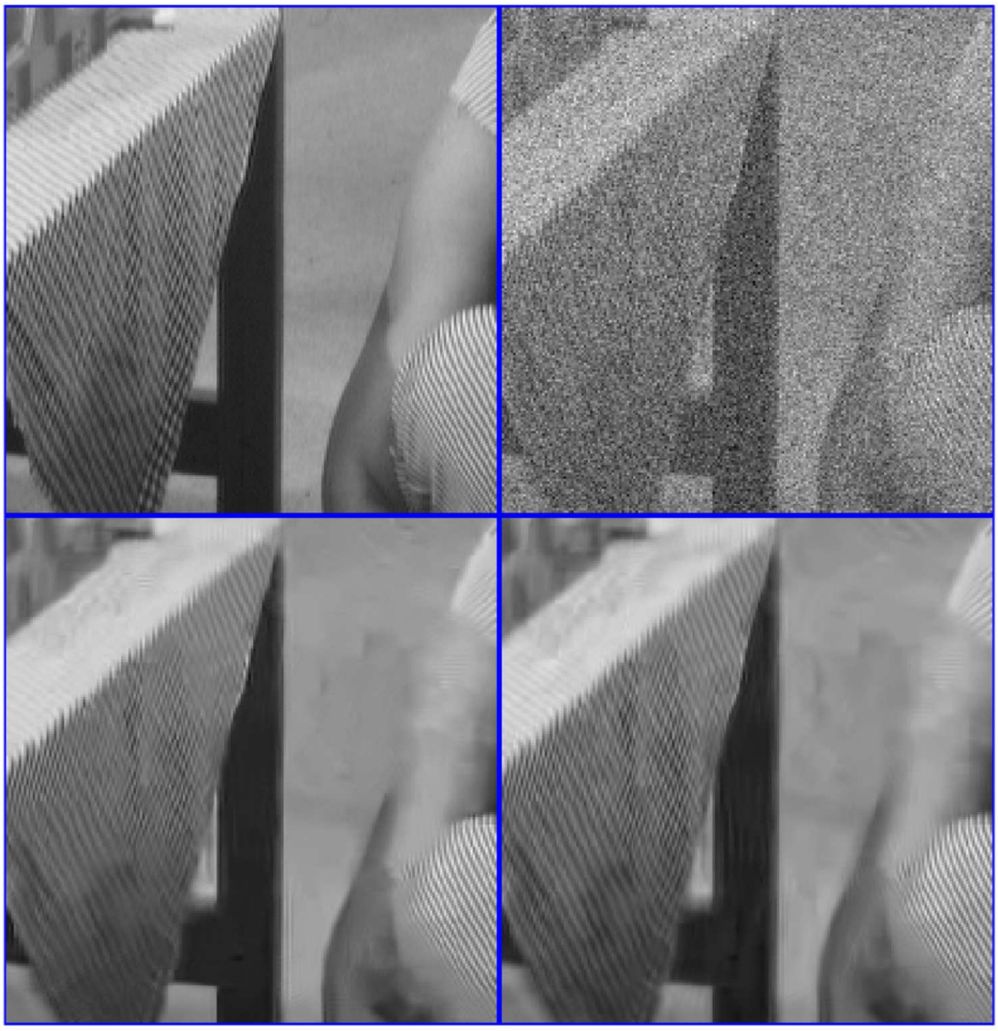

Fig. 7.4. Fragments of the images shown in Fig. 7.3.

scheme as in [6] with the difference that the directional qWPs designed in Section 6 are used instead of wavelet frames.

7.2.1. Brief outline of the restoration scheme

Images are restored by the application of the *split Bregman iteration* (SBI) scheme [19] that uses the so-called *analysis-based* approach (see for example [27]).

Denote by $\mathbf{u} = \{u[\kappa, \nu]\}$ the original image array to be restored from the degraded array $\mathbf{f} = \mathbf{K}\,\mathbf{u} + \varepsilon$, where $\mathbf{K}$ denotes the operator of 2D discrete convolution of the array $\mathbf{u}$ with a kernel $\mathbf{k} = \{k[\kappa, \nu]\}$, and $\varepsilon = \{e_{k,n}\}$ is the random error array. $\mathbf{K}^*$ denotes the conjugate operator of $\mathbf{K}$, which implements the discrete convolution with the transposed kernel $\mathbf{k}^T$. If some number of pixels are missing then the image $\mathbf{u}$ should be restored from the available data

$$\mathbf{P}_\Lambda\,\mathbf{f} = \mathbf{P}_\Lambda\,(\mathbf{K}\,\mathbf{u} + \varepsilon), \tag{7.1}$$

where $\mathbf{P}_\Lambda$ denotes the projection on the remaining set of pixels.

The solution scheme is based on the assumption that the original image $\mathbf{u}$ can be sparsely represented in the qWP domain. Denote by $\tilde{\mathbf{F}}$ the operator of qWP expansion of the image $\mathbf{u}$. To be specific, the 2D

Please cite this article in press as: A. Averbuch et al., Analytic and directional wavelet packets in the space of periodic signals, Appl. Comput. Harmon. Anal. (2023), https://doi.org/10.1016/j.acha.2023.06.006

Fig. 7.5. Top left: Original "Barbara" image. Top right: Image corrupted by noise with σ=60 dB, PSNR=12.57 dB. Bottom right: The qWPT–BM3D-restored image $\mathbf{X}_h$, PSNR=26.51 dB. Bottom left: BM3D-restored image $\mathbf{X}_{nd}$, PSNR=26.34 dB.

transform of the signal $\mathbf{X}$ with directional qWP $\Psi^{2r}_{++[m]}$ and $\Psi^{2r}_{+-[m]}$ down to level M is implemented to generate two sets of the coefficients arrays $\left\{\mathbf{Z}^{j,l}_{+[m]}\right\}$ and $\left\{\mathbf{Z}^{j,l}_{-[m]}\right\}$, $m = 1, ...M,\ j, l = 0, ..., 2^m - 1$. In each of the sets $\left\{\mathbf{Z}^{j,l}_{\pm[m]}\right\}$ either "Best Basis" or "basis", which consist of shifts of all the WPs from the decomposition level M, are selected. The bases are designated by $\mathbf{B}_{\pm[M]}$. The number of the transform coefficients $\mathbf{Z}_{\pm[B]}$ associated with each basis is the same as the number N^2 of pixels in the image. Thus, $\mathbf{C} \stackrel{\text{def}}{=} \tilde{\mathbf{F}}\,\mathbf{u} = \mathbf{Z}_{+[B]} \bigcup \mathbf{Z}_{-[B]}$ is the set of the transform coefficients.

Denote by $\mathbf{F}$ the reconstruction operator of the image $\mathbf{u}$ from the set of the transform coefficients. We get $\mathbf{F}\,\mathbf{C} = \mathbf{u} = \mathfrak{Re}(\mathbf{u}_+ + \mathbf{u}_-)/8$, $\mathbf{F}\,\tilde{\mathbf{F}} = \mathbf{I}$, where $\mathbf{I}$ is the identity operator.

An approximate solution to Eq. (7.1) is derived via minimization of the functional

$$\min_u \frac{1}{2} \left\|\mathbf{P}_\Lambda \left(\mathbf{K}\,\mathbf{u} - f\right)\right\|_2^2 + \lambda \left\|\tilde{\mathbf{F}}\,\mathbf{u}\right\|_1, \tag{7.2}$$

where $\|\cdot\|_1$ and $\|\cdot\|_2$ are the l_1 and the l_2 norms of the sequences, respectively. If $\mathbf{x} = \{x[\kappa, \nu]\}$, $\kappa = 0, ..., k,\ \nu = 0, ..., n$, then

Please cite this article in press as: A. Averbuch et al., Analytic and directional wavelet packets in the space of periodic signals, Appl. Comput. Harmon. Anal. (2023), https://doi.org/10.1016/j.acha.2023.06.006

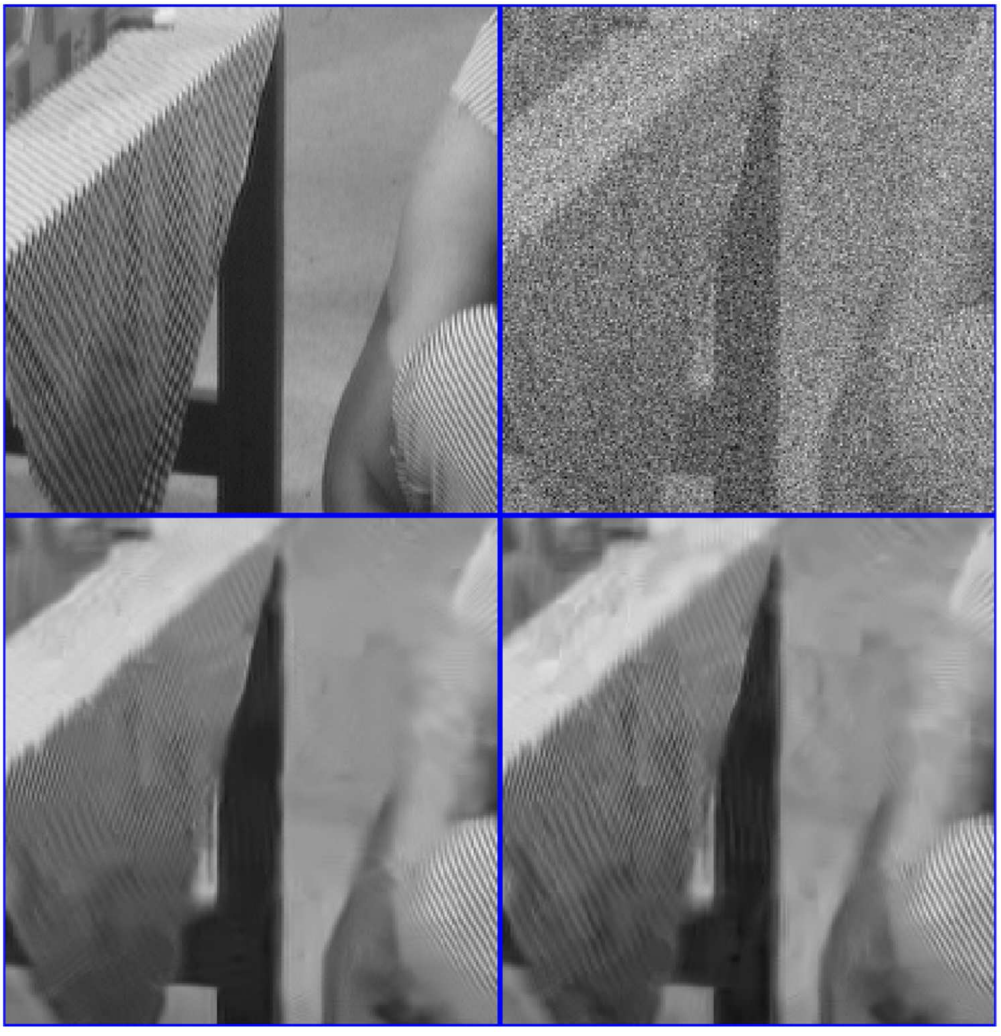

Fig. 7.6. Fragments of the images shown in Fig. 7.5.

$$\|\mathbf{x}\|_1 \stackrel{\text{def}}{=} \sum_{\kappa=0}^{k-1}\sum_{\nu=0}^{n-1} |x[\kappa,\nu]|, \quad \|\mathbf{x}\|_2 \stackrel{\text{def}}{=} \sqrt{\sum_{\kappa=0}^{k-1}\sum_{\nu=0}^{n-1} |x[\kappa,\nu]|^2}.$$

Denote by $\mathbf{T}_\vartheta$ the operator of soft thresholding:

$$\mathbf{T}_\vartheta\,\mathbf{x} = \{x_\vartheta[\kappa,\nu]\}\,, \quad x_\vartheta[\kappa,\nu] \stackrel{\text{def}}{=} \operatorname{sgn}(x[\kappa,\nu])\,\max\{0, |x[\kappa,\nu]| - \vartheta\}\,.$$

Following [27], we solve the minimization problem in Eq. (7.2) by an iterative SBI algorithm. We begin with the initialization $\mathbf{u}^0 = 0,\ \mathbf{d}^0 = \mathbf{b}^0 = 0$. Then,

$$\begin{aligned} \mathbf{u}^{k+1} &:= (\mathbf{K}^*\,\mathbf{P}_\Lambda\,\mathbf{K} + \mu\,\mathbf{I})\,\mathbf{u} = \mathbf{K}^*\,\mathbf{P}_\Lambda\,\mathbf{f} + \mu\,\mathbf{F}\,(\mathbf{d}^k - \mathbf{b}^k), \\ \mathbf{d}^{k+1} &= \mathbf{T}_{\lambda/\mu}(\tilde{\mathbf{F}}\,\mathbf{u}^{k+1} + \mathbf{b}^k), \\ \mathbf{b}^{k+1} &= \mathbf{b}^k + (\tilde{\mathbf{F}}\,\mathbf{u}^{k+1} - \mathbf{d}^{k+1}). \end{aligned} \tag{7.3}$$

The linear system in the first line of Eq. (7.3) is solved by the application of the *conjugate gradient* algorithm. The operations in the second and third lines are straightforward. The choice of the parameters λ and μ depends on experimental conditions.

Please cite this article in press as: A. Averbuch et al., Analytic and directional wavelet packets in the space of periodic signals, Appl. Comput. Harmon. Anal. (2023), https://doi.org/10.1016/j.acha.2023.06.006

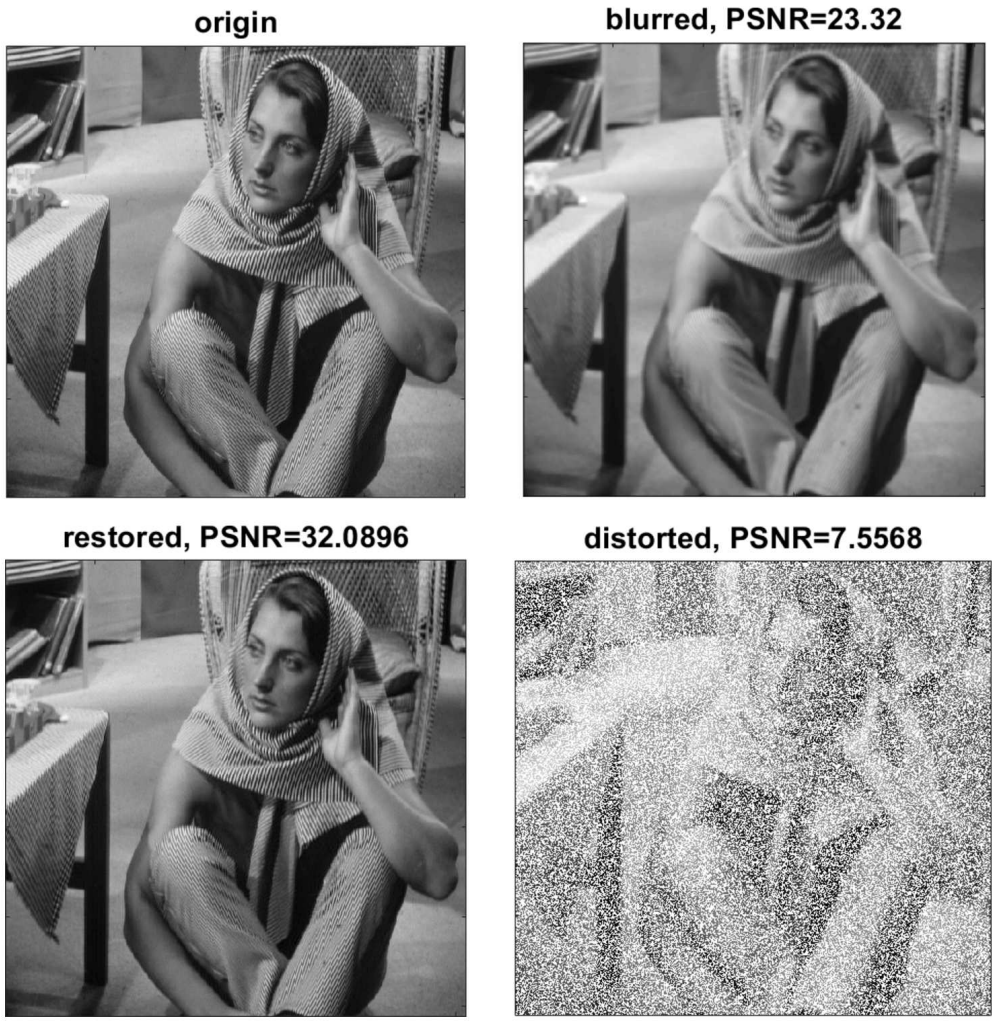

Fig. 7.7. Top left: Source input - "Barbara" image. Top right: Blurred, PSNR=23.32 dB. Bottom right: After random removal of 50% of its pixels. PSNR=7.56 dB. Bottom left: The image restored by the directional qWPT. PSNR=32.09 dB.

7.2.2. Examples

Example I: "Barbara" blurred, missing 50% of pixels: The "Barbara" image was restored after it was blurred by a convolution with the Gaussian kernel (MATLAB function `fspecial`('gaussian',[5 5])) and its PSNR became 23.32 dB. Then, 50% of its pixels were randomly removed. This reduced the PSNR to 7.56 dB. Random noise was not added. The image was restored by 50 SBI using the parameters $\lambda = 0.0015,\ \mu = 0.00014$ in Eq. (7.3). The conjugate gradient solver used 150 iterations. qWPs originating from discrete splines of sixth order were used. For "bases", 8-samples shifts of all the WPs from the third decomposition level were selected. Matlab implementation of the restoration procedures took 59.6 seconds.

Fig. 7.7 displays the restoration result. The image is deblurred and the fine texture is restored completely with PSNR=32.09 dB. Note that the best result in an identical experiment reported in [6] achieved PSNR=30.32 dB.

Example II: "Barbara" blurred, added noise, missing 50% of pixels: The "Barbara" image was restored after it was blurred by a convolution with the Gaussian kernel (MATLAB function `fspecial` ('gaussian',[5 5])). Random Gaussian noise with σ=10 dB was added and the image PSNR became 22.08 dB. Then, 50% of its pixels were randomly removed. This reduced the PSNR to 7.53

Please cite this article in press as: A. Averbuch et al., Analytic and directional wavelet packets in the space of periodic signals, Appl. Comput. Harmon. Anal. (2023), https://doi.org/10.1016/j.acha.2023.06.006

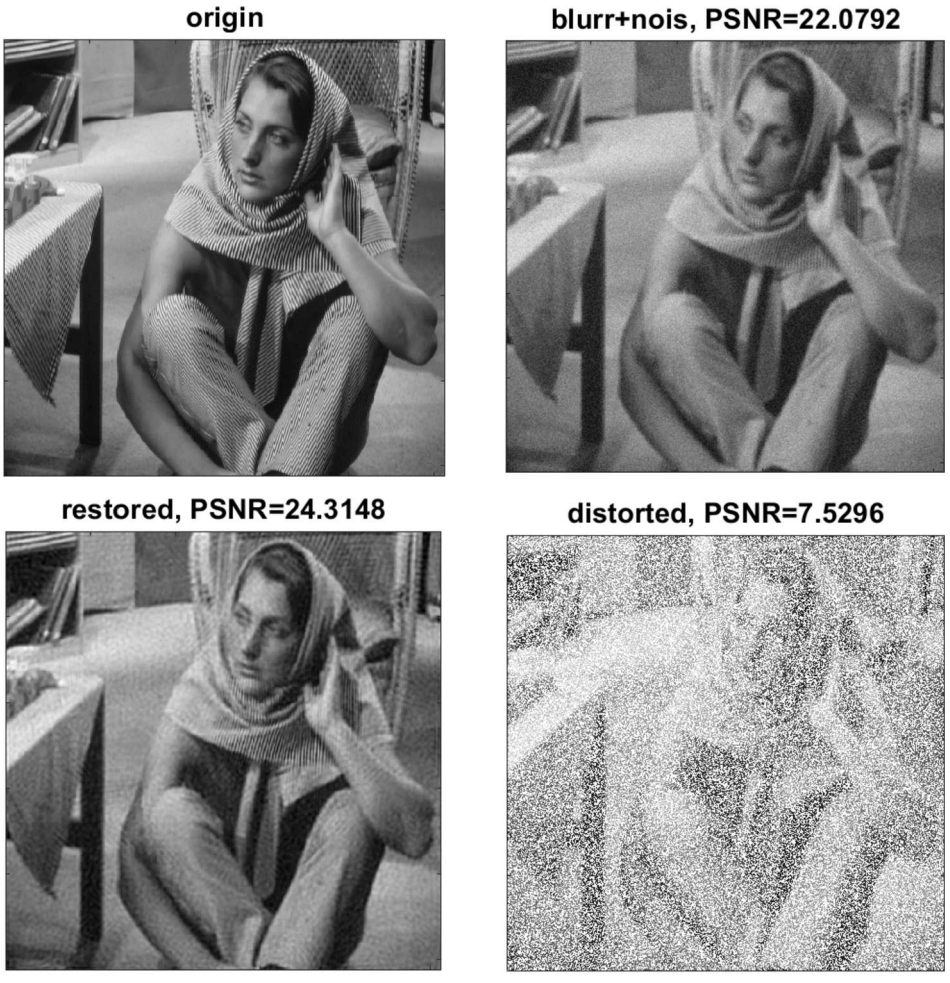

Fig. 7.8. Top left: Source input - "Barbara" image. Top right: Blurred and noised, PSNR=22.08 dB. Bottom right: After random removal of 50% of its pixels. PSNR=7.53 dB. Bottom left: The restored image by the directional qWPT. PSNR=24.31 dB.

dB. The image was restored by 70 SBI using the parameters $\lambda = 3,\ \mu = 0.025$ in Eq. (7.3). The conjugate gradient solver used 15 iterations. qWPs originating from discrete splines of fourth order were used. For the "bases", 16-samples shifts of all the WPs from the fourth decomposition level were selected. Matlab implementation of the restoration procedures took 51.9 seconds.

Fig. 7.8 displays the restoration result. The image is deblurred, noise is removed and the fine texture is partially restored producing PSNR=24.31 dB. Note that the best result in an identical experiment reported in [6] achieved PSNR=24.19 dB.

Example III: "Barbara" blurred, missing 90% of pixels: The "Barbara" image was restored after it was blurred by a convolution with the Gaussian kernel (MATLAB function `fspecial`('gaussian',[5 5])) and 90% of its pixels were randomly removed. This reduced the PSNR to 5.05 dB. The image was restored by 150 SBI using the parameters $\lambda = 0.0025,\ \mu = 0.000025$ in Eq. (7.3). The conjugate gradient solver used 150 iterations. qWPs originating from discrete splines of eighth order were used. For the "bases", 16-samples shifts of all the WPs from the fourth decomposition level were selected. Matlab implementation of the restoration procedures took 226.8 seconds.

Fig. 7.9 displays the restoration result. The image is deblurred and the fine texture is partially restored. The output has PSNR=25.24 dB.

Please cite this article in press as: A. Averbuch et al., Analytic and directional wavelet packets in the space of periodic signals, Appl. Comput. Harmon. Anal. (2023), https://doi.org/10.1016/j.acha.2023.06.006

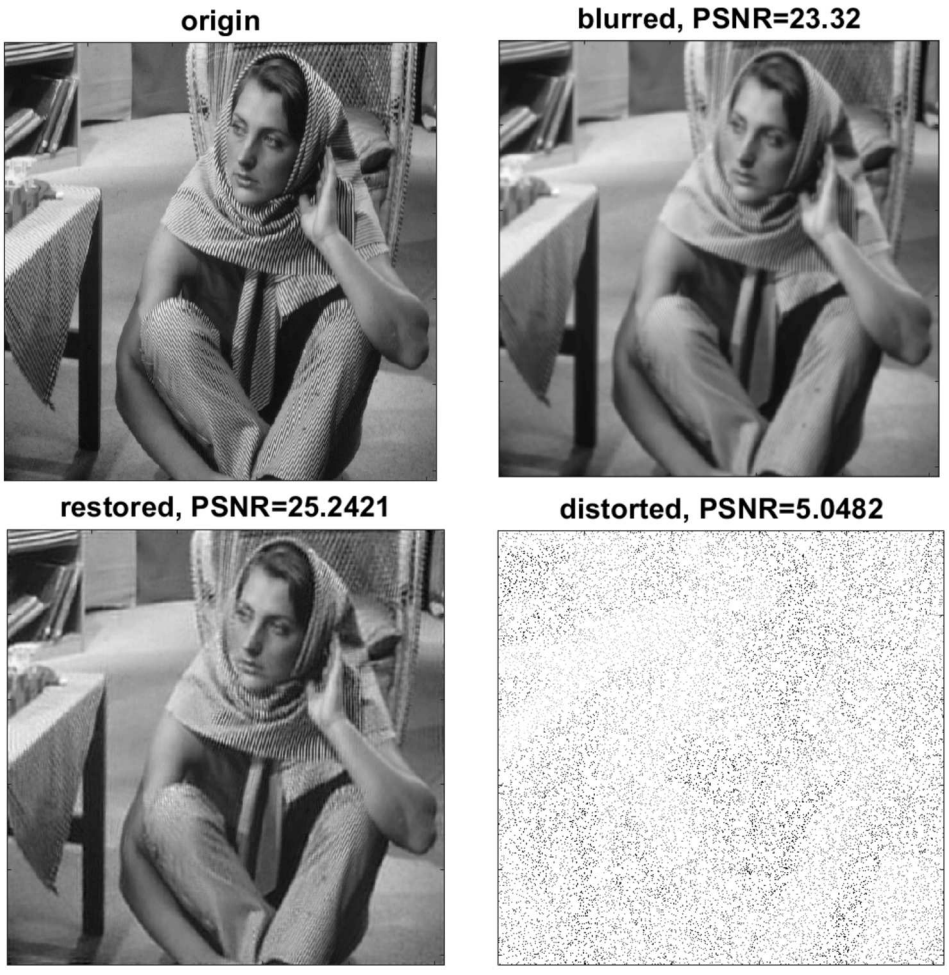

Fig. 7.9. Top left: Source input - "Barbara" image. Top right: Blurred, PSNR=23.32 dB. Bottom right: After random removal of 90% of its pixels. PSNR=5.05 dB. Bottom left: The image restored by the directional qWPT. PSNR=25.24 dB.

8. Discussion

We presented a library of complex discrete-time wavelet packets operating in one- or two-dimensional spaces of periodic signals. Seemingly, the requirement of periodicity imposes some limitations on the scope of signals available for processing, but actually these limitations are easily circumvented. Any limited signal can be regarded as one period of a periodic signal. In order to prevent boundary effects, the signals can be symmetrically extended beyond the boundaries before processing and shrunk to the original size after that. We used such a trick in the "Barbara" denoising examples.

On the other hand, the periodic setting provides a lot of substantial opportunities for the design and implementation of WP transforms such as

- A unified computational scheme based on 1D and 2D FFT.
- Opportunity to use filters with infinite impulse responses, which enables us to design a variety of orthonormal WP systems where WPs can have any number of local vanishing moments.
- The number of local vanishing moments does not affect the computational cost of the transforms implementation.
- A simple explicit scheme of expansion of real WPs to analytic and quasi-analytic WPs with perfect frequency separation.

Please cite this article in press as: A. Averbuch et al., Analytic and directional wavelet packets in the space of periodic signals, Appl. Comput. Harmon. Anal. (2023), https://doi.org/10.1016/j.acha.2023.06.006

The library of qWP transforms described in the paper has a number of free parameters enabling the designer to adapt the transforms to the problem under consideration:

- Order of the generating spline, which determines the number of local vanishing moments.
- Depth of decomposition, which in 2D case determines the directionality of qWPs. For example, fourth-level qWPs are oriented in 314 different directions.
- Selection of an optimal structure, such as, for example, separate Best Bases in the real and imaginary parts of 1D qWP transforms, separate "Best Bases" in positive and negative branches of 2D dual-tree qWP transforms, a wavelet-basis structure or the set of all wavelet packets from a single level.
- Controllable redundancy rate of the signal representation. The minimal rate is 2 when one of options listed in a previous item is utilized. However, several basis-type structures can be involved, for example, all wavelet packets from several levels can be used for the signal reconstruction and results can be averaged.

The goal of the paper is to design qWPs with an efficient computational scheme for the corresponding transforms. A few experimental results highlight exceptional properties of these WPs. The directional qWPs are tested on image restoration examples. In the denoising examples, compared the performance of the popular BM3D denoising algorithm ([16]) with the performance of the hybrid qWP-BM3D algorithm, which exploits best features of the BM3D and qWP-based methods. The hybris algorithm demonstrated an advantage over the original BM3D algorithm.

The second group of experimental results dealt with the restoration of the "Barbara" image which was blurred by convolving the image with a Gaussian kernel and degraded by removing randomly either 50% or 90% of the pixels. The image was restored by using a constrained l_1 minimization of the qWP transform coefficients from a certain decomposition level and implemented via the split Bregman Iterations procedure. In Example I with missing 50% of the pixels, the image was satisfactorily restored with PSNR-32.1 dB and practically whole fine structure reconstructed although it was blurred even before the removal of the pixels. Addition of the Gaussian noise with $\sigma = 10$ dB to the blurred image in Example II depleted the reconstruction result. Although the noise became suppressed and the image was deblurred, most of the fine structure was lost. Restoration results were better in Example III where, instead of adding noise, the number of pixels missing from the blurred image was raised to 90%. The image was deblurred and an essential part of fine structure was restored.

Summarizing, we can state that, having such a versatile and flexible tool at hand, we are prepared to address multiple data processing problems such as signal and image deblurring and denoising, target detection, segmentation, inpainting, superresolution, to name a few. In one of the applications, directional qWPs are used with Compressed Sensing methodology for the conversion of a regular digital photo camera to an hyperspectral imager. Preliminary results appear in [20].

Data availability

Data will be made available on request.

Acknowledgment

This research was partially supported by the Israel Science Foundation (ISF, 1556/17, 1873/21), Blavatnik Computer Science Research Fund, Israeli Ministry of Science, Technology and Space (3-13601, 3-16414, 3-17927) and by Academy of Finland (grant 311514).

Please cite this article in press as: A. Averbuch et al., Analytic and directional wavelet packets in the space of periodic signals, Appl. Comput. Harmon. Anal. (2023), https://doi.org/10.1016/j.acha.2023.06.006

Appendix A

A.1. Proof of Proposition 4.2

Proof. Let $\mathbf{M}^q \stackrel{\text{def}}{=} \mathbf{M}^q_+$.

$$\mathbf{M}^q[n]\cdot\begin{pmatrix}\hat{z}^0_{[1]}[n]_1\\ \hat{z}^1_{[1]}[n]_1\end{pmatrix} = (\mathbf{M}[n]+i\,\mathbf{M}^c[n])\cdot\left(\begin{pmatrix}\hat{y}^0_{[1]}[n]_1\\ \hat{y}^1_{[1]}[n]_1\end{pmatrix} - i\begin{pmatrix}\hat{c}^0_{[1]}[n]_1\\ \hat{c}^1_{[1]}[n]_1\end{pmatrix}\right)$$

$$= \mathbf{M}[n]\cdot\begin{pmatrix}\hat{y}^0_{[1]}[n]_1\\ \hat{y}^1_{[1]}[n]_1\end{pmatrix} + \mathbf{M}^c[n]\cdot\begin{pmatrix}\hat{c}^0_{[1]}[n]_1\\ \hat{c}^1_{[1]}[n]_1\end{pmatrix} + i\vec{P}[n] = 2\begin{pmatrix}\hat{x}[n]\\ \hat{x}[\vec{n}]\end{pmatrix} + i\vec{P}[n],$$

$$\vec{P}[n] \stackrel{\text{def}}{=} \mathbf{M}^c[n]\cdot\begin{pmatrix}\hat{y}^0_{[1]}[n]_1\\ \hat{y}^1_{[1]}[n]_1\end{pmatrix} - \mathbf{M}[n]\cdot\begin{pmatrix}\hat{c}^0_{[1]}[n]_1\\ \hat{c}^1_{[1]}[n]_1\end{pmatrix}.$$

The vector $\vec{P}[n]$ can be represented by $\vec{P}[n] = \mathbf{R}[n]\cdot\begin{pmatrix}\hat{x}[n]\\ \hat{x}[\vec{n}]\end{pmatrix}$, where

$$\mathbf{R}[n] = \frac{1}{2}\left(\mathbf{M}^c[n]\cdot\tilde{\mathbf{M}}[-n] - \mathbf{M}[n]\cdot\tilde{\mathbf{M}}^c[-n]\right).$$

For $n\neq 0$ and $\vec{n} = n + N/2$, the product $\mathbf{M}^c[n]\cdot\tilde{\mathbf{M}}[-n]$ is

$$\mathbf{M}^c[n]\cdot\tilde{\mathbf{M}}[-n] = \begin{pmatrix}-i\beta_{[0]}[n] & -i\alpha_{[0]}[n]\\ i\beta_{[0]}[\vec{n}] & i\alpha_{[0]}[\vec{n}]\end{pmatrix}\cdot\begin{pmatrix}\beta_{[0]}[-n] & \beta_{[0]}[\vec{-n}]\\ \alpha_{[0]}[-n] & \alpha_{[0]}[\vec{-n}]\end{pmatrix}$$

$$\begin{pmatrix}-i|\beta_{[0]}[n]|^2 - i|\alpha_{[0]}[n]|^2 & -i\beta_{[0]}[n]\,\beta_{[0]}[\vec{-n}] - i\alpha_{[0]}[\vec{n}]\,\alpha_{[0]}[\vec{-n}]\\ i\beta_{[0]}[\vec{n}]\,\beta_{[0]}[-n] + i\alpha_{[0]}[\vec{n}]\,\alpha_{[0]}[-n] & i|\beta_{[0]}[n]|^2 + i|\alpha_{[0]}[\vec{n}]|^2\end{pmatrix}.$$

Equations (2.3) imply that

$$|\beta_{[0]}[n]|^2 + \alpha_{[0]}[n]|^2 = 2\frac{\cos^{4r}\frac{\pi\,n}{N} + \sin^{4r}\frac{\pi\,n}{N}}{\cos^{4r}\frac{\pi\,n}{N} + \sin^{4r}\frac{\pi\,n}{N}} = 2,$$

$$\beta_{[0]}[\vec{n}]\,\beta_{[0]}[-n] + \alpha_{[0]}[\vec{n}]\,\alpha_{[0]}[-n] = 2\frac{\sin^{2r}\frac{\pi\,n}{N}\,\cos^{2r}\frac{\pi\,n}{N} - \cos^{2r}\frac{\pi\,n}{N}\,\sin^{2r}\frac{\pi\,n}{N}}{\cos^{4r}\frac{\pi\,n}{N} + \sin^{4r}\frac{\pi\,n}{N}} = 0,$$

$$\beta_{[0]}[n]\,\beta_{[0]}[\vec{-n}] + \alpha_{[0]}[n]\,\alpha_{[0]}[\vec{-n}] = 0.$$

Thus, for $n\neq 0$, the product $\mathbf{M}^c[n]\cdot\tilde{\mathbf{M}}[-n] = 2\begin{pmatrix}-i & 0\\ 0 & i\end{pmatrix}$. Similarly, the product $\mathbf{M}[n]\cdot\tilde{\mathbf{M}}^c[-n] = 2\begin{pmatrix}i & 0\\ 0 & -i\end{pmatrix}$.

When $n=0$, the product is $\mathbf{M}^c[0]\cdot\tilde{\mathbf{M}}[0] = \begin{pmatrix}\sqrt{2} & 0\\ 0 & -\sqrt{2}\end{pmatrix}\cdot\begin{pmatrix}\sqrt{2} & 0\\ 0 & -\sqrt{2}\end{pmatrix} = 2\mathbf{I}_2$ and, similarly, the product $\mathbf{M}[0]\cdot\tilde{\mathbf{M}}^c[0] = 2\mathbf{I}_2$, where $\mathbf{I}_2$ is the 2×2 identity matrix. As a result, we have

Please cite this article in press as: A. Averbuch et al., Analytic and directional wavelet packets in the space of periodic signals, Appl. Comput. Harmon. Anal. (2023), https://doi.org/10.1016/j.acha.2023.06.006

$$\mathbf{R}[n] = 2(1-\delta[n]) \begin{pmatrix} -i & 0 \\ 0 & i \end{pmatrix} \Longrightarrow \vec{P}[n] = \begin{cases} \begin{pmatrix} 0 \\ 0 \end{pmatrix}, & \text{if } n = 0; \\ 2 \begin{pmatrix} \hat{x}[n]/i \\ -\hat{x}[n+N/2]/i \end{pmatrix}, & \text{otherwise.} \end{cases}$$

For $\mathbf{M}^q \stackrel{\text{def}}{=} \mathbf{M}^q_-$ the proof is similar. □

A.2. Outline of hybrid denoising algorithm

Scheme of qWPdn The original image $\mathbf{X}$ of size $N \times N$ is corrupted by additive Gaussian noise with the standard deviation σ. The corrupted image $\mathbf{X}_\sigma$ is decomposed by the directional qWPs $\Psi^p_{++[m]}$ and $\Psi^p_{+-[m]}$ originating from the p-order discrete splines down to (M+1)-th level. In this way, two sets $\left\{\mathbf{Z}^{j,l}_{+[m]}\right\}$ and $\left\{\mathbf{Z}^{j,l}_{-[m]}\right\}$, $m = 1, ...M+1$, $j, l = 0, ..., 2^m - 1$, of the transform ş are produced. The transform ş from the (M+1)-th level are used for the bivariate shrinkage of M-th-level ş, which are used for the shrinkage of the ş from the (M-1)-th level, which in turn, are used for the shrinkage of the (M-2)-th-level ş. Then, the reconstruction from the "cleaned" (M-2)-, (M-1)- and M-level ş is implemented, which produces three restored images $\{\mathbf{X}_s\}$, $s = M-2, M-1, M$. The final qWP-based approximated image $\mathbf{X}_W$ is produced as a weighted average of the three images $\mathbf{X}_s$.

Boosting Denote by $\mathbf{W}$ and $\mathbf{B}$ the operators of application of the qWPdn, which is described above, and BM3D denoising algorithms, respectively, to a degraded array $\mathbf{A}$: $\mathbf{W}\,\mathbf{A} = \mathbf{D}_W$ and $\mathbf{B}\,\mathbf{A} = \mathbf{D}_B$.

Assume that we have an array $\mathbf{X}_\sigma$, which represents an image $\mathbf{X}$ degraded by additive Gaussian noise with the standard deviation σ. Denote $\check{\mathbf{X}}^0 \stackrel{\text{def}}{=} \mathbf{X}_\sigma$ (in the above setting, $\mathbf{W}\,\mathbf{X}_\sigma = \mathbf{X}_W$). The denoising processing is implemented along the following boosting scheme.

First step: Apply the operators $\mathbf{W}$ and $\mathbf{B}$ to the input array $\check{\mathbf{X}}^0$: $\mathbf{Y}^1_W = \mathbf{W}\,\check{\mathbf{X}}^0$ and $\mathbf{Y}^1_B = \mathbf{B}\,\check{\mathbf{X}}^0$.
Iterations: $i = 1, ..., I-1$

1. Form new input arrays $\check{\mathbf{X}}^i_W = \frac{\check{\mathbf{X}}^0 + \mathbf{Y}^i_W}{2}$, $\check{\mathbf{X}}^i_B = \frac{\check{\mathbf{X}}^0 + \mathbf{Y}^i_B}{2}$.
2. Apply the operators $\mathbf{W}$ and $\mathbf{B}$ to the new input arrays: $\mathbf{Y}^{i+1}_W = \mathbf{W}\,\check{\mathbf{X}}^i_B$, $\mathbf{Y}^{i+1}_B = \mathbf{B}\,\check{\mathbf{X}}^i_W$.

Estimations of the clean image: Three estimations are used:

1. The updated BM3D estimation $\tilde{\mathbf{X}}_{uB} \stackrel{\text{def}}{=} \mathbf{Y}^I_B$ (**hybrid1**).
2. The updated qWPdn estimation $\tilde{\mathbf{X}}_{uW} \stackrel{\text{def}}{=} \mathbf{Y}^I_W$ (**hybrid2**).
3. The hybrid estimation $\tilde{\mathbf{X}}_H \stackrel{\text{def}}{=} (\mathbf{Y}^I_B + \mathbf{Y}^I_W)/2$ (**hybrid3**).

References

[1] A. Averbuch, R.R. Coifman, D.L. Donoho, M. Israeli, Y. Shkolnisky, A framework for discrete integral transformations I – the pseudopolar Fourier transform, SIAM J. Sci. Comput. 30 (2) (2008) 764–784.
[2] A. Averbuch, R.R. Coifman, D.L. Donoho, M. Israeli, Y. Shkolnisky, I. Sedelnikov, A framework for discrete integral transformations II – the 2d discrete Radon transform, SIAM J. Sci. Comput. 30 (2) (2008) 785–803.
[3] A. Averbuch, P. Neittaanmäki, V. Zheludev, Periodic spline-based frames: design and applications for image restoration, Inverse Probl. Imaging 9 (3) (2015) 661–707.
[4] A. Averbuch, P. Neittaanmäki, V. Zheludev, Splines and Spline Wavelet Methods with Application to Signal and Image Processing, Volume III: Selected Topics, Springer, 2019.
[5] A. Averbuch, V. Zheludev, M. Khazanovsky, Deconvolution by matching pursuit using spline wavelet packets dictionaries, Appl. Comput. Harmon. Anal. 31 (1) (2011) 98–124.
[6] A.Z. Averbuch, P. Neittaanmäki, V.A. Zheludev, Spline and Spline Wavelet Methods with Applications to Signal and Image Processing, Volume I: Periodic Splines, Springer, 2014.
[7] I. Bayram, I.W. Selesnick, On the dual-tree complex wavelet packet and m-band transforms, IEEE Trans. Signal Process. 56 (2008) 2298–2310.

Please cite this article in press as: A. Averbuch et al., Analytic and directional wavelet packets in the space of periodic signals, Appl. Comput. Harmon. Anal. (2023), https://doi.org/10.1016/j.acha.2023.06.006

[8] E. Candés, L. Demanet, D. Donoho, L.X. Ying, Fast discrete curvelet transforms, Multiscale Model. Simul. 5 (2006) 861–899.
[9] E. Candés, D. Donoho, New tight frames of curvelets and optimal representations of objects with piecewise c^2 singularities, Commun. Pure Appl. Math. 57 (2004) 219–266.
[10] E.J. Candès, D.L. Donoho Ridgelets, A key to higher-dimensional intermittency?, Philos. Trans. A, Math. Phys. Eng. Sci. 357 (1760) (1999) 2495–2509.
[11] C. Chaux, L. Duval, J.-C. Pesquet, 2d dual-tree complex biorthogonal m-band wavelet transform, in: 2007 IEEE International Conference on Acoustics, Speech and Signal Processing-ICASSP'07.
[12] C. Chaux, L. Duval, J.-C. Pesquet, Hilbert pairs of m-band orthonormal wavelet bases, in: 2004 12th European Signal Processing Conference (EUSIPCO).
[13] Z. Che, X. Zhuang, Digital affine shear filter banks with 2-layer structure and their applications in image processing, IEEE Trans. Image Process. 27 (8) (2018) 3931–3941.
[14] R.R. Coifman, V.M. Wickerhauser, Entropy-based algorithms for best basis selection, IEEE Trans. Inf. Theory 38 (2) (1992) 713–718.
[15] L. Şendur, I.W. Selesnick, Bivariate shrinkage functions for wavelet-based denoising exploiting interscale dependency, IEEE Trans. Signal Process. 50 (2002) 2744–2756.
[16] K. Dabov, A. Foi, V. Katkovnik, K. Egiazarian, Image denoising by sparse 3d transform-domain collaborative filtering, IEEE Trans. Image Process. 16 (8) (2007) 2080–2095.
[17] M.N. Do, M. Vetterli Contourlets, in: G.V. Welland (Ed.), Beyond Wavelets, Academic Press, San Diego, CA, 2008.
[18] W.-Q. Lim, G. Kutyniok, X. Zhuang, Digital shearlet transforms, in: Shearlets: Multiscale Analysis for Multivariate Data, Birkhäuser, Boston, 2012, pp. 239–282.
[19] T. Goldstein, S. Osher, The split Bregman method for $L1$-regularized problems, SIAM J. Imaging Sci. 2 (2) (2009) 323–343.
[20] M. Golub, A. Averbuch, M. Nathan, V. Zheludev, J. Hauser, S. Gurevitch, R. Malinsky, A. Kagan, Compressed sensing snapshot spectral imaging by a regular digital camera with an added optical diffuser, Appl. Opt. 55 (March 2016) 432–443.
[21] B. Han, Z. Zhao, Tensor product complex tight framelets with increasing directionality, SIAM J. Imaging Sci. 7 (2) (2014) 997–1034.
[22] B. Han, Z. Zhao, X. Zhuang, Directional tensor product complex tight framelets with low redundancy, Appl. Comput. Harmon. Anal. 41 (2) (2016) 603–637.
[23] B. Han, X. Zhuang, Smooth affine shear tight frames with MRA structures, Appl. Comput. Harmon. Anal. 39 (2) (2015) 300–338.
[24] A. Jalobeanu, L. Blanc-Féraud, J. Zerubia, Satellite image deconvolution using complex wavelet packets, in: Proc. IEEE Int. Conf. Image Process. (ICIP), 2000, pp. 809–812.
[25] A. Jalobeanu, L. Blanc-Féraud, J. Zerubia, Satellite image deblurring using complex wavelet packets, Int. J. Comput. Vis. 51 (3) (2003) 205–217.
[26] A. Jalobeanu, N. Kingsbury, J. Zerubia, Image deconvolution using hidden Markov tree modeling of complex wavelet packets, in: Proc. IEEE Int. Conf. Image Process (ICIP), 2001, pp. 201–204.
[27] H. Ji, Z. Shen, Y. Xu, Wavelet based restoration of images with missing or damaged pixels, East Asian J. Appl. Math. 1 (2) (2011) 108–131.
[28] N.G. Kingsbury, Image processing with complex wavelets, Philos. Trans. R. Soc. Lond. Ser. A, Math. Phys. Sci. 357 (1760) (1999) 2543–2560.
[29] N.G. Kingsbury, Complex wavelets for shift invariant analysis and filtering of signals, Appl. Comput. Harmon. Anal. 10 (3) (2001) 234–253.
[30] G. Kutyniok, D. Labate, Shearlets: Multiscale Analysis for Multivariate Data, Birkhäuser, Boston, 2012.
[31] E. LePennec, S. Mallat, Sparse geometric image representations with bandelets, IEEE Trans. Image Process. 14 (4) (2005) 423–438.
[32] S. Mallat, Z. Zhang, Matching pursuits with time-frequency dictionaries, IEEE Trans. Signal Process. 41 (12) (1993) 3397–3415.
[33] François G. Meyer, Ronald R. Coifman Brushlets, A tool for directional image analysis and image compression, Appl. Comput. Harmon. Anal. 4 (1997).
[34] A.V. Oppenheim, R.W. Schafer, Discrete-Time Signal Processing, 3rd edition, Prentice Hall, New York, 2010.
[35] R. Rubinstein, A.M. Bruckstein, M. Elad, Dictionaries for sparse representation modeling, Proc. IEEE 98 (6) (2010) 1045–1057.
[36] N. Saito, R.R. Coifman, Local discriminant bases and their applications, J. Math. Imaging Vis. 5 (4) (1995) 337–358.
[37] N. Saito, R.R. Coifman, Improved discriminant bases using empirical probability density estimation, in: Proceedings of the Statistical Computing Section, Amer. Statist. Assoc., Washington, DC, 1997, pp. 312–321.
[38] I.W. Selesnick, R.G. Baraniuk, N.G. Kingsbury, The dual-tree complex wavelet transform, IEEE Signal Process. Mag. 22 (6) (2005) 123–151.
[39] J.L. Starck, E.J. Candès, D.L. Donoho, The curvelet transform for image denoising, IEEE Trans. Image Process. 11 (6) (2002) 670–684.
[40] Z. Xie, E. Wang, G. Zhang, G. Zhao, X. Chen, Seismic signal analysis based on the dual-tree complex wavelet packet transform, Acta Seismol. Sin. 17 (1) (2004) 117–122.
[41] X. Zhuang, Digital affine shear transforms: fast realization and applications in image/video processing, SIAM J. Imaging Sci. 9 (3) (2016) 1437–1466.

Please cite this article in press as: A. Averbuch et al., Analytic and directional wavelet packets in the space of periodic signals, Appl. Comput. Harmon. Anal. (2023), https://doi.org/10.1016/j.acha.2023.06.006

Sponsor names

Do not correct this page. Please mark corrections to sponsor names and grant numbers in the main text.

Israel Science Foundation, *country*=Israel, *grants*=1556/17, 1873/21

Israeli Ministry of Science, Technology and Space, *country*=Israel, *grants*=3-13601, 3-16414, 3-17927

Academy of Finland, *country*=Finland, *grants*=311514